Systemization of RFID Tag Antenna Design Based on Optimization Techniques and Impedance Matching Charts

By

Munam Butt

Thesis presented to the
Faculty of Graduate and Postdoctoral Studies
In partial fulfillment of the requirements for the degree of

Master of Applied Science

in

Electrical and Computer Engineering

Ottawa-Carleton Institute for Electrical and Computer Engineering

Department of Electrical Engineering and Computer Science
Faculty of Engineering
University of Ottawa

Ottawa, Ontario, Canada, April, 2012

ABSTRACT

The performance of commercial Radio Frequency Identification (RFID) tags is primarily limited by present techniques used for tag antenna design. Currently, industry techniques rely on identifying the RFID tag application (books, clothing, etc.) and then building antenna prototypes of different configurations in order to satisfy minimum read range requirements. However, these techniques inherently lack an electromagnetic basis and are unable to provide a low cost solution to the tag antenna design process. RFID tag performance characteristics (read-range, chip-antenna impedance matching, surrounding environment) can be very complex, and a thorough understanding of the RFID tag antenna design may be gained through an electromagnetic approach in order to reduce the tag antenna size and the overall cost of the RFID system.

The research presented in this thesis addresses RFID tag antenna design process for passive RFID tags. With the growing number of applications (inventory, supply-chain, pharmaceuticals, etc), the proposed RFID antenna design process demonstrates procedures to design tag antennas for such applications. Electrical/geometrical properties of the antennas designed were investigated with the help of computer electromagnetic simulations in order to achieve optimal tag performance criteria such as read range, chip-impedance matching, antenna efficiency, etc. Experimental results were performed on the proposed antenna designs to compliment computer simulations and analytical modelling.

ACKNOWLEDGEMENTS

I would have never been able to finish my thesis without the support and guidance from everyone who helped me every step of the way. I am grateful for the opportunity to complete this thesis and would like to acknowledge a few individuals who deserve my heartfelt thanks.

I offer my sincerest gratitude to my supervisor at the School of Electrical Engineering and Computer Science at the University of Ottawa, Dr. Mustapha C.E. Yagoub. I am grateful for all his guidance, support, motivation and patience throughout the process of my research work.

I would also like to express my gratitude to my colleagues Rijwal C.R., Alexi Borisenko, as well as the Lab Coordinator Mr. Alain Le Hénaff for analyzing my work critically and providing me with suggestions.

Finally, I would like to thank my parents, my brothers, my sister, my brother-in-law, and my nephews, for their support and encouragement throughout my graduate studies at the University of Ottawa.

TABLE OF CONTENTS

LIST OF FIGURES

LIST OF TABLES

CHAPTER 1 Introduction

1.1 Motivation

RFID (radio frequency identification) has become an integral part of modern daily life by enabling the tracking of assets and merchandise. RFID is extensively used for thousands of applications such as auto-theft protection, merchandise tracking, collecting tolls without stopping, access control of people into buildings, dispensing goods, access to ski lifts, etc. An RFID system consists of tags or transponders that are affixed onto objects and readers or interrogators that communicate remotely with these tags to enable identification [1].

There are four classes of RFID tags: semi-active, active, semi-passive, and passive [2]. This thesis focuses solely on passive RFID tag antenna design. As a result, the power needed to turn-on the passive tag's microchip is provided by the reader through a process called backscatter modulation [3].

Chip sensitivity threshold (P_{th}) is the most important tag limitation. It is the minimum received RF power to turn-on the RFID chip. The lower it is, the longer the distance at which the tag can be detected. Chip sensitivity is usually determined in the RF front end architecture and fabrication process [4]. The chip sensitivity of the RFID tag and the tag's antenna play a key role in the overall RFID system performance factors such as reading range, overall size and compatibility with tagged objects [5]. The design goal is to reduce the size of the antenna as well as conjugate impedance match it to the given RFID-IC's impedance. The reason for matching the antenna to the chip is to achieve maximum power transfer [6], i.e. most of the power is delivered to the IC of the tag and very little is lost due to mismatch or environmental losses.

The back-scattered RFID system works in the following way. The reader transmits a modulated signal, which is detected by the tag antenna [5]. The RF voltage developed at the antenna terminal is converted into dc voltage responsible for turning on the chip. Furthermore, the chip sends back information to the reader by varying its front-end complex RF input impedance. Therefore proper impedance matching between the antenna and the chip is very important in RFID. In addition, this complex impedance matching facilitates the RF power necessary to turn on the chip and establish a communication link. Some RFID tag

antenna configurations are widely used in scientific papers and in commercial products as discussed in [4]-[10]. However, the main problem as encountered in [5]-[7], and [9]-[10], is that there is a lack of systemization in the tag antenna's design process. Furthermore, more attention is given to the application requirements of the RFID tag by means of fabrication and measurement procedures as shown in [10] rather than a precise chip impedance matching process. This thesis proposed to fill this gap by providing techniques to develop RFID tags based on the application of use. Furthermore, the tag designs are modelled using computer simulations which account for tag performance characteristics such as impedance matching, tag read range, etc. In addition, the results obtained can help designers optimize the antenna dimensions before the fabrication process. Consequently, this will enhance the antenna design process and reduce the overall RFID tag development costs.

1.2 Thesis Scope and Outline

The objective of this thesis is to help Radio Frequency (RF) designers to better select the most suitable antenna based on the application of use and design it. This requires the design process to include several stages. First, the antenna theory necessary for a tag designed for a specific application is investigated to ensure the success of the antenna design. For example, in the case of supply chain tags, the antenna may not require a sophisticated geometry and this helps in less material being used thereby reducing costs. Second, antenna-chip impedance matching techniques as well as antenna size reduction techniques are explored, which results in the generation of computer aided simulations. The simulations help the designer pick the optimal dimensions of the tag antennas based on tuning of geometrical and electrical parameters of the antenna. Finally, the designs are fabricated and measured to match the conditions set out by the simulation process. Furthermore, the RF designers can use similar simulation results in order to produce different antenna geometries for a wide variety of commercially available chips.

This thesis is organized into 8 chapters. Chapter 2 deals with background of RFID fundamentals and related work necessary for understanding the subsequent chapters. It can be decomposed into two major parts. The first part gives a brief introduction to RFID systems, the history of RFID, its applications and industry standards and regulations. In the second part, antenna theory and tag-reader coupling mechanisms (communication links) are

discussed. Chapter 3 gives an overview of the RFID tag antenna design process and testing procedures. Chapter 4 provides a detailed discussion on RFID tag antenna design procedures which include antenna-IC matching and size reduction techniques. In chapter 5, a literature survey is conducted to classify existing passive RFID tags into families/classes based on their application of use. In Chapter 6, electromagnetic modeling and simulations of a selection of tag antennas are presented. In Chapter 7, the obtained simulated results are compared to experimental measurements. Chapter 8 provides a conclusion and the contributions of the thesis and future work.

1.3 Contributions

The main contribution of this thesis is the systemization of the RFID antenna design process for RF designers by providing techniques to develop application-specific passive RFID tags. As an example of this process, tag antenna designs (A, B, C, D and E) were achieved through simulations and tag performance measurements. Furthermore, the results obtained can help the designer select optimal impedance-matching antenna dimensions before the fabrication process. As a result, this process will significantly reduce the RFID tag developments costs.

.

CHAPTER 2 – Background to RFID and Antenna Theory fundamentals

In recent years the need for automatic identification techniques (Auto-ID) in the service industry, manufacturing companies and distribution and supply chain has led to the development of Auto-ID systems. Auto ID collects data related to objects and feeds this data into a database management system with minimal human intervention. This process of identification and data collection is automated to provide a high level of efficiency with reduced costs. Auto ID technology is a big superset of different technologies such as Magnetic Ink Character Recognition (MICR), Voice Recognition, Biometrics, Barcodes, and RFID (radio-frequency identification [3, 12]. Until recently, barcodes were prevalent in the service industry in regards to tagging objects. However, barcodes are limited in the data storage capability and require LOS (line of sight). To address these issues, RFID technology was introduced. The RFID system employs RF communication which overcomes the LOS problem and uses IC (integrated chip) technology that can store large amounts of data. Therefore, this makes RFID technology an attractive alternative to barcodes in regards to tagging or tracking objects.

In this chapter we will discuss the history and the fundamentals of RFID technology. It comprises of two major parts, the first part gives a brief introduction to RFID systems; the history of RFID, its applications and industry standards and regulations. In the second part, antenna theory fundamentals and tag-reader coupling mechanisms (communication links) are discussed.

2.1 Introduction to RFID technology

Radio Frequency Identification (RFID) is a wireless technology that allows for automated remote identification of objects [13]. The major components of an RFID system are tags or transponders that are affixed on to objects and readers or interrogators that communicate remotely with these tags to enable identification. RFID systems are part of the Auto-ID procedures as shown in the Figure 2.1.

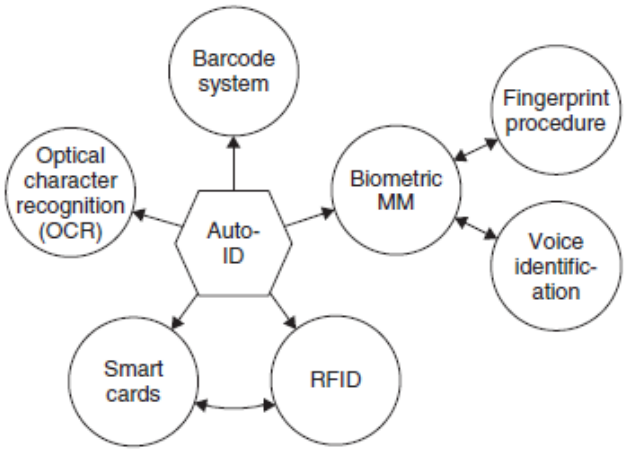

Figure 2.1 Overview of Auto-ID technologies [11]

The basic RFID system as shown in Figure 2.2 consists of two components: (i) the transponder (or tag) that is located on the object to be identified as well as (ii) the reader (or transceiver) that is designed to communicate with the tag by performing either a read or a write/read operation. The RFID system operates as follows: The reader broadcasts signals via its attached antenna. The tag receives these signals and responds by either writing the receive data into the IC memory or replying with another signal that contains some data, usually the identity code or a measurement value [11]. In addition, the tag may rebroadcast the signal to the reader with a predetermined time delay.

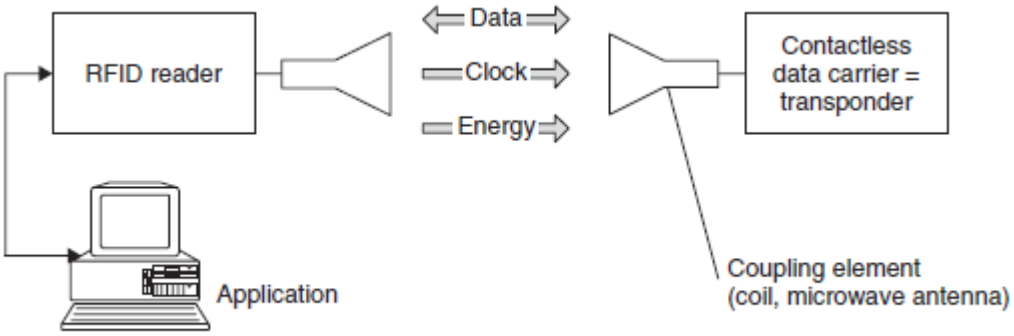

Figure 2.2 Main components of an RFID system [13]

The tag IC contains a unique identification of the object to be tracked. As this object moves through the various processes such as manufacturing, warehousing, and transportation, more data can be written on the attached tag IC. Therefore, data is stored and can be retrieved and manipulated with minimal human intervention. This ease of data manipulation and storage has made RFID technology very popular compared to other forms of Auto ID technologies.

2.1.1 History of RFID

RFID technology can be traced back to as early as World War II, where British airplanes were identified as a 'friend of foe' using this technology. Under the supervision of Scottish physicist Sir Robert Alexander Watson-Watt, the British developed the first active identify friend of foe (IFF) system [15]. A transmitter was installed on each British plane and the radar-on-ground would be able to identify the plane based on the signal it received back from the transmitter.

In 1948, Harry Stockman first showed how a communication link could be established using reflected power [16], and in 1950 the first patent was lodged for passive transponders. However, the optical barcode, a close rival of RFID, came to commercially usage in the 1960s and 1970s. In addition, the cheap implementation of optical barcodes made it a huge success and is still prevalent in the most of the products today (2012). However, due to the increased complexity and volume of business caused the industry to look for alternatives to the barcode and hence started the journey for RFID.

Until 1979, RFID research was confined to laboratory experiments only. However, the first commercial use of RFID was in animal tracking in the United States in the early 1980s. This was followed by the first motor toll collection using RFID in Norway in 1987 and then in US rail cars in 1994 [14]. In 1999, the Auto-ID center was established at the Massachusetts Institute of Technology (M.I.T.) to research and develop worldwide protocols and standards for RFID technology.

Absence of related technologies and global standards restricted the initial development of this technology. Different countries and even different companies used RFID as proprietary technology. There was minimal interoperability among different players. This problem was addressed by UCC (Uniform Code Council) together with EAN (European Article

Numbering) create EPCglobal to commercialize EPC (Electronic Product Code) technology [4]. EPCglobal ratified a second generation standard Gen2 in 2005, for broad adoption of RFID [8]. This revolutionized the RFID industry creating numerous demands from industry giants like Wal-Mart, US Department of Defense, Gillete, and so on.

2.1.2 Overview of RFID Technology

RFID system is a multidisciplinary system that can provide a complete solution and be deployed independently or in compatibility with other existing systems such as the optical barcode [11]. The basic goal of RFID is to make operations more accurate and user friendly for businesses. This includes better quality control, automated tracking and product loss prevention. As seen in Figure 2.3, the RFID system is divided into two layers: physical layer and the IT layer [11]. The physical layer comprises tag, reader and the interrogation zone (IZ).

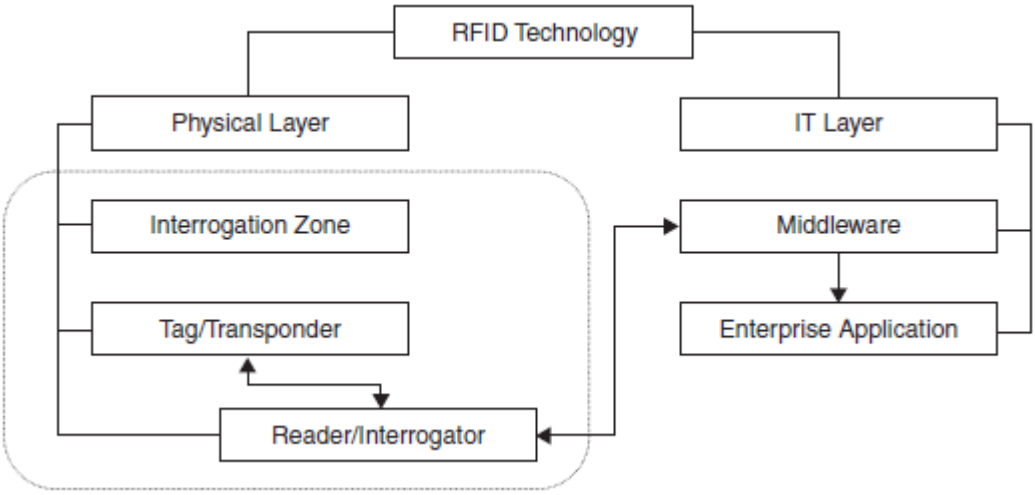

Figure 2.3 RFID system divided into layers [11]

Tag: Tags are similar in purpose to optical barcodes, which are attached to objects and store unique identification of the object/product. The tags primarily consist of two components: the tag antenna and the IC chip. The tag antenna communicates with the reader by means of electromagnetic waves. Based on the type of tag (active, passive, semi-passive or semi-active) energy to turn-on the IC may be either acquired from the environment (reader RF

signal) or via an onboard battery supply. The IC chip stores the unique identification of the system like product description, product code, product origin, etc. In unique tags sensors might be attached on the tag to monitor environmental conditions such as temperature, humidity, etc.

Reader: The reader is a device that is used to communicate with tags that are affixed onto products. They usually are handheld, mobile, or stationary. Readers are made up of two components: the antenna and the reader circuitry. The antenna communicates with the tag using electromagnetic waves. Based on the application of use, the reader circuitry is responsible for sending data through the reader antenna as well receiving data and processing/storing it in the back end.

Interrogation Zone (IZ): The interrogation zone is an area where the reader is able to read/write data to or from a tag. This area is a three-dimensional space in the vicinity of the tag and the reader where electromagnetic waves can travel. The IZ is included in the physical layer because the tag-reader communication link is influenced by the surrounding environment that includes, interferences caused by other objects in the present in the IZ, reflection of waves, etc.

The **IT layer** comprises the *middleware* and *enterprise applications*.

Middleware: The middleware is responsible for collecting data from the interrogator, storing the data and sending it to the enterprise application. It also consists of software that monitors, configures and manages the hardware of the reader.

Enterprise Application: Data is collected by the middleware by this application for business processes like the creation of invoices.

RFID processes are geared to be application specific depending on the nature of the business process. As a result, the process requires different combinations of readers and tags. For example, applications criteria could involve read range, frequency protocol, form factors (shape and size of tags) etc. Therefore, the RFID process is unique and its components have to be carefully selected to meet specific application requirements. Other issues involve standards and regulations. For standard EPCglobal was created, as a worldwide RFID standard. The regulations are region specific such as FCC (USA), ERO (Europe), ACA (Australia) etc. It is the responsibility of the RFID manufactures to comply with these

regulations when developing their products. In addition, mandates provided by some big companies like Wal-Mart also need to be adhered to while developing the RFID products.

2.1.3 RFID Technology Applications

The areas of application of RFID are very vast and are projected to cover every single item in the future [11]. Some broad areas where RFID is used in large volumes are manufacturing, logistics, supply chain and tracking [3, 12]. These include healthcare, pharmaceutical, livestock, baggage handling, access control, contactless payments, etc. To make the concept of RFID application clear, two examples from manufacturing and supply chain process are mentioned below.

Manufacturing: manufactures send their products to the shipping yard for transportations. At the manufacturer's end each item is tracked and placed into a box and then a pallet. The boxes and pallets also are tracked and information about the quantity of the products is stored.

Supply-Chain: At the yard, the items are read and information such as time, place and date etc. are stored on a database. This data is available for manufacturers as well as supply-chain companies like Fedex, UPS to track items and account for any losses or theft.

In this way the items are tracked and any lost or stolen items can be reported immediately with information such as date, time, place where the items went missing. The manufacturers also track the products throughout the supply chain process until they reach the customer. In this way quality control is maintained.

2.1.4 Benefits of RFID

Although the RFID technology has become very popular in recent years, the main rival optical barcode is still prevalent today. This is largely due to the fact that barcodes have the competitive advantage of a cheaper technology to employ for business processes. However, RFID is gaining steam, and with the reduction in the costs of RFID components (tags, readers, ICs) the gap is narrowing. Some of the advantages and disadvantages of RFID technology when compared to barcodes is mentioned in the Table 2.1 below.

Table 2.1 RFID technology compared to traditional barcodes [1].

RFID	Barcode
1. No line of sight (LOC) required. Tags may have any orientation.	1. LOC required or else to scan item for data.
2. Identification of items, cases and pallets is possible.	2. Only one category (items, pallets) identification.
3. Simultaneous identification (read//write) possible.	3. Only one item can be scanned at a time.
4. High data capacity (16-64 Kilobytes).	4. Low data capacity (1-100 bytes).
5. High read distance (0-5m).	5. Lower reading distance (0-50cm).
6. Wear and tear has minimal influence.	6. If barcode ink is smudged then, it is impossible to scan the item.
7. Cost of tag is high ($0.15+)	7. Barcode can be printing on item, minimal costs.
8. RFID tags are application specific so require time to create specific tags to meet requirement.	8. Barcode can be printed on items almost immediately.

2.1.5 RFID Antenna Characteristics

There is a lot of terminology associated with RFID technology from the perspective of electromagnetic (EM) waves. The EM waves are essentially composed of mutually interchanging electric and magnetic fields that are perpendicular to each other as well as the direction of propagation [11]. As these EM waves propagate, they radiate energy in the three dimensional space surrounding them. Therefore, as the waves travel further away from the source the radiated power density decreases in magnitude. The terminology seen throughout the RFID system is shown in Figure 2.4 [11].

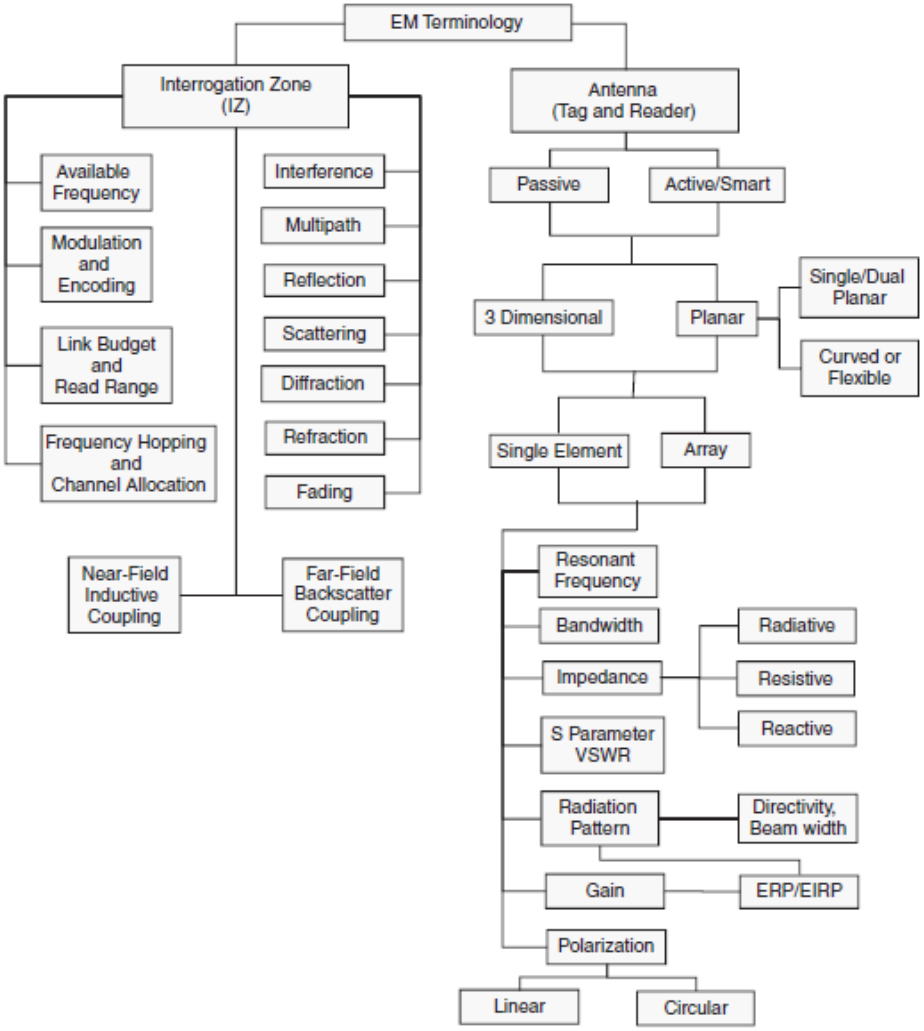

Figure 2.4 RFID system related to EM terminology [11]

The terminology related to the RFID antenna such as resonant frequency, bandwidth, impedance, etc. is unavoidable when it comes to antenna design. Some of the more important terms that are needed for the subsequent chapters are mentioned below.

Resonant Frequency: Any antenna transmits or receives EM waves efficiently at one or more frequencies, depending on the design and matching considerations related to the Friis equation. These frequency/frequencies in the RFID context are called resonant frequency [11].

Bandwidth: The range of frequency surrounding the resonant frequency of the antenna. The efficiency of the RFID tag antennas in transmitting or receiving EM waves is close to 90% (-

10dB) and this is known as the bandwidth for the RFID system [11]. This is typical for RFID system antennas, but may differ for antennas for different technologies.

Impedance: The impedance is divided into three resistances namely, radiative, resistive, and reactive. Power absorbed by the radiative resistance is transmitted as EM energy or vice versa. The radiative resistance is directly proportional to the antenna length. The resistive radiation just dissipates power absorbed in the form of heat. The reactive resistances act as barriers and inhibit the transfer of energy. These are typically capacitive or inductive and at resonant frequency cancel out each other, hence the antenna can freely radiate energy efficiently at the resonant frequency.

Radiation Pattern: For any antenna the radiation pattern is never spherical [11]. In the RFID context, reader antennas have a directional radiation pattern (all the energy is beamed into one direction) and the tag antennas have a toroid shaped pattern (they can be read from all direction).

Polarization: This is a very important concept to grasp. The EM waves radiated from the antenna have an electric and magnetic field that are perpendicular to each other. Based on the orientation of the electric field, the polarization of the antenna may be linear or circular. In the RFID context, readers are typically circularly polarized whereas tags are linearly polarized. Furthermore, the circular polarization allows the reader to be compatible with any linearly polarized tag thereby reducing costs associated with polarization mismatch. This polarization mismatch causes only half the power to be received by the tag antenna, a 3dB loss. The term that describes the amount of power lost due to mismatch is called *polarization loss factor* (PLF). The PLF ranges from 0 to 1, where 0 indicates no transfer or power and 1 represents maximum power transfer as seen in table 2.2 for different polarizations.

Table 2.2 Effect of polarization mismatch resulting in different values for PLF [19].

Incident Wave Polarization (Transmit Antenna)	**Receive Antenna Polarization**	***PLF***
Vertical Linear	Vertical Linear	1
Linear (V or H)	Circular (RH or LH)	0.5
Vertical Linear	Horizontal Linear	0
RH Circular	RH Circular	1
RH Circular	LH Circular	0

2.1.6 RFID Tags

RFID tags are required in large quantities as they have to be attached to all the products that need to be tracked. The main components of the RFID tags are the antenna and the integrated circuit (IC) chip. The other components include the dielectric substrate, packaging, etc. and will be discussed in this section.

2.1.6.1 Tag IC

This is a semiconductor-based circuitry that is designed by a chip manufacturer (Texas Instruments, NXP Semiconductors, etc). The tag manufacturers buy these ICs based on the application requirements. The IC is divided in to three parts:

Analog front end: this part is responsible for controlling the power. The power may be supplied by either the battery or external EM radiation. The analog front end part consists of components such as voltage regulators, modulators, clock cycle generators, and so on.

Detection, Encoding/Decoding unit: This unit is responsible for the modulation and demodulation of signals and encoding the received signal into bits to be stored to the memory unit of the IC.

Memory unit: The memory is divided into blocks which may be either read only or read/write enables depending on the application. The unique identification code, error checking codes, passwords, etc. are stored in the IC memory [11].

2.1.6.2 Substrate

The substrate is a dielectric material and forms the base of the RFID tag. The conductive material (copper, aluminum) is etched on top of the substrate and the IC is attached to either ends of the conductor. The substrates are usually used are thin, flexible and can stand harsh environmental conditions. Some commonly used materials for RFID substrates are PVC, PET, FR-4, Rogers Duriod, etc.

2.1.6.3 Tag Packaging

After the tag has been manufactured it is important to make sure that the tag is packaged properly in order to protect it from the physical environment. Some important tag packaging terms are mentioned below.

Strap: In cases where the IC pads are small, two pads are provided by the manufacturer to help attach the IC to the antenna. This is called the strap.

Inlay: The strap when added to the antenna with some additional substrate is called the inlay. These inlays are typically produced by label makers with the help of an RFID printer.

Smart Label: The inlay is inserted inside a paper label. The paper label has readable information printed outside it like a barcode, the EPC logo, etc. This is called a smart label.

Encapsulated tag: In some applications (supply chain process) the tag need to be protected from the physical environment from damage. In such cases the tags are encapsulated in hard RF translucent outer covers such as polypropylene, polyacetate, etc [11]. This protects the tag from damage.

2.1.6.4 Tag Classification

Tags are separated into different categories based on criteria such as power source, frequency of operation, protocols, functionality, etc. An overview of the RFID tag classification in shown in Figure 2.5 [11] and some of these criteria will be explained in the following sections.

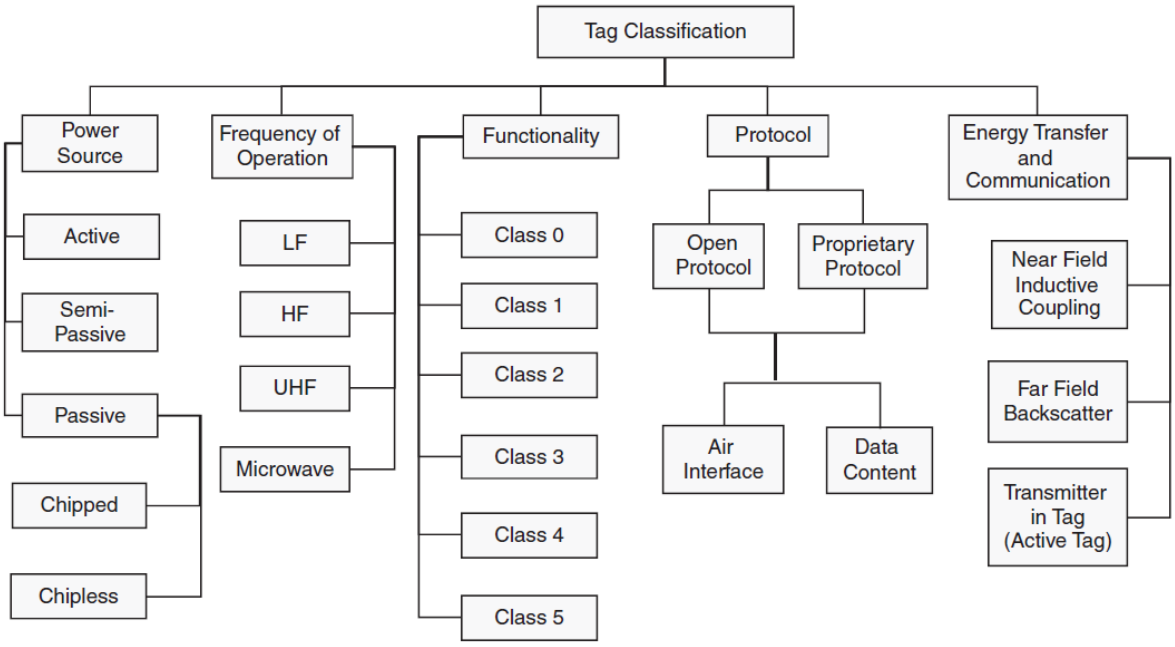

Figure 2.5 RFID tag classification [11]

2.1.6.5 Power Source

Since tags depend on a power source for operation they can be divided into four classes: semi-active, active, semi-passive, and passive [13].

Active-tags: use battery power for powering the logic and communications link. As a result, these tags have greater read-range when compared to passive or semi-active tags. Active tags have the disadvantage of relying on a battery source, which once depleted must be replaced.

Semi-passive tags: use batteries to power only the logic part of the tag once the tag is activated through incident energy from the reader. The semi-passive tag modulates the incident signal to communicate with the reader. The process of reflecting the energy back to the reader as a means of communication is called back scattering [12].

Semi-active tags: harvest energy from their environment to power the logic and communications link. These tags can use solar energy, vibration energy (piezoelectric rectification) or another means to power the logic on the tag. They are also known as energy harvesting

Passive tags: do not have any source of power such as batteries and rely solely on the power that is rectified by the reader to power the tag. Like semi-passive tags, these tags also use the back-scattering process to communicate with the reader. Semi-passive and passive tags can be distinguished through their coupling mechanism: near-field and far field operation [13].

Table 2.3 RFID Tag Types based on power source

Active Tag • Communication and logic powered by onboard battery. • Increased range	Semi-Active Tag • Logic powered by onboard battery • Communications enabled by back scattering incident signal.
Semi-Passive Tag • Logic powered by energy harvesting methods (solar, vibration, etc) • Communications enabled by back scattering.	Passive Tag • No on-board battery, relies on RF waves emitted by the reader to power logic • Communications enabled by back scattering.

2.1.6.6 Frequency of Operation

There are several frequency bands of operation for the RFID tags namely, low frequency 125-134 kHz (LF), high frequency 13.56 MHz (HF), ultra high frequency 400-960 MHz (UHF), and microwave 2.4 GHz and 5.8 GHz [2],[3] and [11]. The operation of frequency for RFID is regulated by each country. For example, the UHF RFID frequency in North America is 915 MHz but for most of Europe it is 860 MHz. Furthermore, RFID tags are designed to meet these frequency specification based on the application such as short read range, long read range, enhanced security, better data transfer rate, etc.

Low frequency tags (125-134 kHz): were among the first tags to be deployed for RFID applications. The main advantage of these tags was that they could be read while attached to objects containing water, animal tissues, metal, wood, and liquids [11]. However, the LF tags had several drawbacks such as use in close proximity applications, only a short read range of a few centimeters, very low data storage capacity and no anti-collision measures which are necessary if the reader requires to be read multiple tags simultaneously.

High frequency tags (13.56 MHz): are currently the most widely used in the RFID industry. The HF tags use inductive coupling as a source of power to communicate with the readers [11]. These tags have several advantages such as better read range, typically half a meter, high data storage capacity, good anti-collision measures for readers to communicate with multiple tags. All these features make HF tags an ideal choice for applications such as credit cards, library book tags, airline baggage tags and asset tracking [11].

Ultra high frequency tags (433 MHz and 860-960 MHz): use far-field coupling or back scatter coupling to communicate with each other [11]. These UHF tags have several advantages such as good memory size for the data, up to 240 bits, and very long read range, typically 20 meters under good conditions. However, the main disadvantage of UHF tags is that their performance is severely degraded when attached to objects containing water, biological tissues and metals. Some typical applications of the UHF tags include supply chain, inventory and logistics, apparel and aviation baggage.

Microwave tags (2.4GHz and 5.8GHz): have high data transfer rate that allow communication between devices at a very high rate [11]. Consequently, the microwave tags are most suited for application where real-time asset tracking is required. The main drawback of the microwave tag is higher cost to develop and most of the tags are active tags

i.e. they require an external battery to power the microchip on the tag. Typical applications include highway toll collection, real-time location system, etc.

2.1.6.7 Functionality (EPC Global Classes)

EPCGlobal (RFID standardization body) has classified RFID tags into six different classes based on the certain criteria such as power, memory capacity, protocols, etc [3], [13], [11] and [16]. These classes are mentioned in the Table 2.4 below.

Table 2.4 RFID classes and their functionality

Class	Functionality
0	Passive tags that have 'write once read many' (WORM) IC chips. The data is written when the IC is manufactured.
1	Passive tags with WORM chips. The data is either written during chip manufacturer or by the customer before use.
2	Passive tags with read/write capability. The user can add additional information to the tag for encryption.
3	Semi-passive tags with on-board sensors. Have read/write capability and additional memory space available for use.
4	Active tags with on-board sensors. Have read/write capability. User memory. Peer communication provision with similar active tags and readers.
5	This class defines readers. These readers can communicate and power tags in the aforementioned classes [0 - 4].

2.1.6.8 Protocols

Protocols are a given set of codes ('language') that allow communication between the tag and the reader. There also exist protocols where a reader can communicate with other readers in close vicinity.

Protocols are divided into the following categories:

Open Protocols: These are developed by standardization bodies such as ISO 18000-6(A/B), ISO 14443 (A/B), etc. Open protocols are available globally and can be used by anyone.

Proprietary Protocols: These are developed by manufacturers for their own business such as Texas Instrument's 'TI Tag-IT', Intermec's IntelliTag, etc.

The protocols mentioned above can be divided into sub sections where the readers might need to use multiple protocols to for different tags. These types of protocols are mentioned below:

Air Interface Protocols: These protocols depend on how the tag and reader communicate based on frequency of operation, bit rate, modulation, anti-collision algorithms, etc.

Data Content Protocols: These protocols define the layout of the memory structure in the IC. Therefore, these protocols make it easier to locate specific data on the tag's IC.

2.1.6.9 Tag Antenna

In UHF tags, the antennas preferred are usually a dipole or patch structures [11]. The main considerations while choosing the antenna for design are mentioned below.

- Must be small enough to attach on to object (typically 50.8mm x 101.6 mm) [10].
- Have an omnidirectional radiation pattern so that the tag can be read from any direction.
- Must have minimum turn-on impedance for the tag-IC.
- Avoid polarization mismatch (discussed in section 2.1.5)
- Be very robust and cheap.

2.2 RF in RFID

This section starts with the discussion of antenna fundamentals such as field regions, dipole radiation patterns. The second part of this sections deals with coupling mechanisms such as inductive coupling, or modulated back-scatter coupling.

2.2.1 Antenna fundamentals

It is important to understand the field of operation (near-field, far-field) and the radiation pattern (omnidirectional) of RFID antennas before the design process of the antenna. These concepts are discussed in this section.

Field regions: The space surrounding the antenna is divided into three regions, based on the behaviour of the fields [20]. These regions: the reactive near-field, radiating near-field (or Fresnel), and the far field (or Fraunhofer) are shown in figure 2.6, for an antenna whose largest dimension is D.

The **reactive near-field region** is the region immediately surrounding the antenna where the fields predominately do not radiate [19]. For an electrically small antenna, the radius of this sphere is denoted by, $R = \lambda/2\pi$ [13]. For larger antennas, this region is denoted by [19]:

$$R = 0.62\sqrt{\frac{D^3}{\lambda}} \quad (1)$$

The tags at LF and HF frequencies are mostly loop or inductive coil antennas and operate in this region [19].

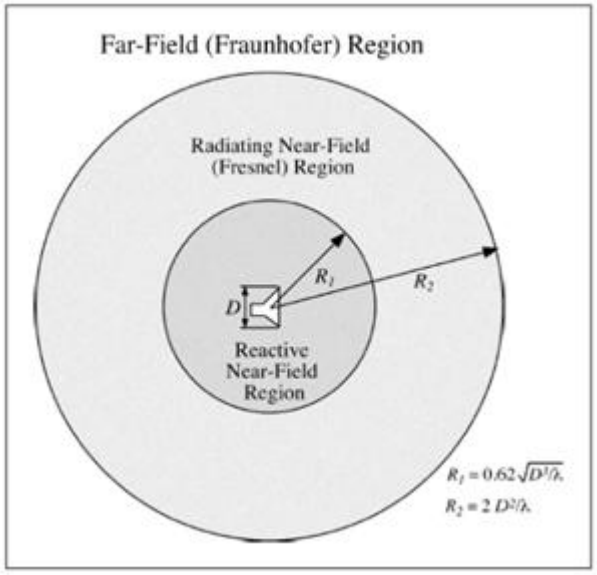

Figure 2.6 Field regions [19].

The **radiating near field**, or **Fresnel region**, lies between the reactive near-field region and the far-field region. In this region the fields are predominately radiating, and the angular field distribution depends on the distance from the antenna [19]. If the antenna is small this region may not exist [19]. For larger antennas, the inner radius of this spherical region is given by (1) while the outer region is given by [19]:

$$R = \frac{2D^2}{\lambda} \quad (2)$$

The **far-field**, or **Fraunhofer**, region is the region where the fields are radiating and their angular variation is essentially independent of the distance from the antenna, and the fields components lie essentially in the transverse plane to the direction of propagation [19]. The traveling waves dominate in this region where the decay rate is $1/r$ (where r is the distance from the antenna to the observation point in the far-field region) [19]. These traveling waves carry the electromagnetic power to the passive and semi-passive UHF and microwave transponders [19].

Radiation Pattern: An accurate model for the dipole is quite complex, but forming a reasonable approximation for the radiation of the dipole is simple. We can achieve this by looking at small segments of a dipole. For each segment we assume that the current is uniform. The dipoles examined here known as Hertzian dipoles. As seen in figure 2.7a, the distance *R* from a point z' on the dipole to the observation point *P* is given by [9]:

$$\boldsymbol{R = \sqrt{x^2 + y^2 + (z - z')^2}} \quad (3)$$

In the far-field region of the dipole (where $R > 2l^2/\lambda$), as shown in figure 2.7b, the following approximations can be made for determining the radiated patterns:

$$R \approx r, \text{ for amplitude terms}$$
$$R \approx r - z'\cos\theta, \text{ for phase terms}$$

Since the length of the wire is so small, the electric current (I) along the wire is assumed to be constant and flowing solely in the z-direction[20]:

$$\boldsymbol{I\,(x', y', z') = Io\hat{z}} \quad (4)$$

l is the length of the dipole, *P* is the observation point (typically more than a wavelength away).

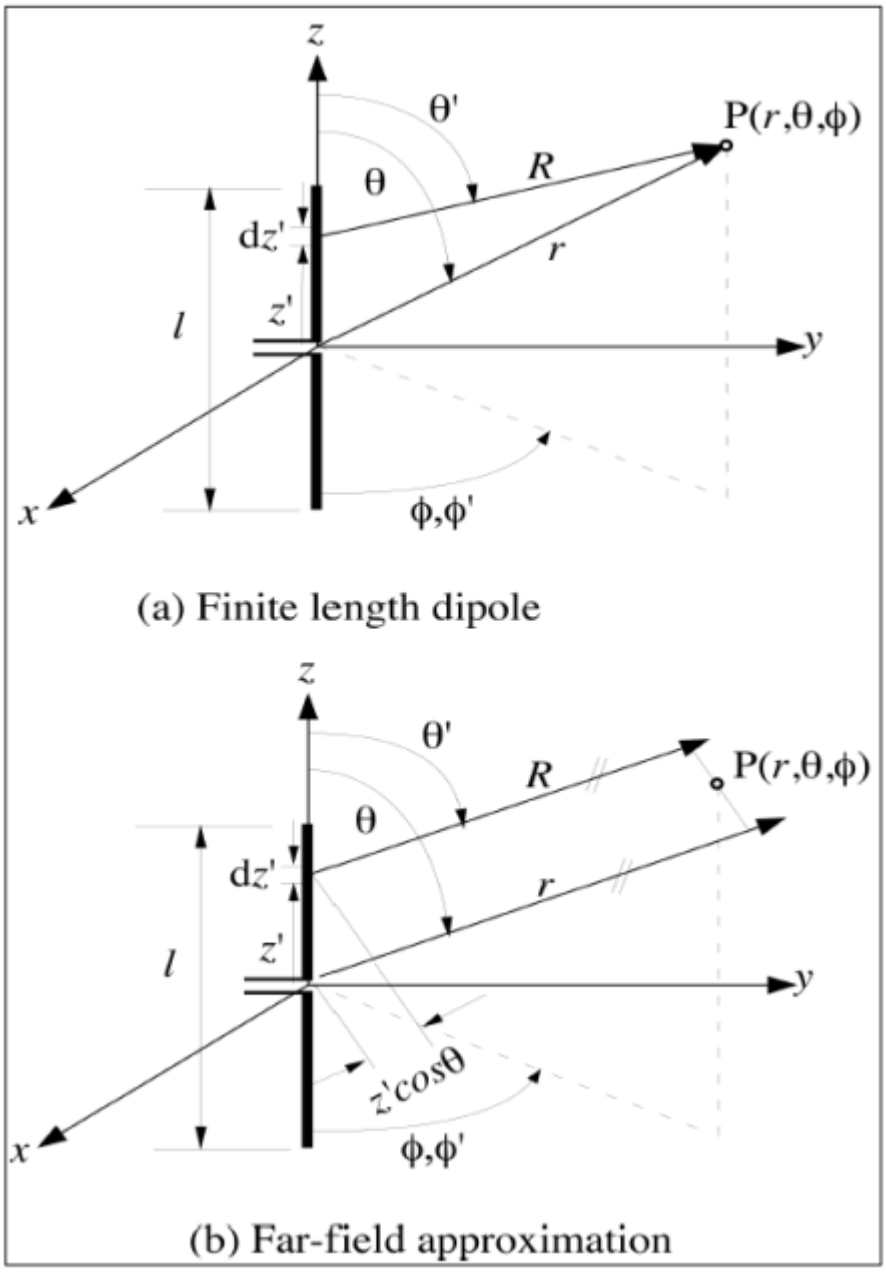

Figure 2.7 Far field approximation of R for a finite length dipole [19]

Normalized radiation patterns of the dipole of various lengths [18] are shown in Figure 2.8. As the length of the antenna increases, the beam narrows and the directivity increases. When the length of the dipole exceeds a wavelength, additional lobes will appear in the radiation pattern.

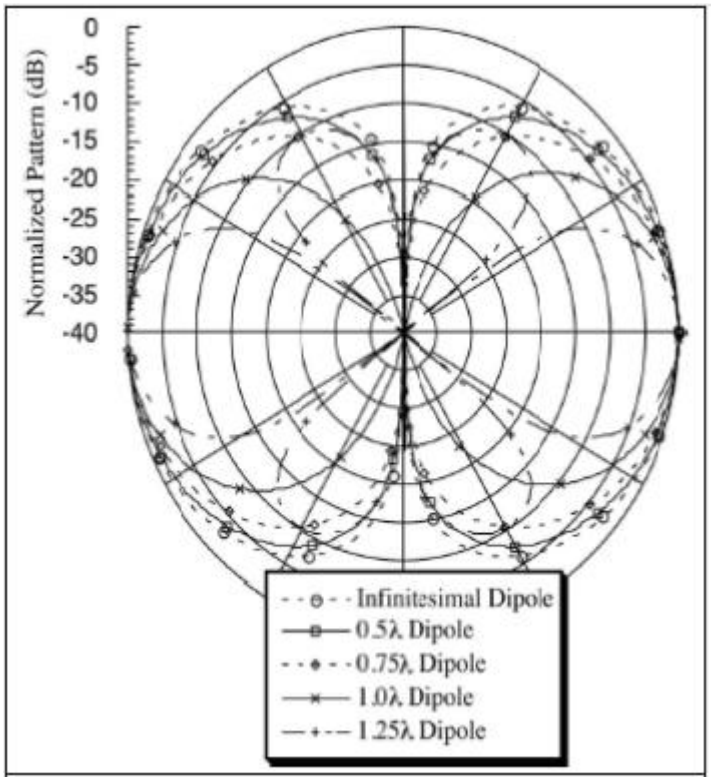

Figure 2.8 Radiation pattern of dipole of various lengths [18]

The intensity of the electric field is given by [19].

$$\boldsymbol{E = -\frac{jIo\sin\theta}{2\varepsilon ocd}\frac{L}{\lambda}e^{-j(\omega t-kd)}} \quad (5)$$

In the above equation, $j^2 = -1$,ε_0 is the free space permittivity, c is the speed of light, $k = 2\pi / \lambda$ and $\omega = 2\pi f$

Two important points observed from the above equation are

(1) The power intensity is the square of the E-field intensity, and the E-field power drops off as $1/d$, and this makes the power drop off as $1/d^2$.
(2) The E-field intensity falls off with θ as sin θ, resulting in a radiation pattern that looks like a toroid-like or 'donut-shaped' pattern.

The half-wave dipole does not have a uniform current distribution over its length. At resonance, it is a half sine wave. The bottom line is that the dipole radiation is at maximum in the broadside direction, and essentially goes to zero in the direction of the poles.

2.2.2 Coupling Mechanisms

The coupling mechanisms of different classes of tags are important when it comes to the operation characteristics such as reading distance and operating power. The coupling mechanisms related to RFID tags can be divided into two categories namely**, near-field coupling** (inductive coupling) and **far-field coupling** (modulated back-scattering). This section will discuss these types of coupling mechanisms.

Near field coupling: This is the three dimensional space immediately surrounding the antenna. Low frequency (LF), High frequency (HF) tags and Near Field Communication (NFC) tags use this type of coupling mechanism. The antenna used for this type of coupling is referred to as a 'transformer' [15] and has an 'inductive coil' shape. Since the reading distance is limited to a few centimeters the typical applications for this type of coupling include, animal tagging, proximity cards, contactless payments, etc. The inductive coupling operation between the reader and the tag/transponder is shown in the figure 2.9.

Far-field coupling: This is the three-dimensional space beyond the near field and encompasses the reader as well as the tag. The electromagnetic energy is radiated in a radial manner in the far field with the power dropping off with increasing distance. The EM energy radiated by the reader's antenna is reflected or absorbed by the tag's antenna based on the tag antenna's radar cross section (RCS). The tag's IC switches between a load and open/short circuit and thus is able to control the reflected EM wave. The reflected EM wave is picked up by the reader's antenna, is amplified and decoded to extracts the sent data. This type of coupling is used in ultra high frequency (UHF) tags and microwave tags. Since the

reading distance is several meters (20 meters, [19]) the typical applications for this type of coupling include, supply chain processes, pharmaceutical, healthcare, etc. The modulated backscatter operation between the reader and the tag/transponder is shown in the figure 2.10.

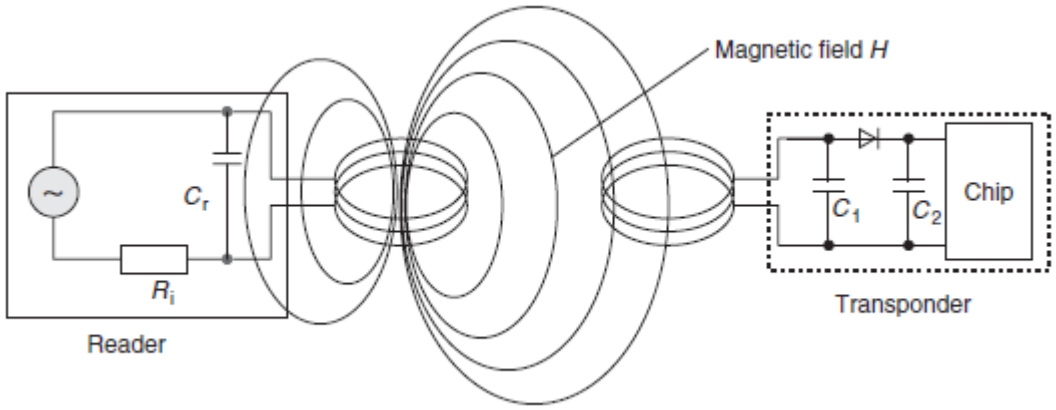

Figure 2.9 Power supply to an inductively coupled tag from magnetic alternating field generated by the reader [11]

2.3 Chapter Summary

In this chapter we discussed the history and the fundamentals of RFID technology (RFID tags, tag antenna theory, coupling mechanisms, etc). The different classes of RFID tags based on their criteria such as power, protocols, frequency of operation were discussed. In the second part, antenna theory fundamentals and tag-reader coupling mechanisms (communication links) were mentioned briefly. The chapter aims to give its reader an overall view of the RFID technology with emphasis on RFID tags.

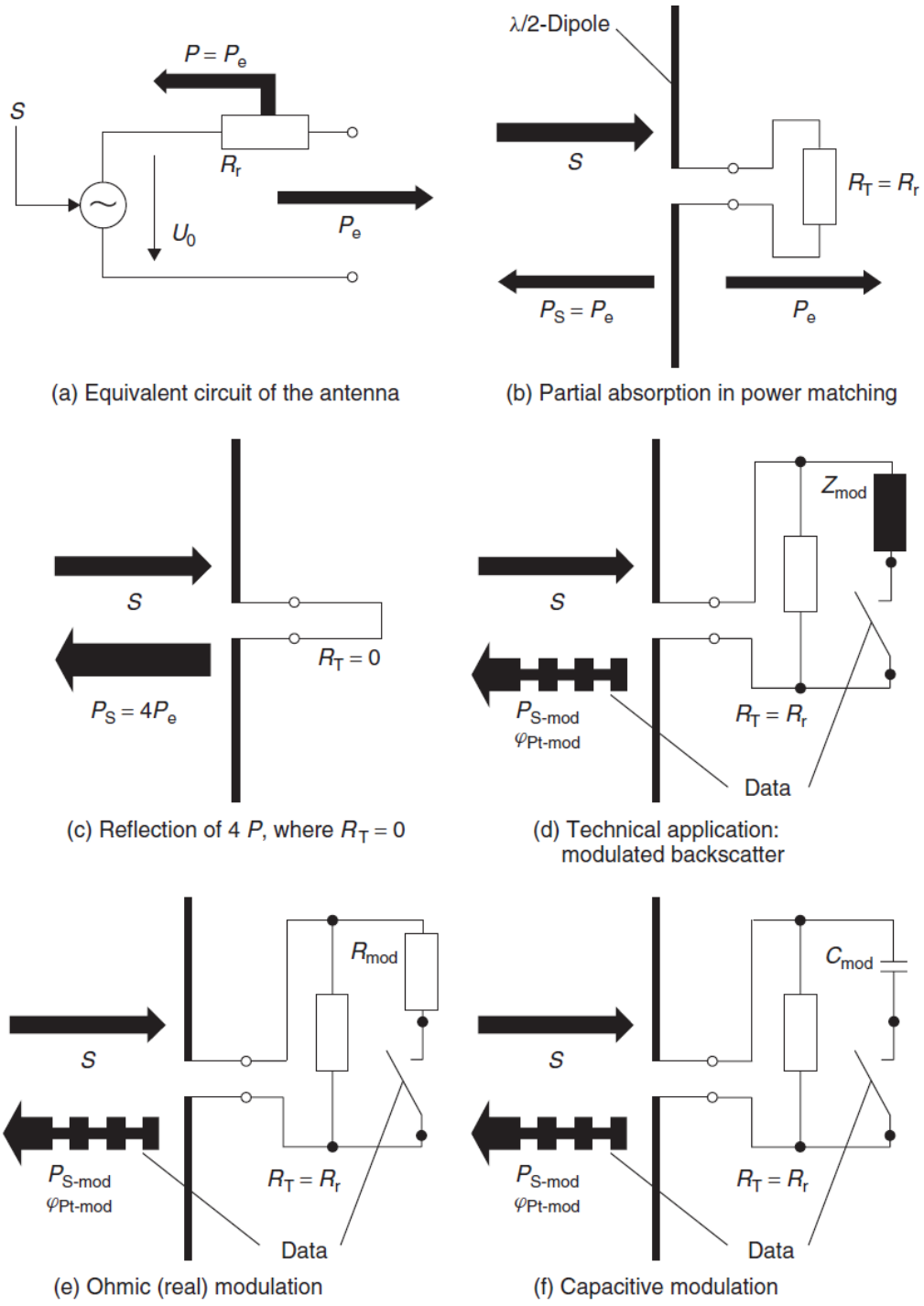

Figure 2.10 Modulated backscatter by modulation of the transponder impedance Z_T (=R_T) [19]

CHAPTER 3 – RFID tag antenna design requirements and testing procedures

The design requirements for a passive RFID tag antenna have been extensively investigated [4]-[6], [10] and [21]. The first step involves understanding tag performance criteria such as increased read-range, orientation sensitivity, reduced environmental impacts (humidity, metals) etc. Secondly, the passive RFID design process as suggested by [5] should be addressed which includes antenna-chip impedance matching and read range measurement. Finally, the tag antenna impedance itself (excluding the chip) needs to be tested using the measurement setup as proposed by [21].

In this chapter we will discuss the RFID tag antenna design requirements and the test procedures. It comprises of three parts; the first part introduces different tag performance criteria. The second part highlights the design process which includes optimization, analysis and prototype construction. The last section deals with the testing procedures that include antenna measurement setup (vector network analyzer) and reading-range setup (anechoic chamber).

3.1 Tag Performance Criteria

Although there are many different tag performance criteria such as tag orientation sensitivity, chip sensitivity, frequency of operation, etc. the most important one is read range. The tag read range is defined as the maximum distance at which the RFID reader can detect the RFID tag. The reader has a higher sensitivity than the tag and as a result the read range can be considered as the tag response threshold. Furthermore, the read range is also dependant on other factors such as tag orientation and environmental losses [5]. The read range is calculated using the Friis free-space equation (6) shown below [5].

$$r_{max} = \frac{\lambda}{4\pi}\sqrt{\frac{P_t G_t G_r \tau}{P_{th}}} \quad (6)$$

In equation (6), λ is the wavelength, P_t is the power transmitted by the reader, G_t is the gain of the transmitting antenna, G_r is the gain of the tag antenna, P_{th} is the minimum threshold power necessary to turn on the chip and τ is the power transmission coefficient.

It is given by

$$\tau = \frac{4R_cR_a}{|Z_c + Z_a|^2}, \quad 0 \leq \tau \leq 1 \ (7)$$

In the equation (7) above, Z_c represents the chip impedance ($R_c - jX_c$) and Z_a represents the antenna impedance ($R_a + jX_a$) (Figure 3.1). In addition, when $\tau = 1$, maximum power is transferred and the antenna is said to be perfectly matched to the chip impedance at a particular frequency. However, if $\tau = 0$ then, the antenna is not matched to chip impedance at all. Typically for RFID tags, impedance matching deteriorates when $\tau < 0.5$ [23]. In addition, good impedance matching for RFID tags is considered only when $\tau > 0.8$ [5].

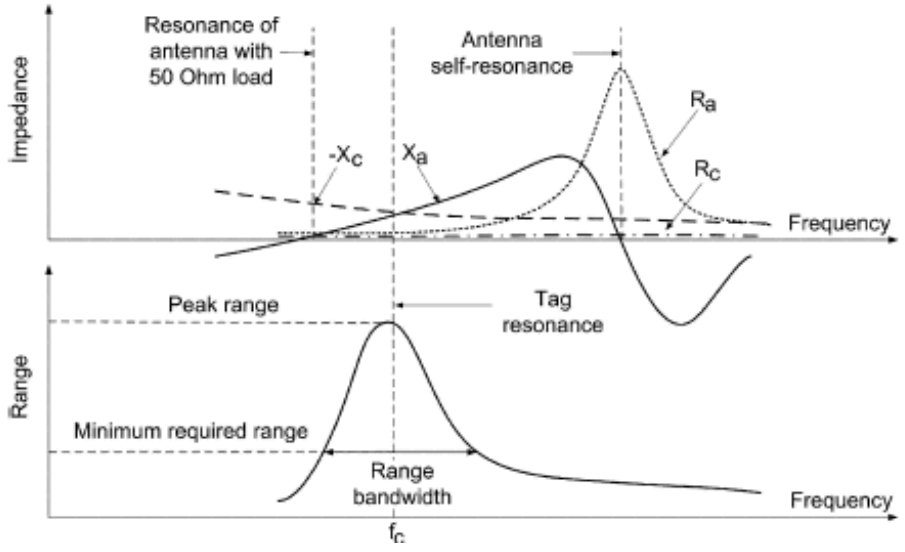

Figure 3.1 Antenna impedance, chip impedance and read range as functions of frequency for a typical RFID tag [5].

The figure 3.1 illustrates the qualitative behavior of the antenna impedance, chip impedance and the read range for a typical RFID tag at a given frequency. The frequency of peak range is defined as the tag resonance. In addition, the range bandwidth shown in figure 3.1 is defined as the frequency band in which the tag offers acceptable minimum read range. From (6) we conclude that τ is frequency dependant and determines the tag resonance.

Another important concept as indicated in figure 3.2 is the tag performance chart [5]. This chart helps the designer to estimate the range tradeoff between the impedance matching and the gain. Basically, the range in (6) is normalized by a factor r_0 as shown in (8). This factor is the range of the tag with 0 dBi antenna perfectly matched ($\tau = 1$) to the chip impedance at a fixed frequency.

$$r_0 = \frac{\lambda}{4\pi}\sqrt{\frac{P_t G_t}{P_{th}}} \quad (8)$$

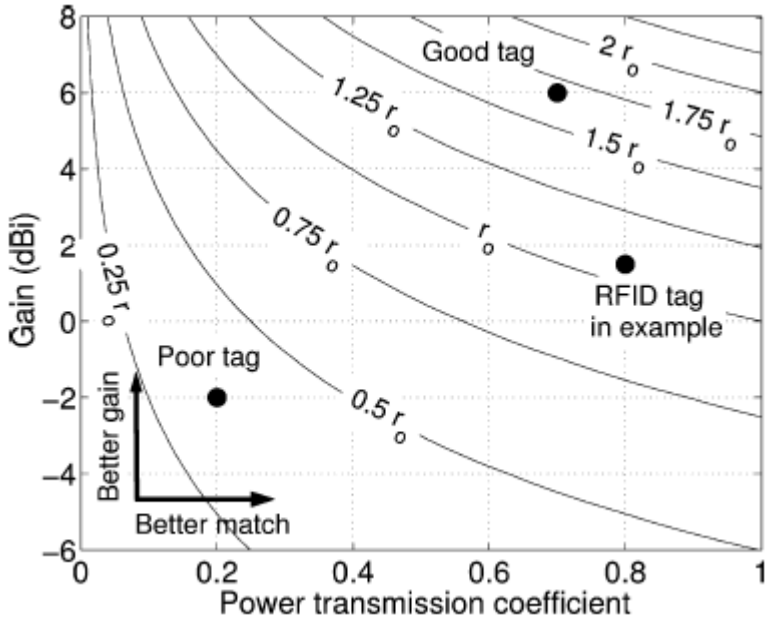

Figure 3.2 Tag performance chart: contours of the constant normalized range in the gain-transmission coefficient plane [5].

The antenna designer realizes that the design process involves tradeoffs between antenna gain, impedance and bandwidth. The figure 3.2 is one such tool that the antenna designer can use to determine the requirements for a 'good tag' based on the read range.

Other important tag performance criteria such as chip sensitivity, orientation sensitivity, etc. are mentioned below.

Chip Sensitivity: Chip sensitivity threshold (P_{th}) is an important tag limitation. It is the minimum received RF power to turn on the RFID chip. The lower it is, the longer the distance at which the tag can be detected. Chip sensitivity is usually determined in the RF front end architecture and fabrication process [4].

Orientation Sensitivity: The EM waves radiated from the antenna have an electric and magnetic field that are perpendicular to each other. Based on the orientation of the electric field, the polarization of the antenna may be linear or circular. In the RFID context, readers are typically circularly polarized whereas tags are linearly polarized. This polarization mismatch causes only half the power to be received by the tag antenna, a 3dB loss.

Environmental Limitations: The antenna designed for an RFID chip using computer simulations, or even through measurements may work very well in theory. However, in practice, there are several environmental factors that degrade the tag performance. Environmental issues that will degrade tag performance like placing the tag near a plastic bin, on a cardboard box, on a bottle of water, or even near metals are hard to assess. Typical ways to mitigate these effects are placing foam separators between the tag and the environment (water, metal, etc) [10].

3.2 Tag Design Process

In this section the RFID tag antenna design process will be mentioned briefly. The overall chain of steps to follow in the successful realization of the RFID tag is illustrated in figure 3.3 which is self-explanatory. However, each section from the figure 3.3 will be briefly addressed for clarity.

1. **Select application and define tag requirements**: this is perhaps the most important step. The designer needs to determine beforehand several tag requirements such as frequency band (915 MHz or 868 MHz), tag size, maximum read range, operation environment (metals, water, etc), orientation (polarization of tag), costs (printed ink,

copper, silver) etc. After the designer has taken into account most of these requirements based on the application then, it is safe to move to the next step.

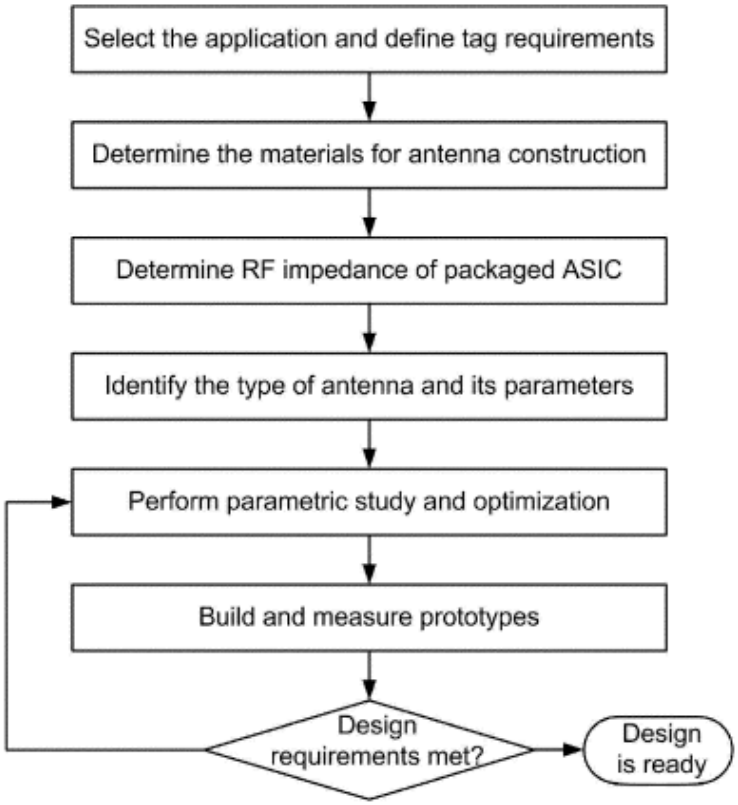

Figure 3.3 RFID tag antenna design process [5].

2. **Select materials for antenna construction**: This process is directly related to the overall cost of the tag. The designer must take into account the material used for the antenna (copper, silver, etc.) as well as the substrate (PVC, FR-4, etc.) in order to ensure that the overall tag production cost (from a manufacturer's perspective) is minimal. Furthermore, the physical properties of the materials (environmental effects) should be investigated by the designer. For example, the substrate might not withstand harsh environments (airport baggage tags) where the tag is under constant physical impact with other bags and the conveyer belts.
3. **Determine the RF impedance of the packaged ASIC**: this step is relatively easy because the chip provided by the chip manufacturers (NXP semiconductors, Texas

instruments, etc) usually come with the datasheet which includes chip impedance values. The designer in most cases trusts this chip impedance value because to measure the exact chip impedance requires further measurement setups and increases the overall cost.

4. **Identify the type of antenna and its parameters:** this step is important because there is a range of antenna shapes and sizes that designers use for RFID tags such as meandered dipole, folded dipole, capacitive-tip loaded dipole, inverted-F … [7], [24]-[26]. Thus, the designer needs to know how the antenna shapes effect the overall tag performance.
5. **Perform parametric study and optimization:** this step usually involves analyzing the tag antennas with electromagnetic (EM) modeling and simulation tools such as method of moments (MoM), finite-element method (FEM) or finite-difference time-domain (FDTD) method. Fast EM analysis tools such as Ansoft HFSS are very important for efficient tag design. For example, the geometrical parameters (height, width) of a meandered dipole antenna designed using HFSS can be investigated to see how incremental changes effect tag performance (impedance, frequency, etc).
6. **Build and measure prototypes**: this is last stage in the design process. The antennas fabricated based on simulation results need to be verified for impedance matching using a vector network analyzer and read range measurement in an anechoic chamber. If the results are in close agreement with the simulation results then, the design is ready. Otherwise, the designer needs to go back to step 5 and modify the simulation setup.

3.3 Tag Testing Procedures

The testing procedures for fabricated RFID tags are mentioned in this section. These testing procedures include 1) read range and 2) impedance measurement as mentioned below.

Read range: range measurement for RFID tags is usually carried out in a controlled environment such as an anechoic chamber as shown in Figure 3.4 [5]. The tag is placed at a fixed distance from the reader. At each frequency, the minimum power P_{min}, needed to communicate with the tag is recorded. Since the loss L of the connecting coaxial cable, the

gain of the transmitting antenna G_t, the distance d to the tag are known, the tag range for any transmitter EIRP (effective isolated radiated power) can be determined from (9).

$$r_0 = d\sqrt{\frac{EIRP}{P_{min}LG_t}} \quad (9)$$

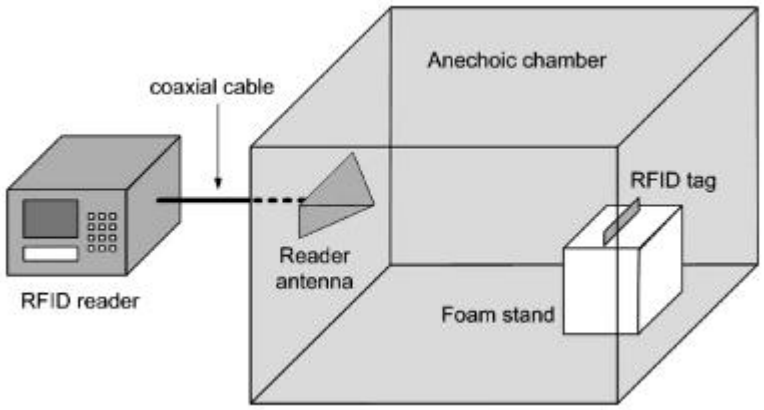

Figure 3.4 RFID tag range measurement using anechoic chamber [5].

Some other general guidelines for selecting tag position using the anechoic chamber setup [5] are listed below.

1. The distance must be such that the tag will respond in the far-field region.
2. The tag must be placed in the quiet zone of the chamber where multipath is minimal.

Impedance measurement: most RFID tags are balanced dipoles [22] and this makes it harder to measure the electrically small antennas directly using a vector network analyzer (VNA). To overcome this problem as suggested by [22], only half of the antenna structure is placed on a metal plate as shown in Figure 3.5 and Figure 3.6.

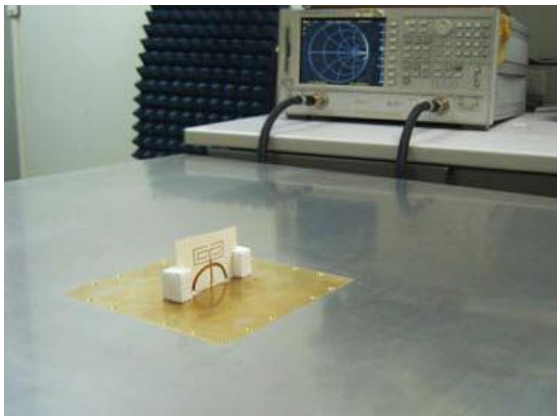

Figure 3.5 measurement setup [23].

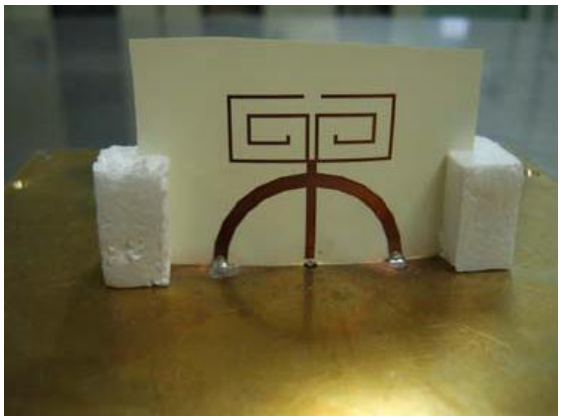

Figure 3.6 Half-antenna mounted on plate [23].

The impedance amounts to only half the impedance overall RFID tag because a mirror image produced by the ground plane as shown in Figure 3.7 [10]. The metal plate is composed of stainless steel part (1m x 1m) and brass sheet (16cm x 16cm). The cable of the VNA is hidden underneath the metal plate. The feeding point of the antenna is soldered to a central pin of the SMA connector. In this way the VNA is used to measure the antenna impedance of half the antenna.

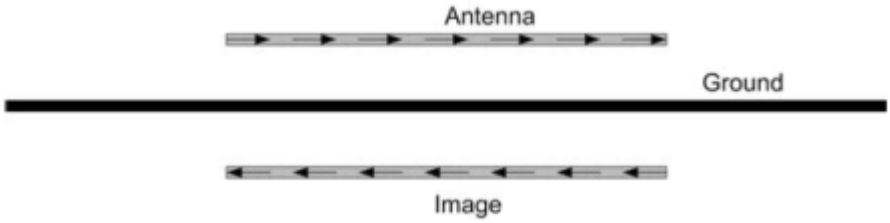

Figure 3.7 Tag operating above a ground plane with the mirror image beneath it [10].

3.4 Chapter Summary

In this chapter RFID tag antenna design requirements and test procedures were discussed. Firstly, tag performance criteria were explored to highlight the concept of impedance matching, chip sensitivity, orientation sensitivity, etc. In the second part, the RFID antenna design process which includes optimization, analysis and prototype construction was

discussed. Finally, the testing procedures for read range and impedance were explored. The RFID tag antenna design process is not a simple process because it requires extensive knowledge of antenna theory as well as the results published by other researchers [4], [7], and [10].

Chapter 4 - Conjugate Impedance Matching Techniques

This chapter presents different design methodologies of UHF (915 MHz) RFID passive tag elements. As already mentioned, passive tags require RF energy supplied by the reader's antenna to power the microchip. Passive ICs are generally highly capacitive because of the necessary power required to bias the IC which is drawn through electromagnetic coupling [3]. As a result, the antennas designed should exhibit a low resistance value and a high inductance value to match the input impedance of the tag IC. Note the impedance value of the IC corresponds to the 'turn-on' impedance of the IC. These values are provided by the IC manufacturer.

The HFSS design tool [27], based on Finite Element Method (FEM), is used to analyze and optimize the antenna design. The FEM is a numerical technique used to solve Boundary Value Problems (BVP's) governed by a differential equation and a set of boundary conditions [28]. In this chapter, T-Match (165mm x 20mm), inductively coupled loop (165mm x 35mm) and nested-slot (163mm x 163mm) antennas were designed to achieve maximum read range.

4.1 T-Match

The equivalent circuit of a T-match structure is shown in Figure 4.1. The input impedance of a planar dipole of length *l* can be changed by using a short circuit stub as explained in detail in section 9.7.3 of [19]. The antenna source is connected to the second dipole of length a< *l* and placed at a distance b from the larger dipole. The electric current distributes along the two radiators according to the size.

The input impedance seen by the source is expressed in equation (10) below taken from [7].

$$\boldsymbol{Z_{in}} = \frac{\boldsymbol{2Z_t(1+\alpha)^2 Z_A}}{\boldsymbol{2Z_t + (1+\alpha)^2 Z_A}} \quad (10)$$

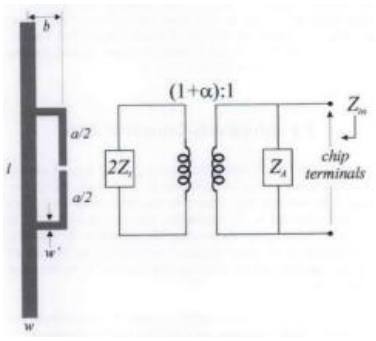

Figure 4.1 T-match of the planar dipole with its equivalent circuit [7].

Z_A- is the dipole impedance taken in the centre in the absence of a T-match connection. Z_t, is the impedance of the short circuit stub and Z_o is the characteristic impedance of the two-conductor transmission line with spacing b. They are given by the following relations.

$$\boldsymbol{Z_t = jZ_0 \tan ka/2} \quad (11)$$

$$\boldsymbol{Z_0 \cong 276\, log_{10}\left(\frac{b}{\sqrt{r_e r`_e}}\right)} \quad (12)$$

$\boldsymbol{r_e}$=0.25w and $\boldsymbol{r`_e}$=8.25w' are the equivalent radii of the dipole and the matching stub, respectively. $\alpha = \ln(b/r_e')/\ln(b/r_e)$ is the current division factor between the two conductors. The geometrical parameters a, b and w' can be adjusted in order to match the complex chip impedance Z_{chip}.

For half-wavelength dipoles, the T-match port is inductive and for smaller wavelength dipoles this impedance can be both inductive and capacitive. Figure 4.2 [7] shows a matching chart for the T-match layout where the ratio between the dipole's cross section is fixed to w/w'=3. The parameters a and b both influence the resistance and the reactance values. Generally, high resistance values are found while using the classic T-match as shown in Figure 4.1.2. Further degrees of freedom may be needed to overcome this problem. For example, we may use multiple T-matches in a layout or use an embedded T-match feed as shown in figure 4.3.

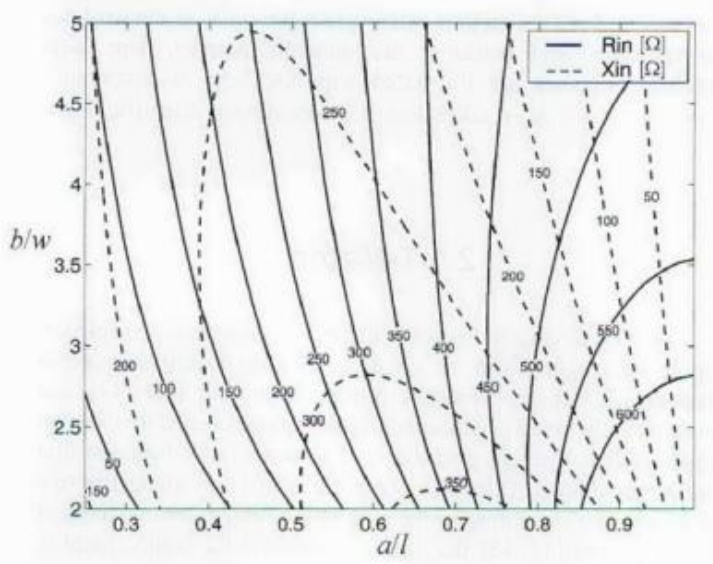

Figure 4.2 Matching chart for the T-match layout. $l = \lambda/2$, w= $\lambda/100$, w'=w/3, and $Z_A = 75\Omega$ [7].

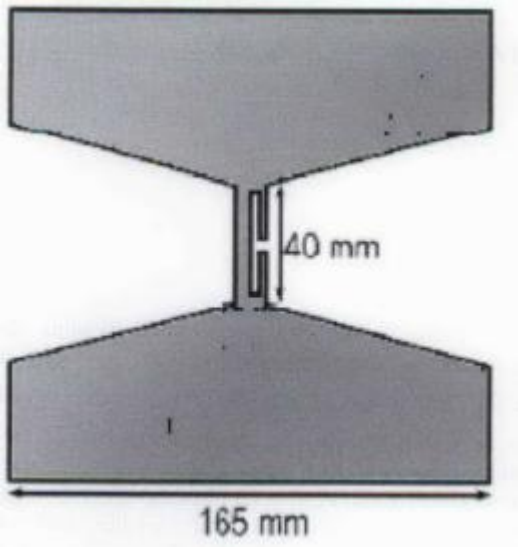

Figure 4.3 Example of an embedded T-match feed as proposed in [7].

4.2 Inductively Coupled Loop

As shown in figure 4.4, the radiating dipole is placed in an inductively coupled small loop, placed close to the main conductor. The terminals of the loop are directly connected to the microchip. This arrangement adds equivalent inductance in the antenna. The reactance is controlled by varying the distance of the loop from the main conductor.

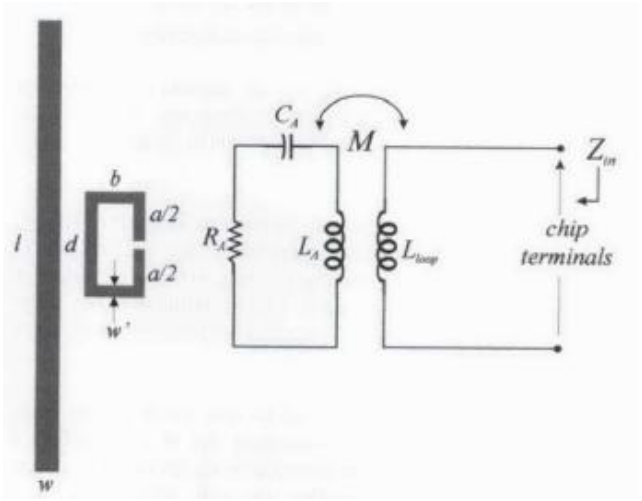

Figure 4.4 Inductively coupled feed with its equivalent circuit [32]

The inductive coupling can be modeled by a transformer. The resulting impedance seen from the loop's terminals is given by [7].

$$\boldsymbol{Z_{in} = Z_{loop} + \frac{(2\pi f M)^2}{Z_A}} \quad (13)$$

In the above equation $Z_{loop} = j2\pi f L_{loop}$ is the loop's input impedance. Whether the dipole is at resonance or not, the total input impedance depends on the loop inductance, L_{loop}. The resistance is related to the transformer mutual inductance M as shown below [7].

$$\boldsymbol{R_{in}(f_0) = \frac{(2\pi f_0 M)^2}{R_A(f_0)}} \quad (14)$$

$$\boldsymbol{X_{in}(f_0) = \left(2\pi f_0 L_{loop}\right)} \quad (15)$$

In equations 14 and 15, R_A represents the antenna's resistive impedance, f_0 is the resonant frequency, M is the mutual inductance of the transformer and L_{loop} is the inductance of the loop. The total input resistance is dependent on the loop's shape and the dipole-loop distance. Figure 4.5 shows the loop-driven dipole for a square loop (a = b). Input reactance is unaffected by loop distance (*d*). For a fixed loop, the resistance reduces as the value of *d*

increases. Therefore, for design purposes, the loop size can first be setup to match the chip's reactance. After the reactance is set, the loop-dipole distance can be adjusted to control the resistance.

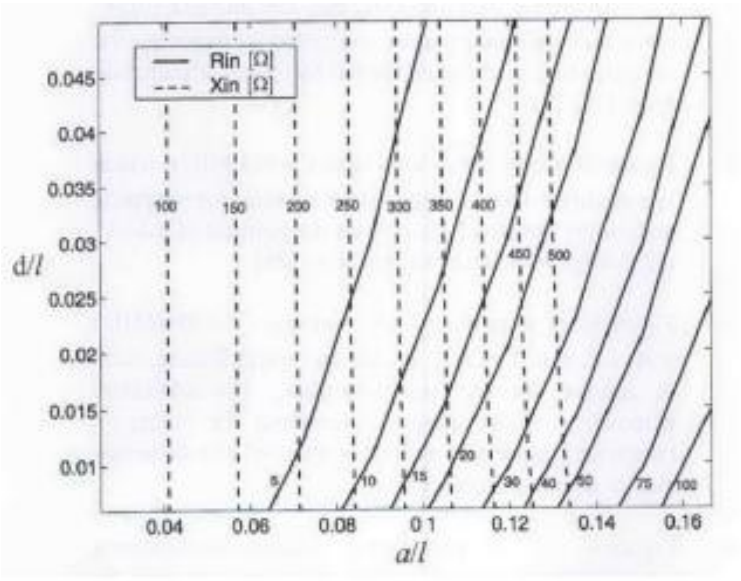

Figure 4.5 Matching chart for the loop-fed dipole. $l = \lambda/2$, w= λ/100, w'=w/3 and a=b (square loop) [7].

4.3 Nested Slot

This is a matching strategy useful for tags with large planar dipoles or suspended patches as shown in Figure 4.6 [31]. The non-resonant slot has an inductive reactance, and this makes it possible for complex impedance matching even when the tag is attached to a high permittivity substrate as shown in Figure 4.8 [22]. The slot-line can be considered as impedance transformer, where each discontinuity (tooth) provides energy for storage and radiation. Increasing the number of teeth can help us miniaturize the design and achieve multi-band features [32].

Maximum antenna gain is fixed by the patch length, *l*, and the impedance tuning can be achieved by changing the slot dimensions a and b. Varying the shape and size of the internal slot may cause the antenna to act as an H-slot, a broadband dipole or a doubly folded dipole.

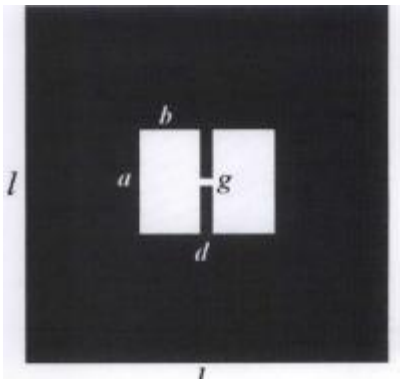

Figure 4.6 Geometry of a nested-slot suspended patch [31], [22]

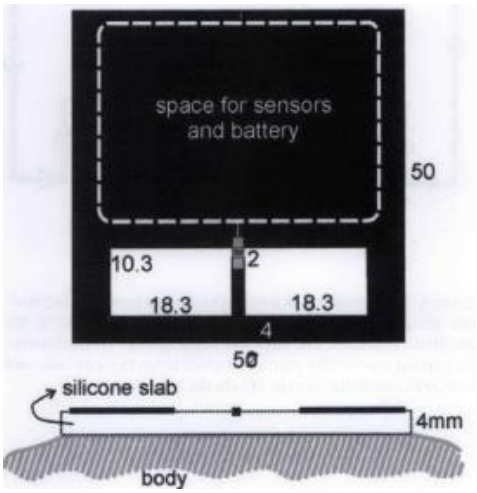

Figure 4.7 A tag attached to the human body with space for fitting sensors [31]

When *b* is much smaller than *l*, RLC behavior is observed, with high reactance. When *b* is very close to *l*, then the reactance is reduced significantly. As observed by [31] the resistance is mainly sensitive to the parameter *b*, while the reactance tends to change almost linearly with the simultaneous change in both *a* and *b*. A matching chart for the nested-slot layout for figure 4.3.3 is shown below.

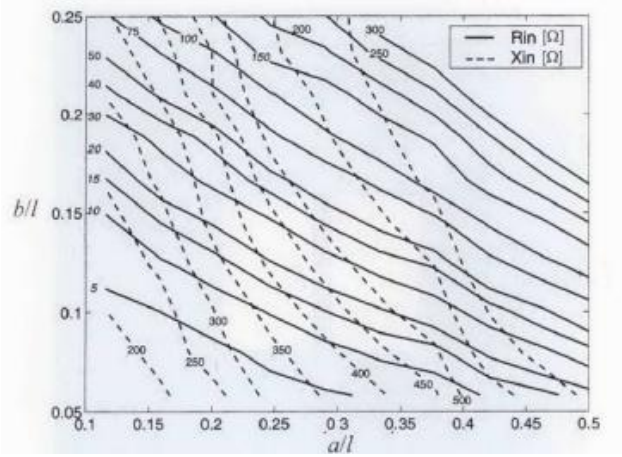

Figure 4.8 Matching chart for the nested-slot matching layout. $l = \lambda/2$, d = g = $\lambda/150$ [7]

4.4 HFSS Modified T-Match Simulation

4.4.1 T-Match Antenna Design

The antenna is made of copper metal with thickness, 0.02 mm. The substrate is made of polyester with thickness, 0.1 mm (with $\varepsilon_r = 3.2$ and loss tangent $\delta = 0.003$). Its dimensions are width = 16.5 mm and length = 180 mm. The geometrical parameters of the antenna as shown in Figure 4.4.1 are as follows:

l = 163 mm
a = 15 mm
b = 8 mm
w = 3mm
w' = 1 mm
Port separation = 2 mm

The IC impedance used for this design at 915 MHz is equal to 12 – j140 Ω (Alien-Higgs). That means that the load antenna impedance should be 12 + j140 Ω for maximum power transfer (conjugate matching).

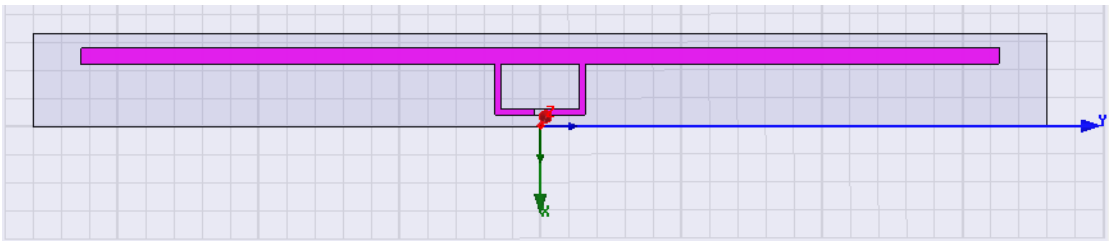

Figure 4.9 T-Match RFID antenna design layout.

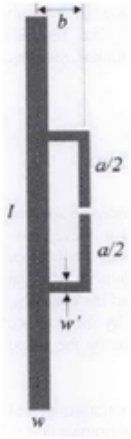

Figure 4.10 T-Match configuration for planar dipoles [7].

4.4.2 T-Match Simulation Results

The results on the following page show the HFSS simulations results for the return loss and the impedance.

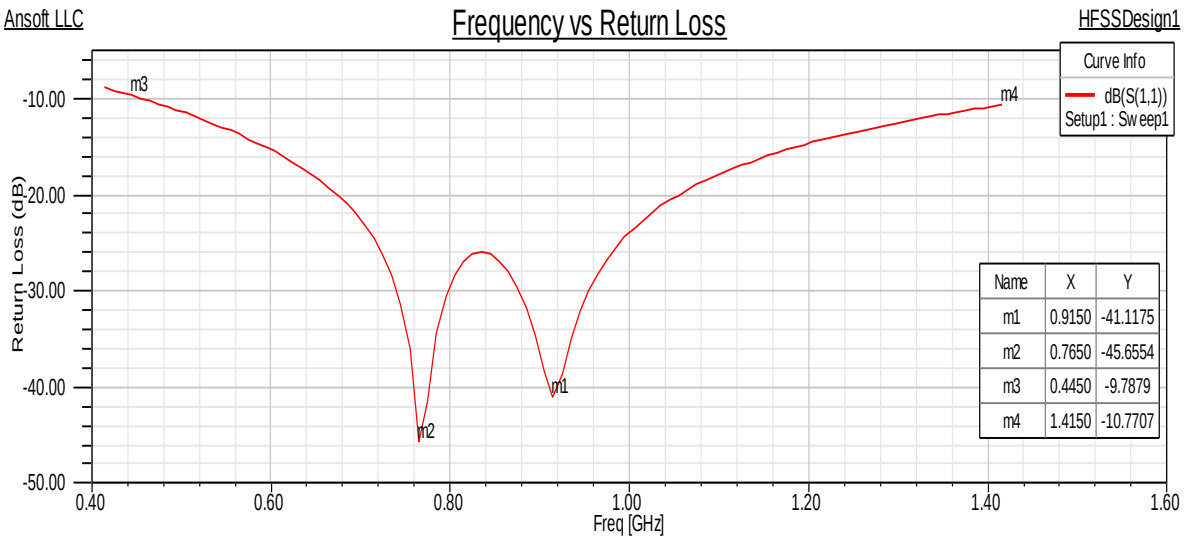

Figure 4.11 Simulation results showing the return loss of the antenna.

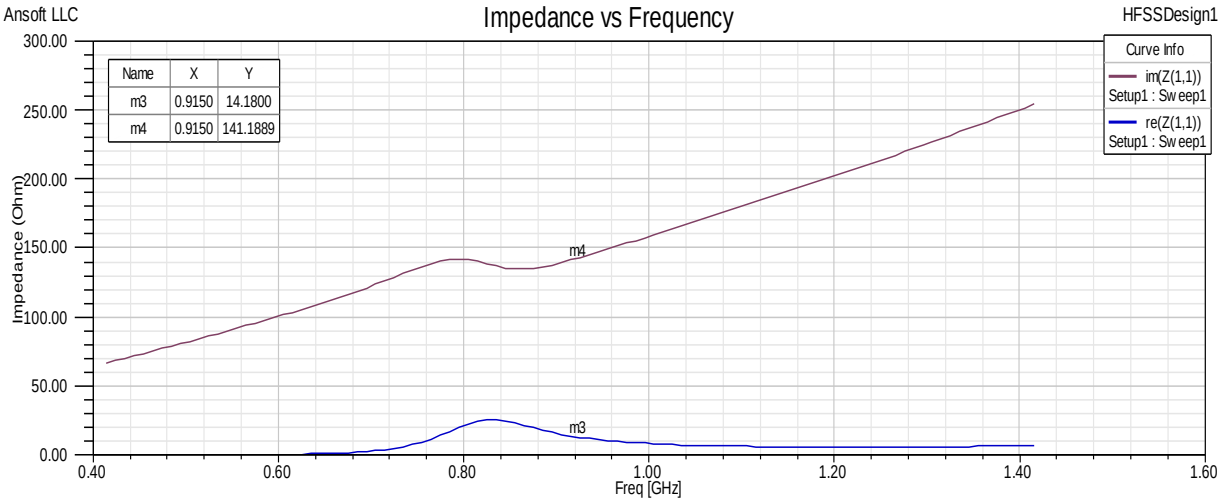

Figure 4.12 Simulated antenna input impedance with respect to frequency.

As seen from Figure 4.11 the antenna has a bandwidth of 97 MHz at a return loss (RL) > 10dB which covers the worldwide RFID UHF band. As seen from Figure 4.12 the simulated resistance and reactance at the required frequency (915MHz) is 14.18 + j141.19 respectively. This is very close to the impedance of 12 + j140 Ω required for conjugate matching.

$$r_{max} = \frac{\lambda}{4\pi}\sqrt{\frac{P_t G_t G_r \tau}{P_{th}}} \quad (16)$$

$$\tau = \frac{4R_c R_a}{|Z_c + Z_a|^2}, \qquad and \;\; 0 \leq \tau \leq 1 \quad (17)$$

The radiation patterns for the T match antenna design are shown in Figure 4.13. The omnidirectional radiation pattern of the T match dipole are in the phi=0 (x-z plane) and phi = 90 (y-z plane) plane. The half wave dipole does not have a uniform current distribution over its length. At resonance, it is a half sine wave, i.e. the current is larger in the centre and falls off to zero at ends.

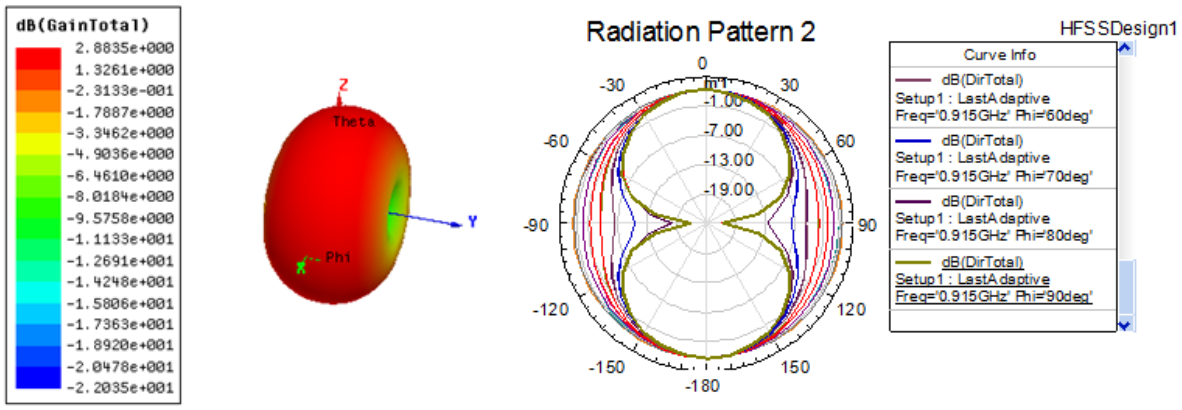

Figure 4.13 Simulated antenna 3-D gain pattern and antenna radiation pattern (Directivity for phi=0 degrees (x-z plane) and phi = 90 degrees (y-z plane))

The resulting field intensity follows a pattern as shown in Figure 4.13 given by [10].

$$\cos\frac{(\frac{\pi}{2}cos\theta)}{\sin\theta} \approx \sin\theta \quad (18)$$

The above approximation of sin θ is good enough for the resulting electric field intensity pattern. The bottom line is that the dipole radiation is at maximum in the broadside direction, and essentially goes to zero in the direction of the poles. In the results obtained for the T-

match, since the antenna is placed horizontally, the radiation intensity is maximum at the broadside direction ((phi=0 degrees (x-z plane) and phi = 90 degrees (y-z plane)) and *nulls* (zero current intensity) at the ends (x-y plane). This makes the RFID tag antenna linearly polarized- horizontal (LHP). Therefore, the reader antenna should either be of the same type of LP (horizontal or vertical) or be circularly polarized (CP) in order to avoid polarization mismatch and provide sufficient power to the tag antenna for communication.

Table 4.1 Simulated Antenna Parameters

Impedance (Ohm)	Return Loss (dB)	Gain (dB)	Directivity (dBi)	Antenna Radiation Efficiency (%)	Theoretical Read Range (m)
14.18 + j141.18	41.12	2.372	2.884	82.2	2.914

The antenna radiation efficiency is given by the formula $G = e_{rad}D$ [19]. Here, G is the gain of the antenna and D is the directivity and e_{rad} is the radiation efficiency. The read range is given by the Friis free-space formula given by [5], equations (16), (17).

The chip to be used is Alien Higgs-2 ($P_{th} = -11\ dBm$). The reader used is Alien ALR 9650 ($P_t = 30db, Gt = 6dBi$), the antenna gain as given above and λ≅ 0.33 m.
Using the equations (16) and (17) from [19], the antenna performance parameters such as Gain, read range were calculated and shown in Table 4.4.

$$r_{max} = \frac{\lambda}{4\pi}\sqrt{\frac{P_t G_t G_r \tau}{P_{th}}} \quad (16)$$

$$\tau = \frac{4R_c R_a}{|Z_c + Z_a|^2}, \qquad and\ \ 0 \le \tau \le 1 \quad (17)$$

4.5 HFSS Inductively Coupled Loop Simulation

4.5.1 Inductively Coupled Loop Antenna Design

The antenna is made of copper metal with thickness, 0.02 mm. The substrate is made of polyester with thickness 0.1 mm (with ε_r = 3.2 and loss tangent δ = 0.003). Its dimensions are width = 31.5 mm and length = 180 mm.

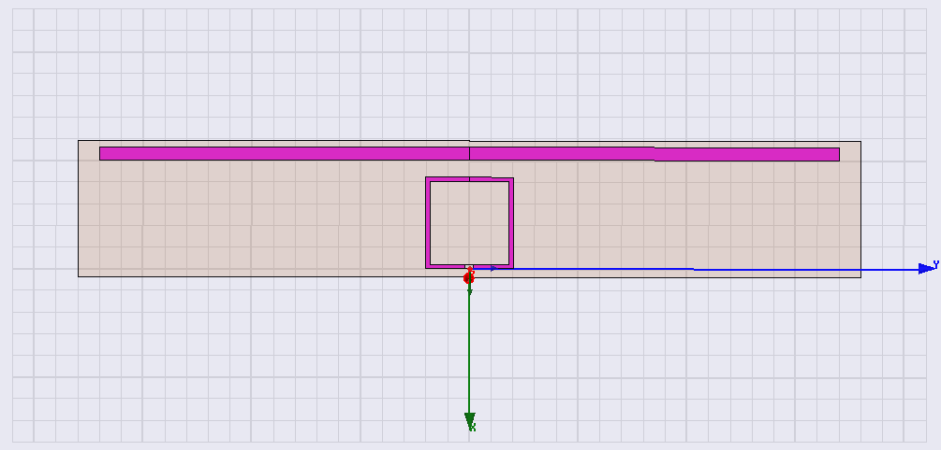

Figure 4.14 Inductively coupled loop RFID antenna design layout.

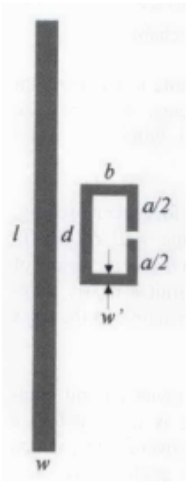

Figure 4.15 Inductively coupled loop configuration for planar dipoles [7].

The geometrical parameters of the antenna as shown in Figure 4.5.1 are as follows:

l = 163 mm

a = 20.1 mm

b = 20.1 mm

d = 3.9 mm

w = 3mm

w' = 1 mm

Port separation = 2 mm

The IC impedance used for this design at 915 MHz has impedance 16 – j350 Ω (Phillips EPC 1.19). That means the load antenna impedance should be 16 + j350 Ω for maximum power transfer (conjugate matching). A different IC was used for the inductively coupled loop design in order to demonstrate the antenna design process can be matched to different ICs instead of just one unique IC.

4.5.2 Inductively Coupled Loop Simulation Results

The results below show the HFSS simulations results for the return loss and the impedance.

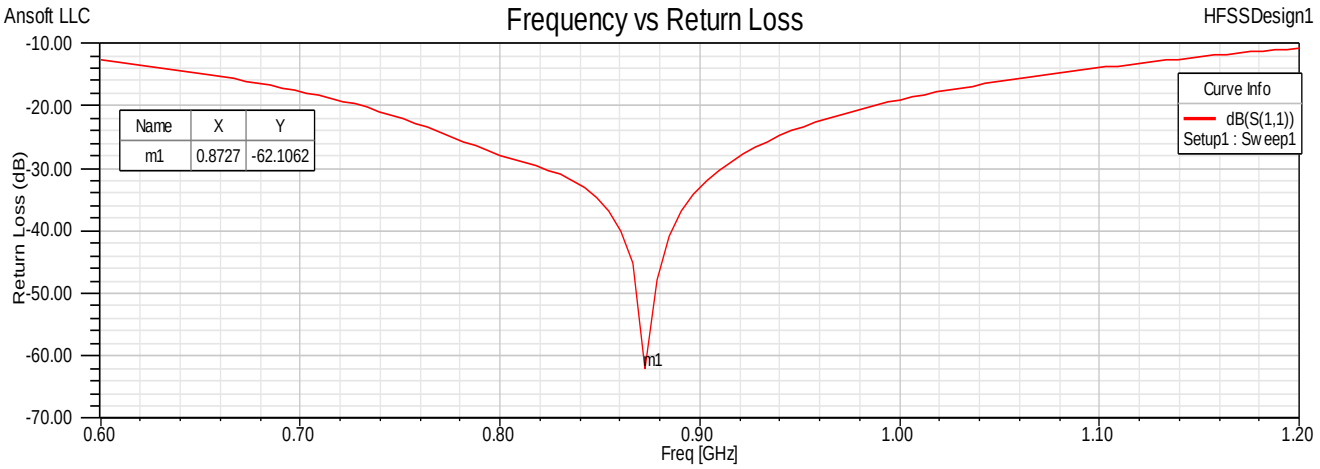

Figure 4.16 Simulation results showing the return loss of the antenna.

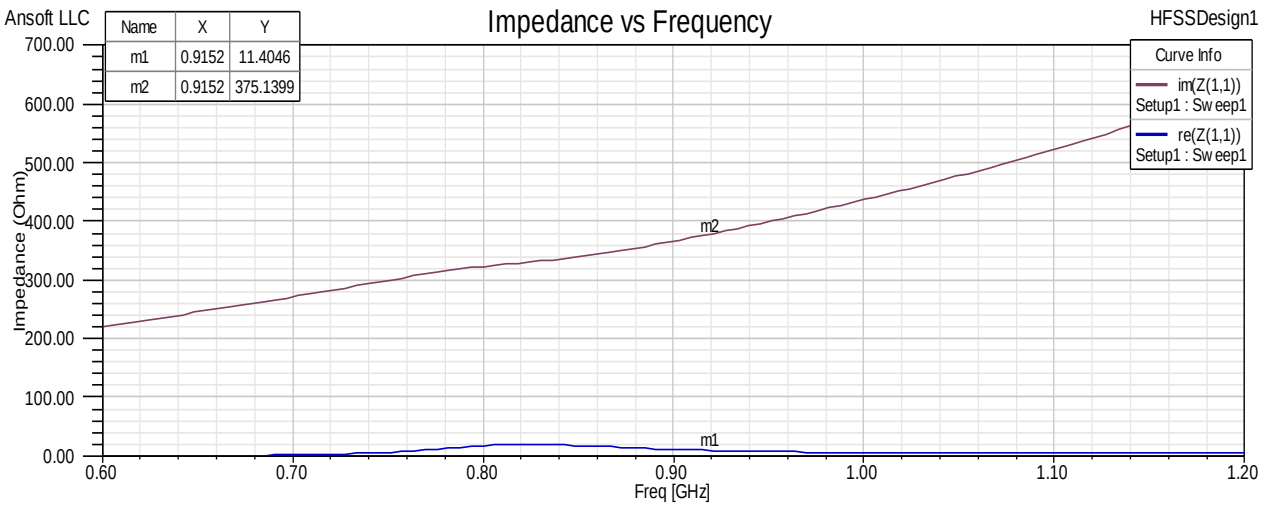

Figure 4.17 Simulated antenna input impedance with respect to frequency.

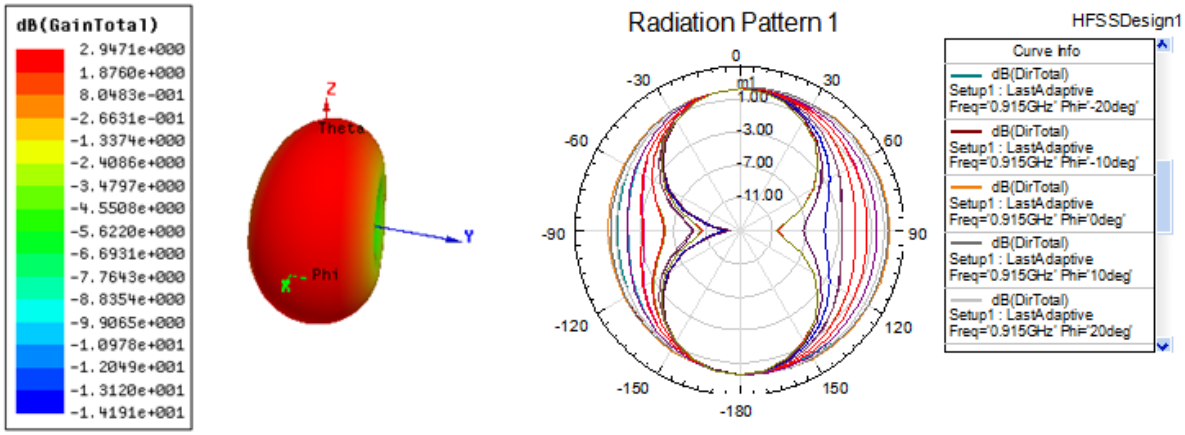

Figure 4.18 Simulated antenna 3-D gain pattern and antenna radiation pattern (Directivity for phi=0 (x-z plane) and phi = 90 (y-z plane))

The radiation patterns for the T match antenna design are shown in Figure 4.5.5. The omnidirectional radiation pattern of the T match dipole are in the phi=0 (x-z plane) and phi = 90 (y-z plane) plane. The half wave dipole does not have a uniform current distribution over its length. At resonance, it is a half sine wave, i.e. the current is larger in the centre and falls off to zero at ends. As mentioned in section 4.4, the dipole antenna is linearly polarized (LP). Therefore, the reader antenna should either be of the same type of LP (horizontal or vertical)

or be circularly polarized (CP) in order to transfer sufficient power to the tag antenna for communication.

Table 4.2 Simulated Antenna Parameters

Impedance (Ohm)	Return Loss (dB)	Gain (dB)	Directivity (dBi)	Antenna Radiation Efficiency (%)	Theoretical Read Range (m)
11.40 + j375.14	62.10	2.350	2.947	79.7	1.56

The antenna radiation efficiency is given by the formula $G = e_{rad}D$ [19]. Here, G is the gain of the antenna and D is the directivity. The read range is given by the Friis free-space formula given above by [5]. The chip to be used is Phillips EPC 1.19 ($P_{th} = -8\ dBm$). The reader used is Alien ALR 9650 ($P_t = 30db, Gt = 6dBi$), the antenna gain as given above and $\lambda \cong 0.33$ m.

4.6 HFSS Nested Slot Simulation

4.6.1 Nested Slot Antenna Design

The antenna is made of copper metal with thickness, 0.02 mm. The substrate is made of polyester with thickness, 0.1 mm (with $\varepsilon_r = 3.2$ and loss tangent $\delta = 0.003$) and its dimensions are width = 31.5 mm and length = 180 mm.

The geometrical parameters of the antenna as shown in Figure 4.6.1 are as follows:

l = 163 mm
a = 45 mm
b = 23 mm
d = 2 mm
g = 2 mm

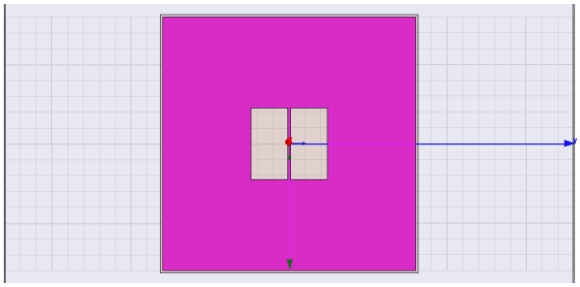

Figure 4.19 The nested-slot RFID antenna design layout.

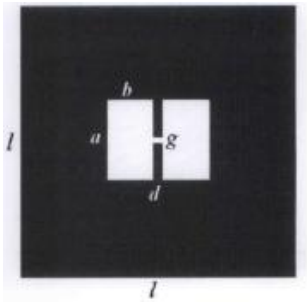

Figure 4.20 The geometry of the nested-slot suspended patch [7]

The IC impedance used for this design at 915 MHz has impedance 16 – j350 Ω (Phillips EPC 1.19). That means the load antenna impedance should be 16 + j350 Ω for maximum power transfer (conjugate matching).

4.6.2 Nested Slot Simulation Results

The results on the following page show the HFSS simulations results for the return loss and the impedance. The radiation patterns for the T match antenna design are shown in Figure 4.23. The omnidirectional radiation pattern of the T match dipole are in the phi=0 (x-z plane) and phi = 90 (y-z plane) plane.

The half wave dipole does not have a uniform current distribution over its length. At resonance, it is a half sine wave, i.e. the current is larger in the centre and falls off to zero at ends. As mentioned in section 4.4, the dipole antenna is linearly polarized (LP). Therefore, the reader antenna should either be of the same type of LP (horizontal or vertical) or be circularly polarized (CP) in order to transfer sufficient power to the tag antenna for communication.

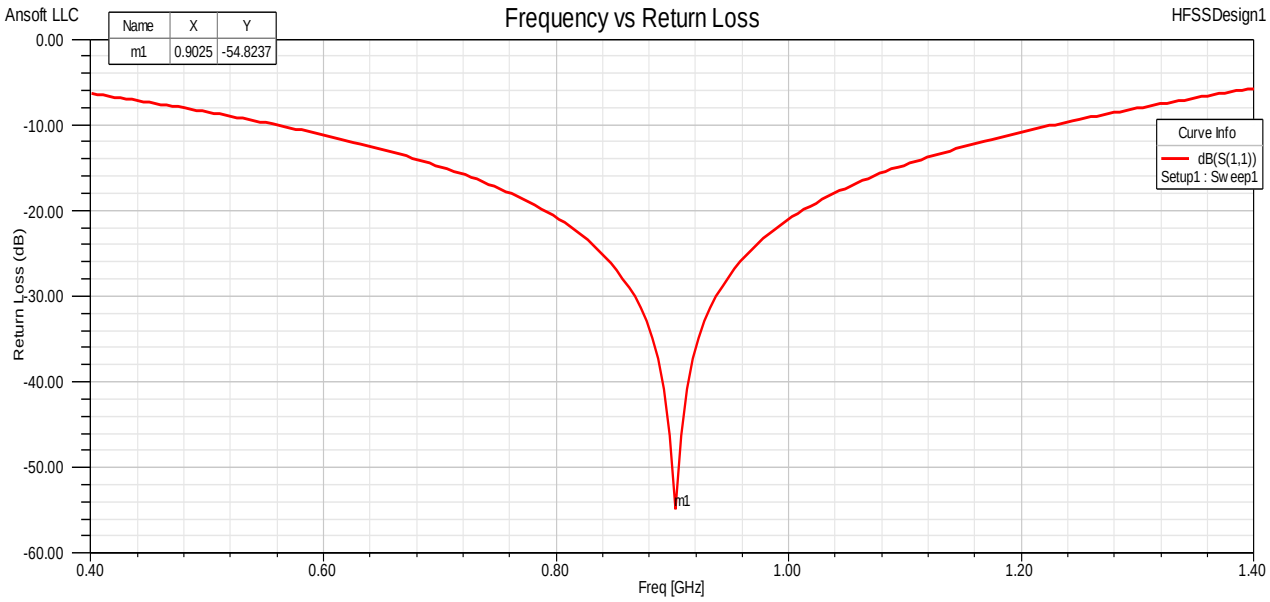

Figure 4.21 Simulation results showing the return loss of the antenna.

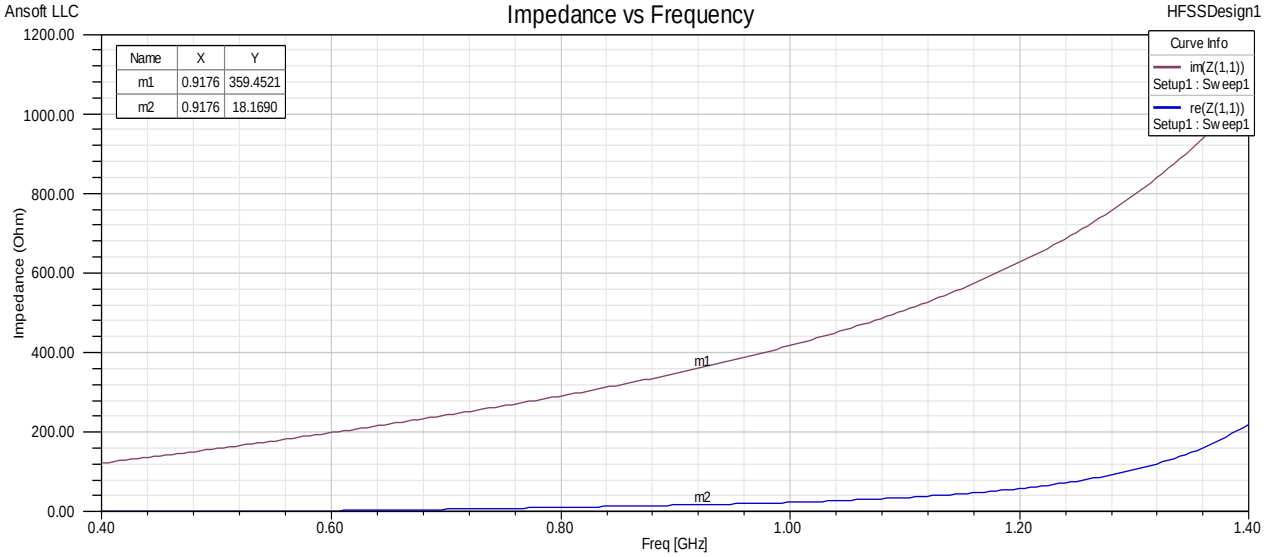

Figure 4.22 Simulated antenna input impedance with respect to frequency.

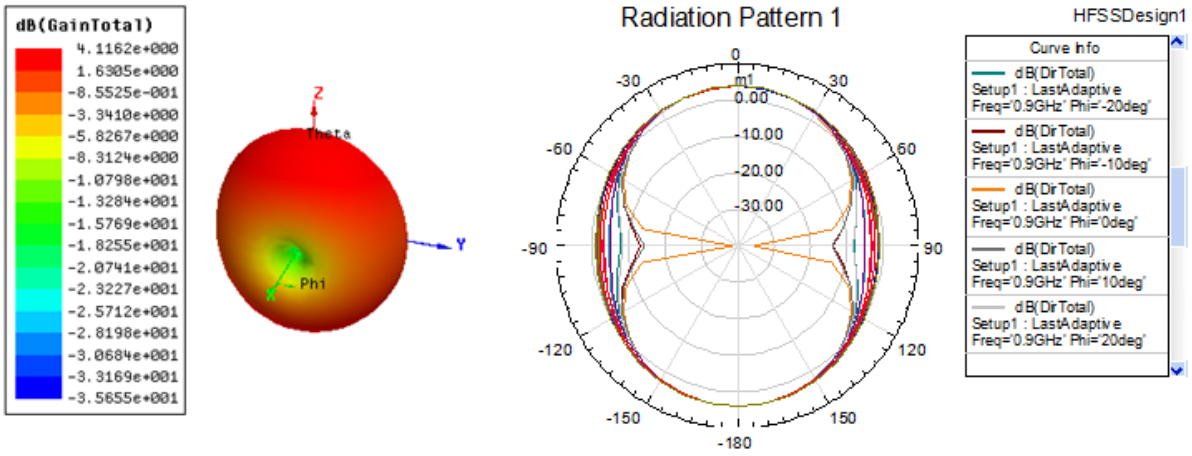

Figure 4.23 Simulated antenna 3-D gain pattern and antenna radiation pattern (Directivity for phi=0 (x-z plane) and phi = 90 (y-z plane))

The antenna radiation efficiency is given by the formula $G = e_{rad}D$ [19]. Here, G is the gain of the antenna and D is the directivity. The read range is given by the Friis free-space formula given by [13]. The chip to be used is Phillips EPC 1.19 ($P_{th} = -8\,dBm$). The reader used is Alien ALR 9650 ($P_t = 30db, Gt = 6dBi$), the antenna gain as given above and $\lambda \cong 0.33$ m.

Table 4.3 Simulated Antenna Parameters

Impedance (Ohm)	Return Loss (dB)	Gain (dB)	Directivity (dBi)	Antenna Radiation Efficiency (%)	Theoretical Read Range (m)
18.17 + j359.45	54.82	3.928	4.116	95.4	2.49

Table 4.6.2 The simulated return loss and impedance value comparison for the above cases shown below

	Return Loss	Simulated Impedance Value	Desired Impedance Value
T-Match	41.118 dB	14.2 + j141.18 Ω	12 + j140 Ω
Inductively Coupled Loop	62.108 dB	11.4 + j375.14 Ω	16 + j350 Ω
Nested Slot	54.803 dB	18.2 + j359.40 Ω	16 + j350 Ω

4.7 Summary

In this chapter we discussed different methodologies for the design of UHF RFID (915 MHz) passive tag elements. These design methodologies include T-match, inductively coupled loop, and nested-slot. All three designs are conjugate matching techniques used to conjugate match the input impedance of the IC. The geometry of the antenna design determines the impedance value of the antennas which generally have low resistance and high inductance. In this chapter, all three designs were simulated using Ansoft HFSS antenna design tool. The simulation results were in close agreement to the desired antenna impedance as seen in Figure 4.6.2. Further optimization of the antenna geometry may improve the conjugate matching. Consequently, the RFID tag antenna will resonate at the required frequency (915 MHz) and improve the most important tag performance requirement 'read range'.

CHAPTER 5 – Classification of commercially available RFID tags

Passive UHF RFID antennas are mainly based on a “printed” dipole configuration [10]. Figure 5.1 shows several commercial tags. As seen in Figure 5.1, the tags have interesting geometries such as long and skinny dipoles, slots, curves and wiggles. The RFID-IC is attached to a loop within the antenna structure. Most of the features are designed for a functional purpose, i.e. they affect the behavior of the antenna to meet a specific design goal.

In this chapter, a literary survey is examined to classify existing passive RFID tags into a family or class based on their application of use. The chapter is divided into three parts; the first part introduces the dipole geometry and radiation resistance. The second part highlights the size reduction techniques such as meandering dipoles and inverted-F configurations. The last section deals with classification of RFID tags into a family based on their application.

5.1 Dipoles

The classic dipole antenna Figure 5.2 consists of two cylindrical wires of equal length placed in a line with an ac source in the middle.

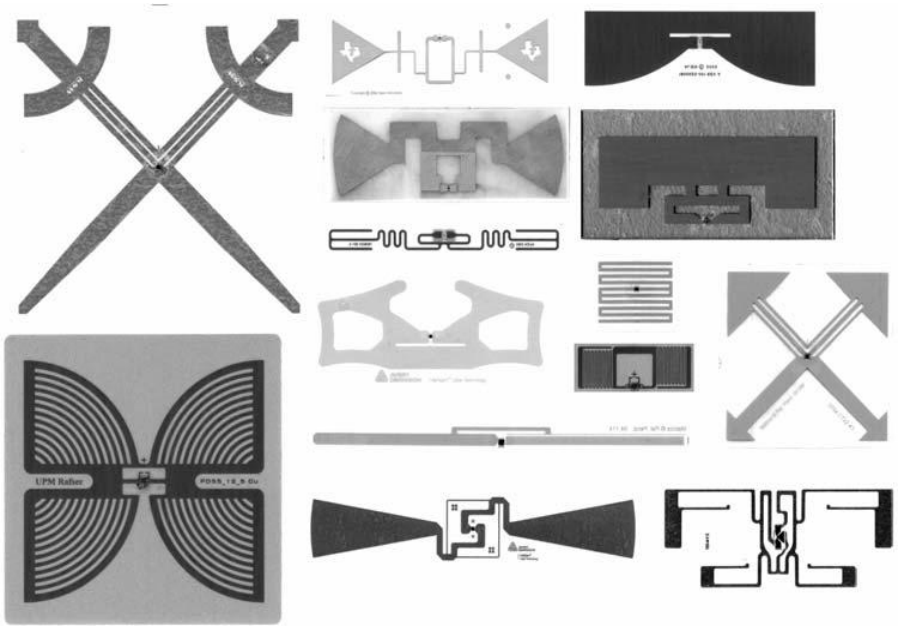

Figure 5.1 Variety of commercially available tags [10].

RFID antennas are not usually made out of cylindrical tubes, but are instead made of "printed" geometry that resembles a dipole. Typically, RFID antennas are printed using conductive silver or metallic inks. Instead of a three dimensional structure of the classic dipole, the RFID antennas are a two dimensional structure where all of the conductive ink or metal resides in one plane.

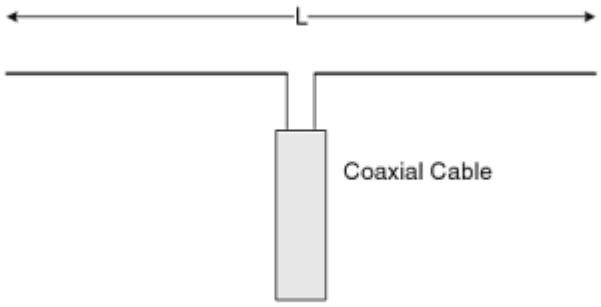

Figure 5.2 Dipole antenna [33].

Predicting the impedance of the dipole antenna is very challenging. However, over a short range of frequencies near resonance, circuit model can to some extent accurately predict the dipole impedance. A series RLC circuit model [10] as shown in Figure 5.3 works very well for the reactance part of the dipole impedance. The model as described by [10] holds reasonably well over short range of frequencies near resonance, 915 MHz (North American RFID standard).

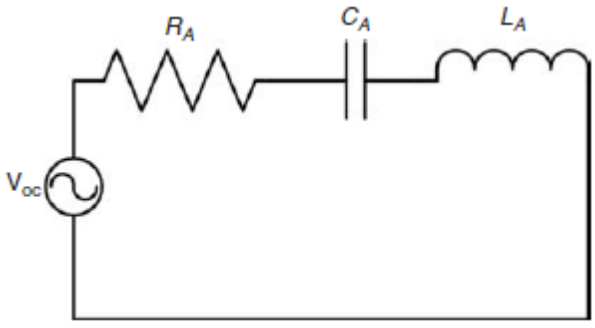

Figure 5.3 Simple circuit model of dipole antenna near resonance [10].

5.1.1 Printed Dipoles

Almost all of RFID antennas are some variant of a printed dipole. The printed dipole is not usually printed using for example an ink-jet printer, but simply means that the antenna is thin and flat, a two dimensional structure. The term ‘printing’ refers to an old printing process used to print a layer of resist before etching the pattern away with some corrosive solution.

So, what is the consequence of using a flat dipole instead of a round dipole? The answer is ‘loss of bandwidth’. As seen in figure 5.4 [10] there is a rough relationship between a wire dipole with radius *r* and a printed dipole with width *W: W* = 4*r*.

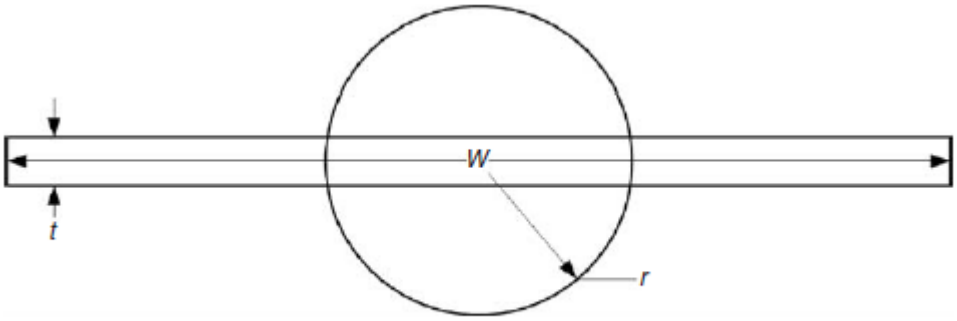

Figure 5.4 Relationship between cylindrical and ribbon dipoles [10].

Wider printed dipoles have larger bandwidths [10]. However, wider dipoles occupy more space, and if the dipole is made out of silver ink, the cost can increase rapidly. Therefore, there is a tradeoff between bandwidth (performance) and cost when designing the RFID antenna [10].

5.1.2 Radiating Resistance

In this section we will look at how the radiation resistance (radiated power) affects RFID tags. Power absorbed by the radiative resistance is transmitted as EM energy or vice versa. The radiative resistance is directly proportional to the antenna length [11]. The resistive radiation just dissipates power absorbed in the form of heat. For example, if we took the dipole and broke it down to small segments then, each segment would induce an electric field at some distance.

If we integrate the square of electric field over all solid angles, we could obtain the total radiated power. A simple formula for the radiation resistance is given by [37].

$$R_A = 80\,\alpha^2(\frac{\pi L}{\lambda})^2 \quad (20)$$

In this equation, L is the total length of the dipole and α is the term dependant on the current distribution along the dipole. If the current is uniform then, α = 1. If the current is triangular than α = 0.5 and if the current is half a sine wave then α = 0.62. The goal is to increase the bandwidth efficiency of the antenna so that the EM energy can be transmitted or received easily.

One method proposed by [19] is to use the dipole structure which is straight in the middle and where the meandered part is pushed towards the end of the dipole as seen in Figure 5.5. The second method proposed is called capacitive tip loading, where the end of the dipole has a large metallic area as shown in Figure 5.6. The last method to increase the value of α as proposed by [34] is to use a spiral inductor as shown in Figure 5.7.

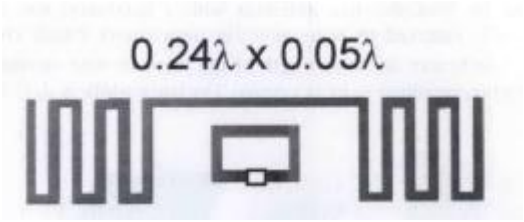

Figure 5.5 A meander-line antenna (*f*=915 MHz) with an inductively coupled loop feed [35].

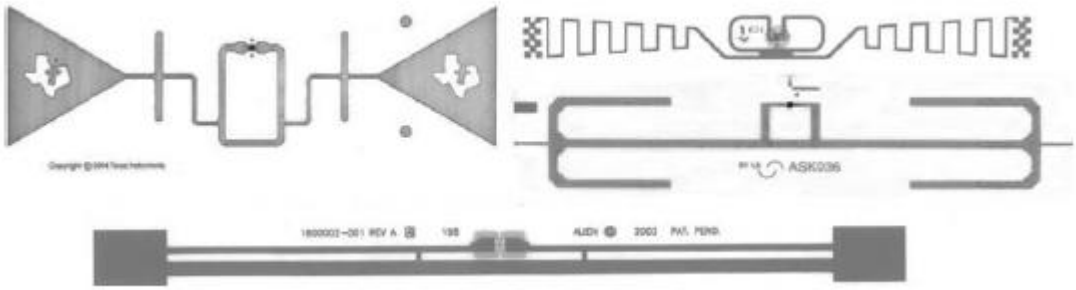

Figure 5.6 Examples of capacitive tip-loaded tags [10].

Figure 5.7 Example of spiral-loaded tag. [10].

5.2 Size Reduction Techniques

Most UHF RFID tags have to be attached to small objects. The dipole as described in section 5.1.1 has to be reduced in length to fit the tag's area as well as not degrade in radiation efficiency. Two methods to achieve this are meandering and inverted-F configurations. Both configurations require a single or multiple folding of the radiating body in order to accommodate the length required for achieving resonance at a particular frequency. Matching charts may be used in the design of simple layouts or optimization tools can be used where a large geometry (many parameters) is used.

5.2.1 Meandering Diploes

The dipole antenna arms are folded along a meandered path as proposed by [7] and shown in Figure 5.8. The wire configuration produced has distributed capacitive and inductive reactance that effect the overall antenna's input impedance. The transmission-line currents do not give a valuable contribution to the radiated power, but instead produce losses. Resonances are achieved at lower frequencies when compared to straight dipoles. In addition, the bandwidth is reduced along with low efficiency.

The shape of the meandered dipole can be periodic or individually optimized to match the chip impedance. As seen in the figures 5.8 to 5.14, the total length of the meander-line antenna increases along with the reactance, and the height of the meandered segment controls the resistance.

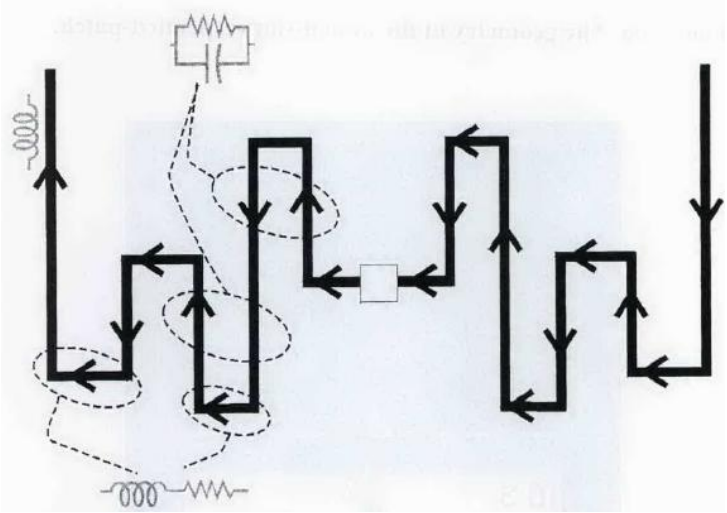

Figure 5.8 The geometry of the meander line antenna with multiple unequal turns. The horizontal lines control the radiation resistance, the adjacent vertical lines act as energy storage elements, and the overall conductor length affects the inductance [7]

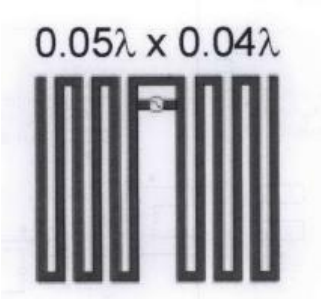

Figure 5.9 An equi-spaced meander line antenna (*f*=953 MHz) with the T-match feed [36]

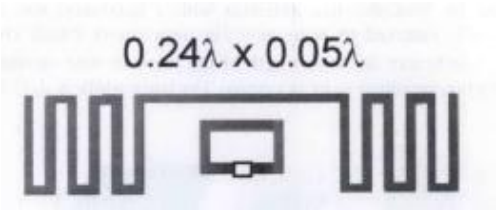

Figure 5.10 A meander-line antenna (*f*=915 MHz) with an inductively coupled loop feed [37].

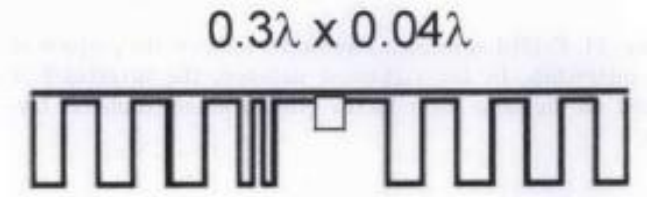

Figure 5.11 A meander-line antenna (*f*=920 MHz) with a loading bar. The antenna's reactance and resistance can be controlled by trimming the meander-line antenna and the bar by punching holes [37].

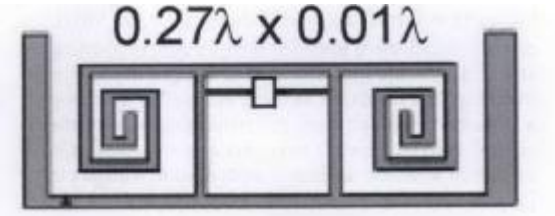

Figure 5.12 A multi-conductor antenna (*f*=900 MHz) with a double T-match scheme and spiral folding, used to achieve the required inductance. The extra material at the end as discussed in section 1.5 helps increase the antenna's bandwidth [38]

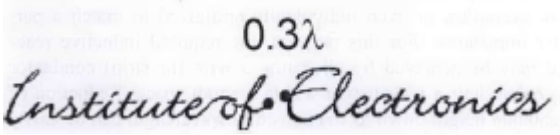

Figure 5.13 A text-shaped meander-line antenna (*f*=870 MHz) where the turns are obtained by attaching the adjacent letters of the text [39]

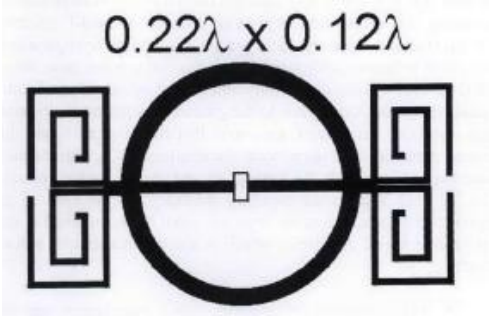

Figure 5.14 A multi-conductor meander-line tag (*f*=900 MHz) with circular-shaped double T-match. This meander arrangement is designed to keep most of the horizontal currents in phase [22].

5.2.2 Inverted-F Configurations

The size of the vertical wire monopole is folded into a wire that is parallel to the ground plane and resembles an inverted-L structure [7] that typically has a low resistance and a high capacitive reactance. A T-match is applied to this structure resulting in an F-type configuration as shown in Figure 5.15. In the inverted structure, the radiating elements are the conductors that are orthogonal to the ground plane. The folded conductor, together with its image (under the ground plane) yields a transmission-line current mode, producing power loss and negligible radiation. The antenna bandwidth may be improved by replacing wire with large strips (**PIFA)** as shown in Figure 5.15.

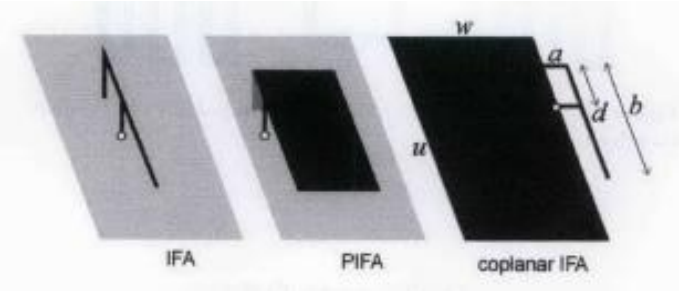

Figure 5.15 Folded antennas: circles indicate the position where the chip is attached. The right most has the inverted-F structure placed on the same layer as the ground plane [7].

In the case of the inverted-F geometry, considered to be an asymmetric dipole as shown in Figure 5.15, a wide variety of input impedances can be obtained by varying the parameters {*a* , *b, d*}. As seen in the chart of Figure 5.16 [7] the input (inductance) reactance monotonically increases with both *b* and *d*. The resistance is controlled by varying the parameter *d*. Finally, the antenna becomes more inductive as the value of *a* increases, since the folded part of the antenna moves away from the ground plane.

5.3 Classification of RFID Tags based on application.

The classification of RFID tags based on their application is a challenging goal because each RFID tag antenna design is based on the tag performance criteria such as read range, chip sensitivity, orientation sensitivity, etc. Therefore, identifying known commercially available RFID inlays into a family based on their application is a good starting point. As seen in table 5.1, RFID tag manufacturer 'Avery Dennison' currently provides the following RFID Inlays. This section aims to classify the tags into a family based on their applications as well as their associated antenna parameters.

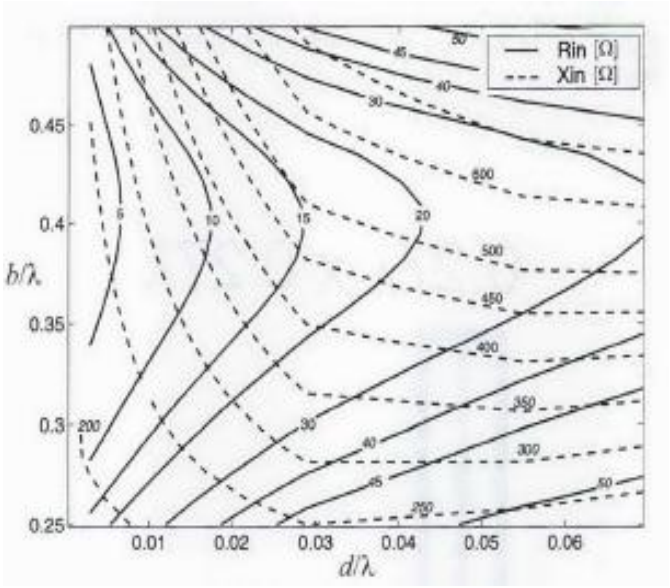

Figure 5.16 The matching chart for the co-planar inverted-F antenna geometry shown in figure 5.15. The parameters that are fixed are w = λ/4, u = λ/2, a = λ/10 and the folded-wire length and the feeding position is varied [7].

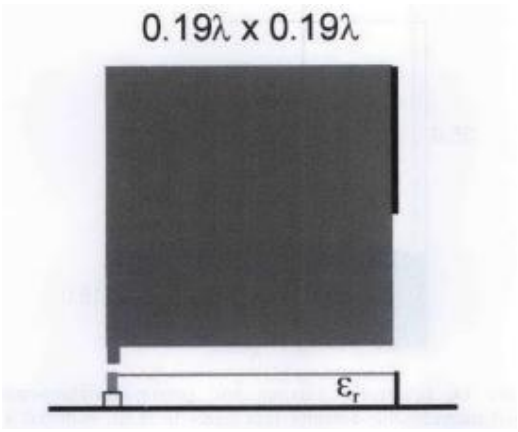

Figure 5.17 A conventional two-layer PIFA (*f*=870 MHz) with a square conductor [7].

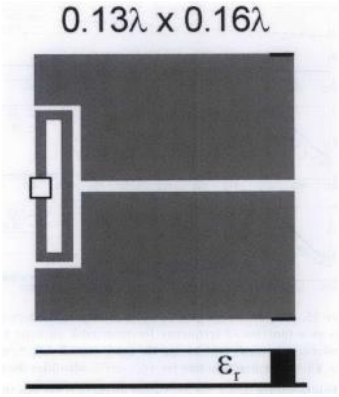

Figure 5.18 A two-layer double PIFA tag with proximity feed loop (*f*=900 MHz). The microchip is placed on the top metallization [40].

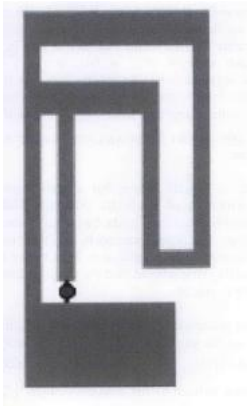

Figure 5.19 A co-planar IFA (*f*=870 MHz) with an additional horizontal stub [41].

Table 5.1a Antennas marketed by Avery Dennison [42].

Tag #	Antenna Type	Dimensions (mm)	Applications	Antenna Parameters linked to literature papers.
1.		95 x 8.15	General purpose applications, with medium read range.	Modified T-Match, no meandering. Therefore, low resonance frequency [42], [43].
2.		70 x 14.5	Distance reading	Modified T-Match, with meandering. Therefore, good resonance frequency [42], [44].
3.		70 x 14.5	Stock management. Low read range	Modified T-Match, with meandering and capacitive tip-loading at ends (section 5.1.2) Therefore, good resonance frequency, good radiation resistance, increased cost –more metal used [42], [45].
4.		50 x 30	Ideal for media denim and cotton based on mechanical properties of antenna.	Modified T-Match, with less meandering and capacitive tip-loading at ends (section 5.1.2) Therefore, lower resonance frequency, good radiator, increased cost – [42], [46].

Table 5.1b Antennas marketed by Avery Dennison [42].

5.		70 x 70	Uniform radiation pattern. Ideal for card support.	PIFA configuration. Large metallic surface. Good resonance frequency, high radiation resistance, increased cost [42], [47].
6.		16 x 16	Very compact. Used on metal supports.	IC pushed to one corner. Small meander. Small size. Good resonating frequency, high radiation resistance. Increased cost (metal surface – refer to section 5.3) [42], [48].
7.		22 x 22	For pharmaceutical products of various sizes and shapes.	PIFA configuration. Large metallic surface. Good resonating frequency, high radiation resistance, increased cost [42], [49].
8.		20 x 10	Excellent on glass support. Used in the United States and Japan.	One-sided meandering, monopole structure, good resonance frequency, reasonable cost [42], [46].
9.		29.99 x 50	For retail sale of various products.	Spiral loaded tag. Excellent radiation resistance [42].

Table 5.1c Antennas marketed by Avery Dennison [42].

10.		18 x 40	Long read range distance. Mainly used in the medical field because of small size and mitigation of the effects of liquids.	Modified T-Match, with higher meandering and capacitive tip-loading at ends (section 5.1.2) Therefore, good resonance frequency, increased cost [42], [50].
11.		Unknown. Expected to be larger than most tags in size.	Orientation Insensitive.	Dual-Dipole RFID tag. Able to deal with polarization mismatch. Lower Q, good resonance. However increased cost (2 RF feeds on IC, plus the metal area) [42], [10].

As seen in table 5.1, the RFID inlays are manufactured based on their applications of use such as retail, clothing, healthcare, pharmaceutical, distance reading, metal supports, etc. Furthermore, the antenna parameters associated with the RFID inlays such as T-match, meandering, capacitive tip-loading, high radiation resistance, etc are also mentioned in the table. Note, good resonance frequency in table 5.1 indicates that the desired antenna return loss value (>10 dB) is close to the frequency of operation, 915MHz.

Now each of these designs is classified into a family based on their application of use shown in table 5.2. The tags are classified into a family based on their applications. The tag numbers ‘A, B, C, D and E’ in table 5.2 represent the tag designs for each application and will be presented in the next chapter.

Table 5.2 Family of RFID tags based on application

Application	Tag Number
1) Broad Band tag (universal RFID bandwidth)	2,4,11, A
2) General purpose tag (Clothing, books)	1, 9, B
3) Medical, healthcare	6,7,8,10,11,C
4) Baggage tag	3, D
5) Contactless card	5, E

5.4 Chapter Summary

In this chapter, a literary survey is examined to classify existing passive RFID tags into a family or class based on their application or use. The first section introduced to dipole geometry and radiation resistance necessary to understand how tags are manufactured in industry. Second, size reduction techniques such as meandering dipoles and inverted-F configurations were studied with respect to changes in the geometrical parameters of the design. Finally, the classification of RFID tags into a family based on their application as presented in table 5.2, was discussed and a few designs (A, B, C, D and E) that will be simulated and fabricated will be presented in the following chapters.

CHAPTER 6 – Simulation of antennas design using HFSS

Passive RFID tags are usually analyzed using electromagnetic modeling and simulation tools such as method of moments (MoM) for planar designs and finite element method (FEM) or finite-difference time-domain (FDTD) methods for other designs. Fast EM analysis tools such as Ansoft HFSS are very important for efficient tag design. For example, the geometrical parameters (height, width) of a meandered dipole antenna designed using HFSS can be investigated to see how incremental changes effect tag performance (impedance, frequency, etc).

In this chapter the simulation results of the designed tags based on the application of use as shown in table 6.1 are presented. The chapter is divided into three parts; the first part briefly introduces the different antenna designs 'A, B, C, D and E' and the advantages for using the particular shape. The second part examines the parametric study and optimization of the proposed antenna geometry using the FEM design tool. Finally, the simulations results are investigated to find the best possible geometrical dimensions for the proposed antennas.

Table 6.1 Family of RFID tags based on application

Application	Tag Number
1. Broad Band tag (universal RFID bandwidth)	A
2. General purpose tag (Clothing, books)	B
3. Medical, healthcare	C
4. Baggage tag	D
5. Contactless card	E

6.1 Proposed Antenna Designs

In this section the proposed antenna designs based on the application as seen in table 6.1 are presented. The antenna designs are chosen specifically based on size reduction and impedance matching techniques [7], [5] such as T-match, meandering, capacitive tip-loading, etc. The goal is to design antennas that will provide optimal tag performance characteristics for the given application.

The first step in the design process involves choosing the materials for the tag. The proposed antennas are made of copper metal with a thickness of 0.05 mm. The substrate chosen for the designs is RogersRT-Duroid 5880 with a thickness of 1.58 mm (62-mil). The copper metal is chosen because of its good conductive properties and relatively low cost. The substrate RogersRT-Duroid is chosen because of its features such as low electrical loss, low moisture absorption, isotropic, uniform electrical properties over frequency and excellent chemical resistance [51].

The second step and perhaps the most crucial step in the antenna design process is the selection of the application-specific integrated circuit (ASIC) chip. The ASIC chip 'turn-on' impedance for a given frequency (915 MHz) is usually provided with datasheet by the chip manufacturer. The ASIC chips chosen for the proposed tags are mentioned in table 6.2 below.

Table 6.2 ASIC Chips used for antennas

ASIC Chip	Manufacturer Part Number	Impedance	Frequency of Operation	Tag Number
1) NXP UCODE G2XM	SL3S1002FTT,118	16-j148 Ω	915 MHz	B, D
2) NXP UCODE G2XM	SL3S1002AC2, 118	34-j142 Ω	915 MHz	A, C
3) NXP MIFARE	MF0MOA4U10/D, 118	17 pF	13.56 MHz	E

As seen in table 6.2, the chip impedances have a low-resistive part and a high-capacitive part. Therefore, for conjugate impedance matching criteria as examined in chapter 4, the antenna impedance must have a low-resistive part and a high-inductive part. For example, antenna 'B' would require an impedance of 16+j148 Ω is to be perfectly matched to the chip impedance.

The proposed antennas are listed in table 6.3 with a brief description on the size reduction and impedance matching techniques such as T-match, meandering, capacitive tip-loading, high radiation resistance, etc. The tabular format was chosen to highlight how the proposed tags fulfill the given application requirements.

Table 6.3a Proposed Antenna Design based on specific applications.

Tag #	Antenna Type	Dimensions (mm)	Applications	Antenna size reduction and Impedance Matching techniques
A.	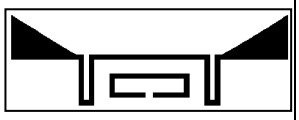	97.5 x 34.7	Broadband tag (universal RFID bandwidth, 868-960 MHz)	Inductively coupled loop, minimal meandering, capacitive tip-loaded. Therefore, increased bandwidth.
B.		94 x 18.5	General purpose tag (Clothing, books)	Inductively coupled-loop Match, with meandering. Therefore, good resonance frequency.
C.	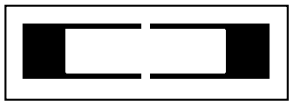	120 x 40	Medical, healthcare	Two-wire folded dipole, and capacitive tip-loading. Therefore, increased read range, good radiation resistance, increased cost –more metal used.

The exact dimensions of the proposed antennas are individually shown in Figure 6.1. The dimensions of the antenna were chosen. The FEM simulation tool is used for modeling the antennas A-D parameters such as return loss, load impedance, read range, etc. However, for design 'E' the antenna design software provided by [52] is used to model the exact dimensions necessary for conjugate impedance matching with the chip impedance (17 pF).

Table 6.3b Proposed Antenna Design based on specific applications.

D.		94 x 24.5	Baggage tag	Inductively coupled-loop Match, with less meandering and capacitive tip-loading at ends. Therefore, lower resonance frequency, good radiator and increased cost.
E.	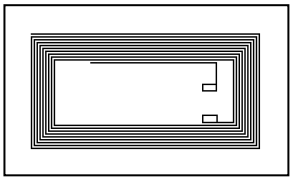	100 x 60	Contactless card	Square coil structure [4]. Good resonance frequency, high radiation resistance, increased cost because more size and material used.

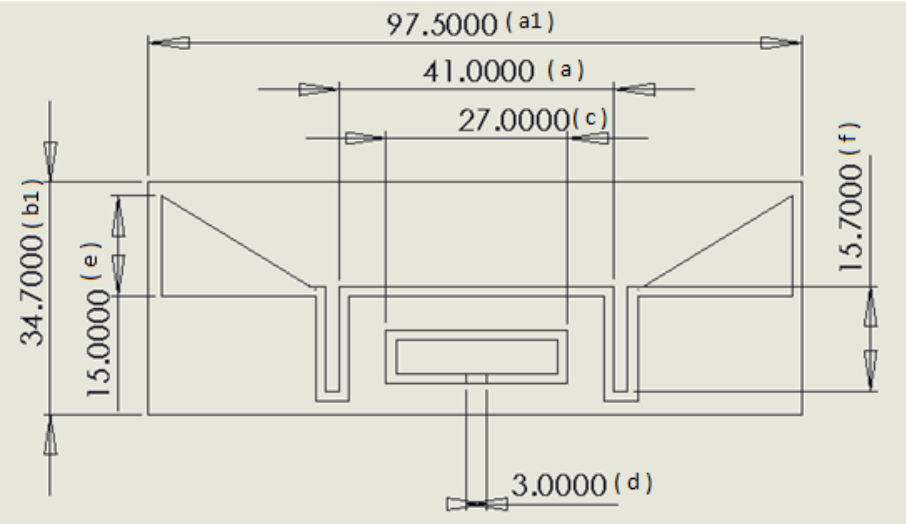

Figure 6.1a Antenna design **A**: the dimensions are a1 = 97.5 mm, bl = 34.7 mm, a = 41 mm, b = 15 mm, c = 27 mm, d = 2 mm, e = 15 mm and f = 15.7 mm. The dimensions a1 and b1 represent the substrate and *d* represents the chip dimensions. The antenna trace thickness is 0.05 mm and the substrate thickness is 1.58 mm.

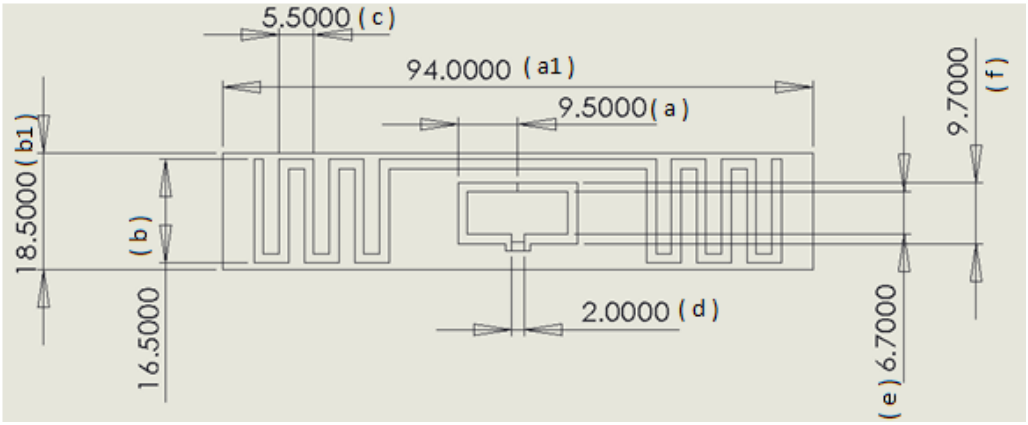

Figure 6.1b Antenna design **B**: the dimensions are a1 = 94 mm, bl = 18.5 mm, a = 9.8 mm, b = 16.5 mm, c = 5.5 mm, d = 2 mm, e = 6.7 mm and f = 9.7 mm. The dimensions a1 and b1 represent the substrate and *d* represents the chip dimensions. The antenna trace thickness is 0.05 mm and the substrate thickness is 1.58 mm.

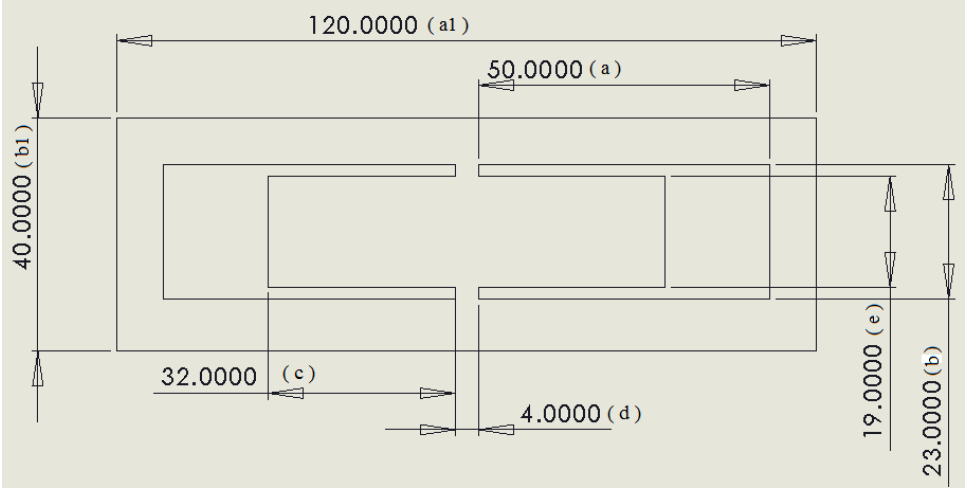

Figure 6.1c Antenna design **C**: the dimensions are a1 = 120 mm, bl = 40 mm, a = 50 mm, b = 23 mm, c = 32 mm, d = 4 mm and e = 19 mm. The dimensions a1 and b1 represent the substrate and *d* represents the chip dimensions. The antenna trace thickness is 0.05 mm and the substrate thickness is 1.58 mm.

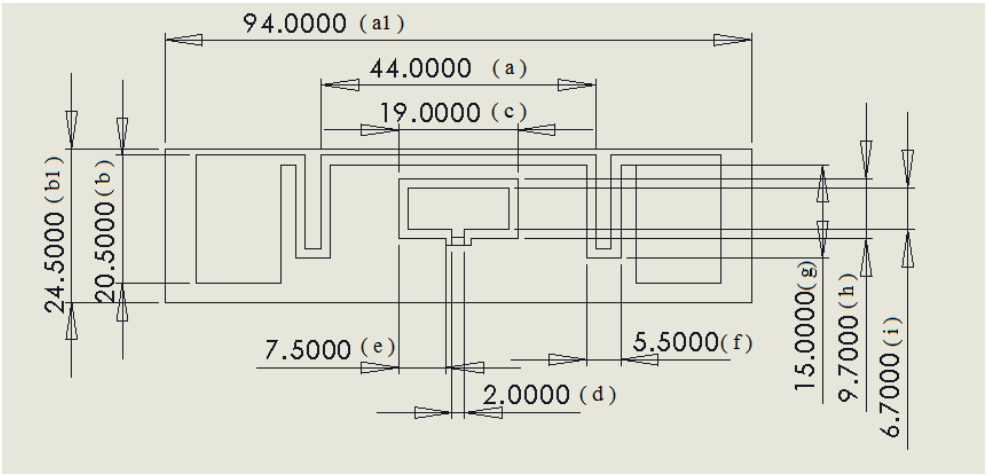

Figure 6.1d Antenna design **D**: the dimensions are a1 = 94 mm, bl = 24.5 mm, a = 44 mm, b = 20.5 mm, c = 19 mm, d = 2 mm, e = 7.5 mm, f = 5.5mm, g = 15 mm, h = 9.7mm and i = 6.7mm. The dimensions a1 and b1 represent the substrate and *d* represents the chip dimensions. The antenna trace thickness is 0.05 mm and the substrate thickness is 1.58 mm.

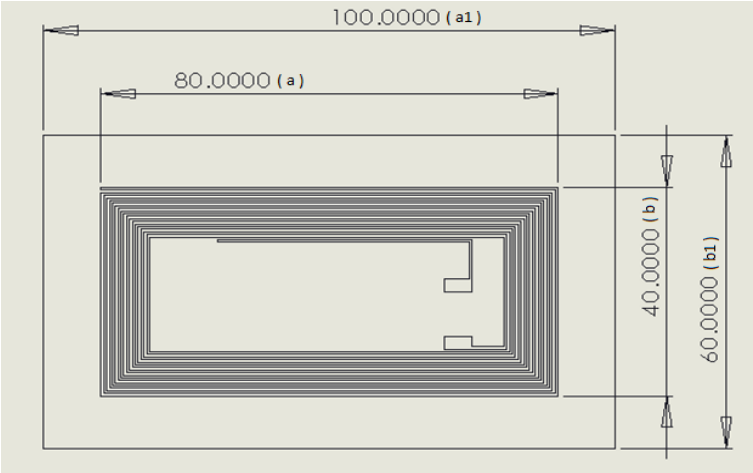

Figure 6.1e Antenna design **E**: the dimensions are a1 = 100 mm, bl = 60 mm, a = 80 mm, b = 40 mm. The dimensions a1 and b1 represent the substrate dimensions. The antenna trace thickness is 0.05 mm and the substrate thickness is 1.58 mm.

Figure 6.1 Dimensions of the proposed antenna designs.

6.2 Optimization of antenna design using HFSS simulations

This section highlights the antenna parameters such as return loss, load impedance, read range, etc. using HFSS simulations. Furthermore, the optimization of the antenna design is achieved by varying the geometrical parameters and analyzing the impact on tag performance (impedance, return loss, etc). For the simulation setup in this chapter the antenna impedance is matched to the impedance of the IC.

6.2.1 Simulation results without optimization

The return loss with respect to frequency for antenna designs A-D is shown in figure 6.2 below.

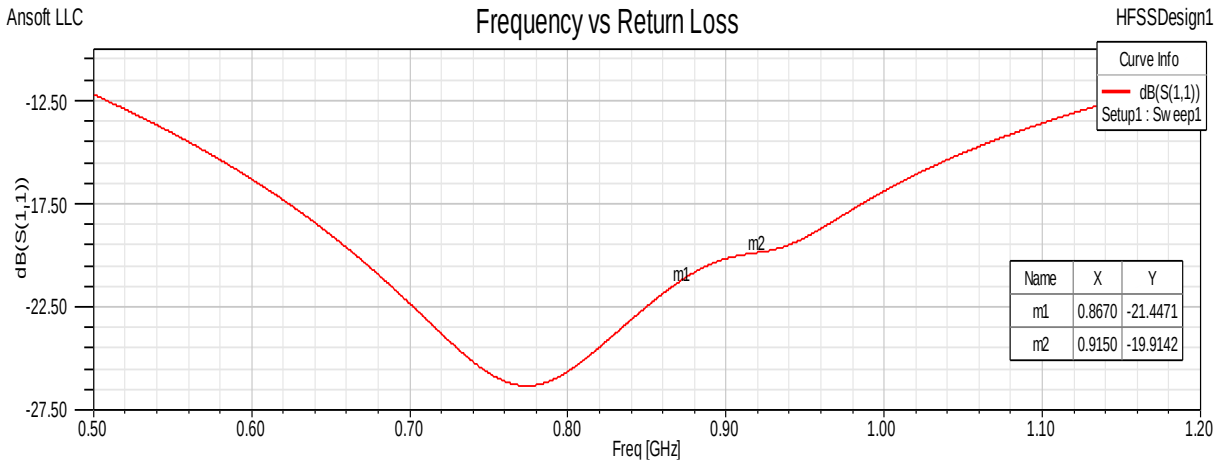

Figure 6.2a Simulation results showing the return loss of the antenna **A**

As seen from Figure 6.2a the antenna has a bandwidth > 70 MHz at a return loss (RL) > 10dB which covers the worldwide RFID UHF band.

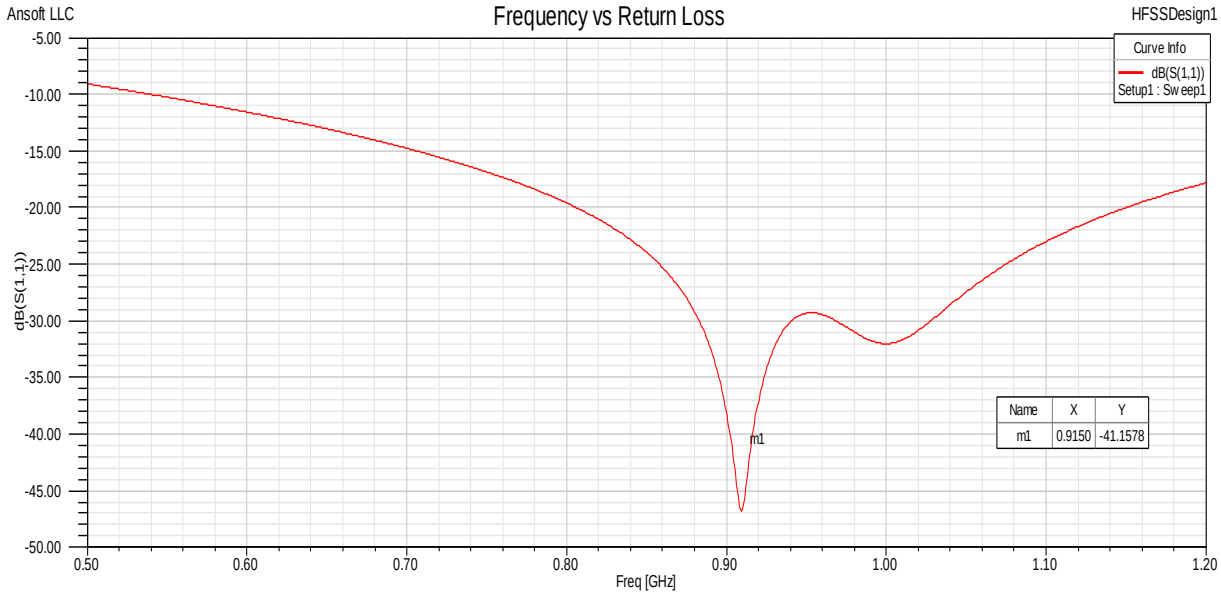

Figure 6.2b Simulation results showing the return loss of the antenna **B**

As seen from Figure 6.2b the antenna has a bandwidth > 70 MHz at a return loss (RL) > 10dB.

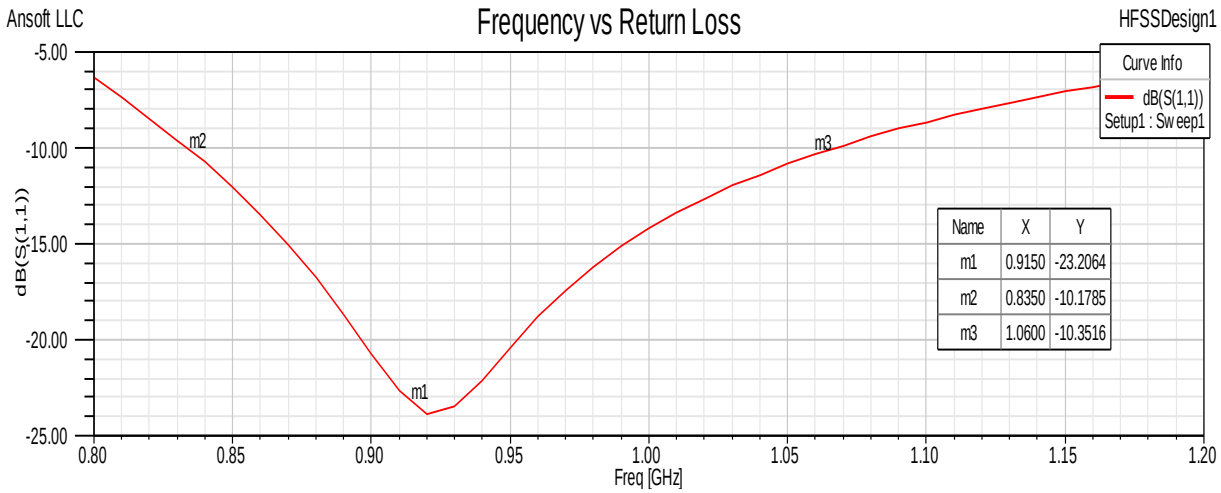

Figure 6.2c Simulation results showing the return loss of the antenna **C**

As seen from Figure 6.2c the antenna has a bandwidth of 22.5 MHz at a return loss (RL) > 10dB.

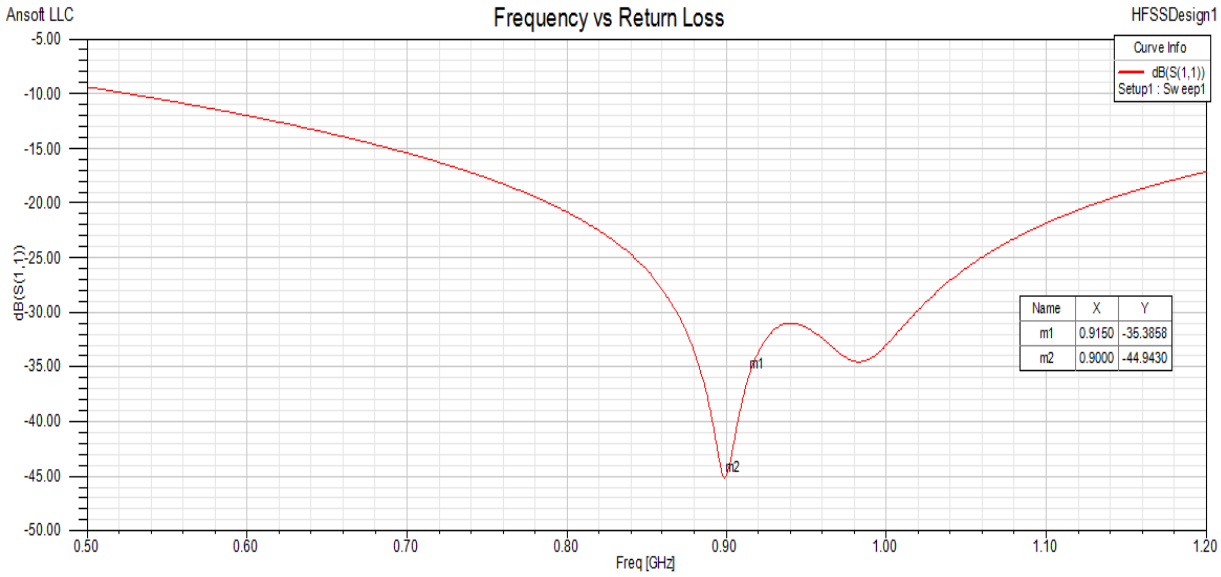

Figure 6.2d Simulation results showing the return loss of the antenna **D**

Figure 6.2 Simulation results showing the return loss proposed antenna designs.

As seen from Figure 6.2d the antenna has a bandwidth > 70MHz at a return loss (RL) > 10dB.

The results obtained in figure 6.2 show that the antenna have a minimum return loss (RL) > 10dB which is standard while designing RFID tag antennas [5]. The next simulation results of interest are the impedance versus frequency. At 915 MHz, the impedance of the simulated results should conjugate match with the chip impedance as seen in figure 6.3.

As seen from Figure 6.3a the simulated resistance and reactance at the required frequency (915MHz) is 10.99 + j180.9 respectively. This is very close to the required impedance of 16 + j148 Ω required for conjugate matching.

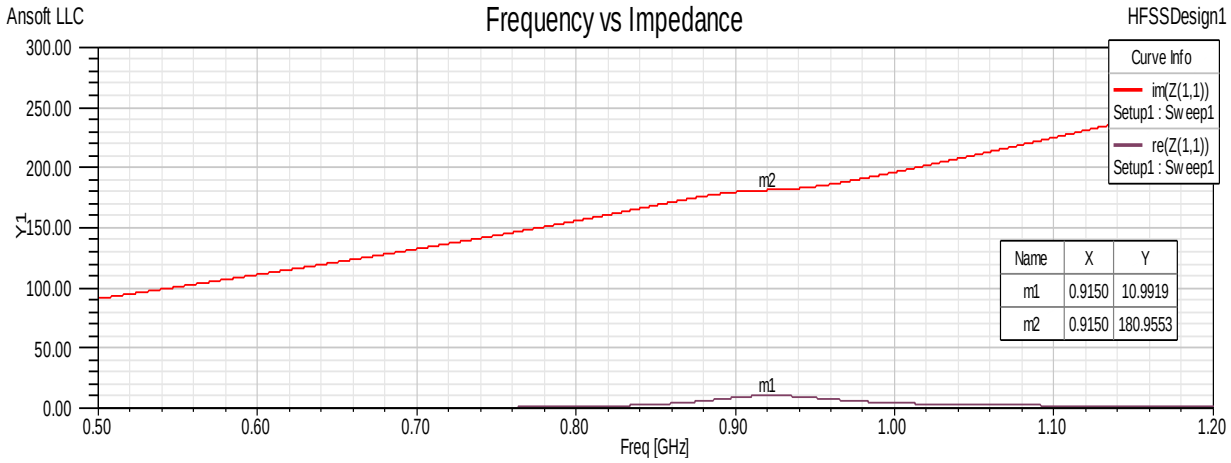

Figure 6.3a Simulation results showing the impedance of the antenna **A**

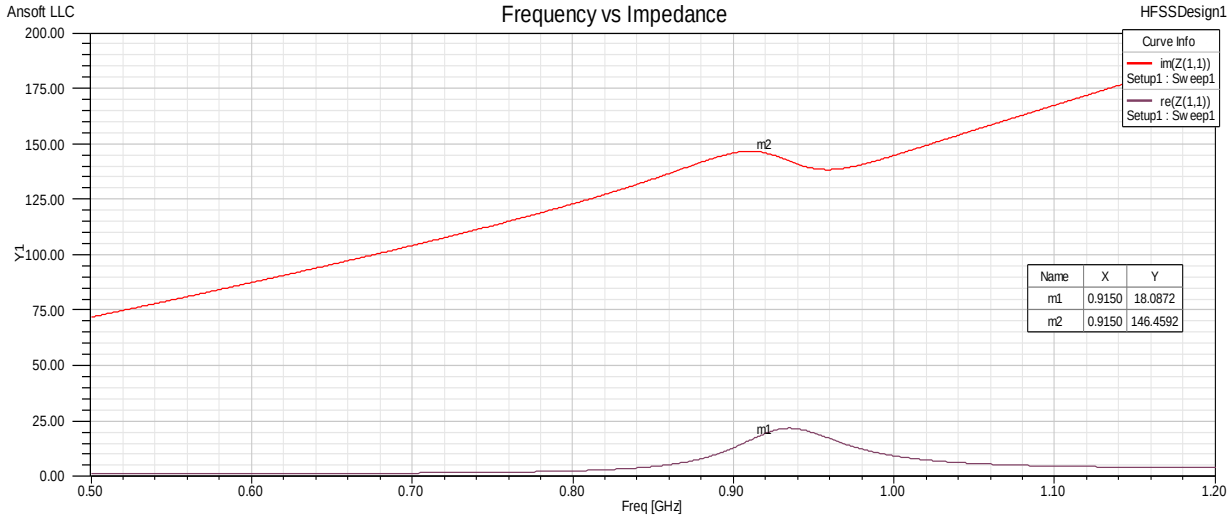

Figure 6.3b Simulation results showing the impedance of the antenna **B**

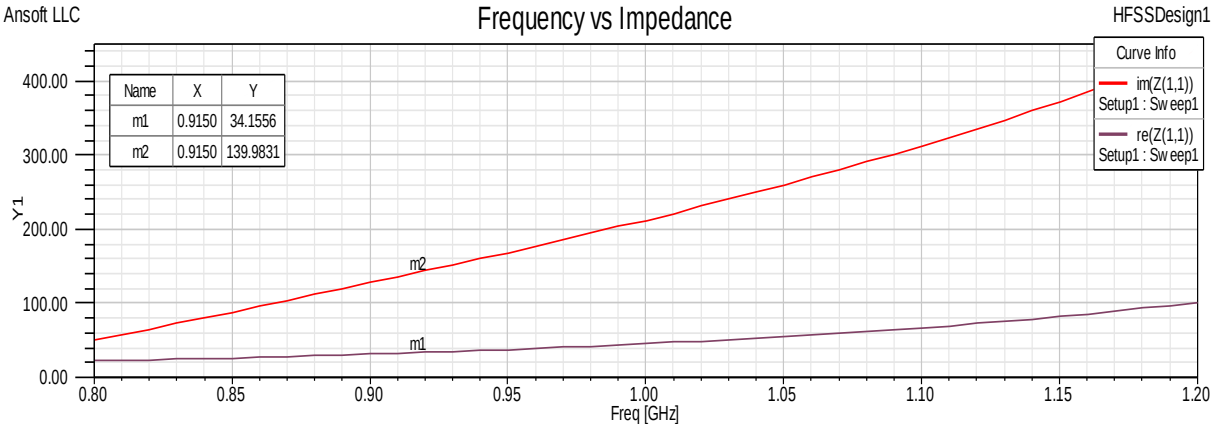

Figure 6.3c Simulation results showing the impedance of the antenna **C**

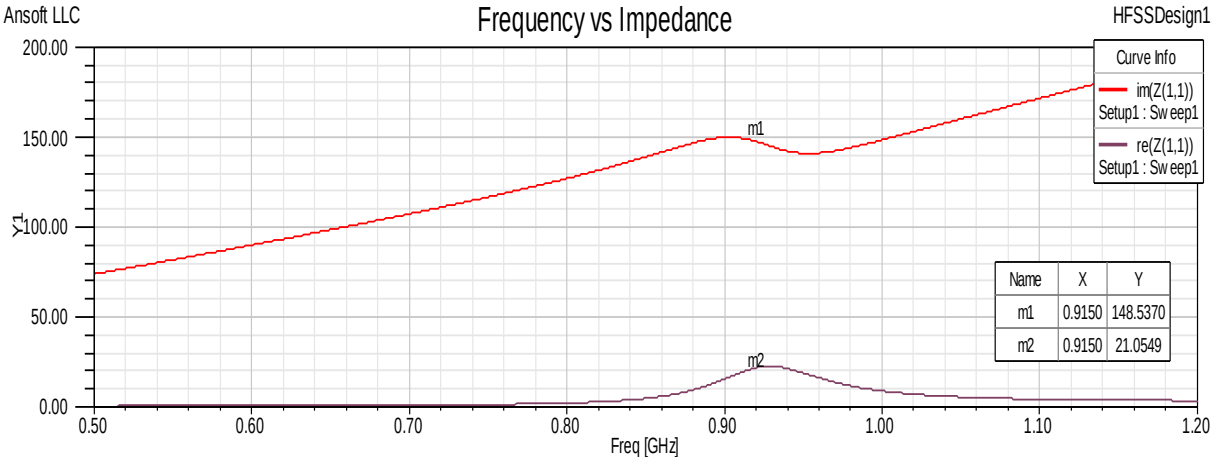

Figure 6.3d Simulation results showing the impedance of the antenna **D**

Figure 6.3 Simulation results showing the return loss proposed antenna designs.

As seen from Figure 6.3b the simulated resistance and reactance at the required frequency (915MHz) is 18.1 + j146.5 respectively. This is very close to the required impedance of 16 + j148 Ω required for conjugate matching.

As seen from Figure 6.3c the simulated resistance and reactance at the required frequency (915MHz) is 14.18 + j141.19 respectively. This is very close to the required impedance of 12 + j140 Ω required for conjugate matching.

As seen from Figure 6.3d the simulated resistance and reactance at the required frequency (915MHz) is 21.05 + j148.5 respectively. This is very close to the required impedance of 34 + j142 Ω required for conjugate matching. The radiation patterns for the antenna designs are shown in Figure 6.3. The omnidirectional radiation pattern of the antenna deigns are in the phi=0 (x-z plane) and phi = 90 (y-z plane).

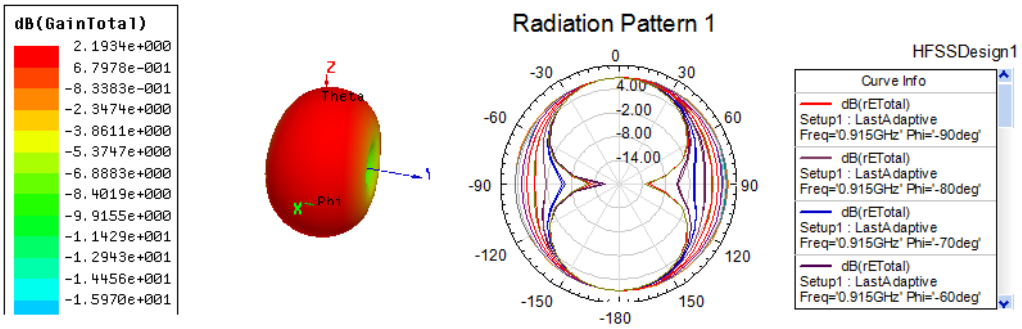

Figure 6.4a Simulated antenna 3-D gain pattern and antenna radiation pattern for antenna **A** (Directivity for phi=0 degrees (x-z plane) and phi = 90 degrees (y-z plane))

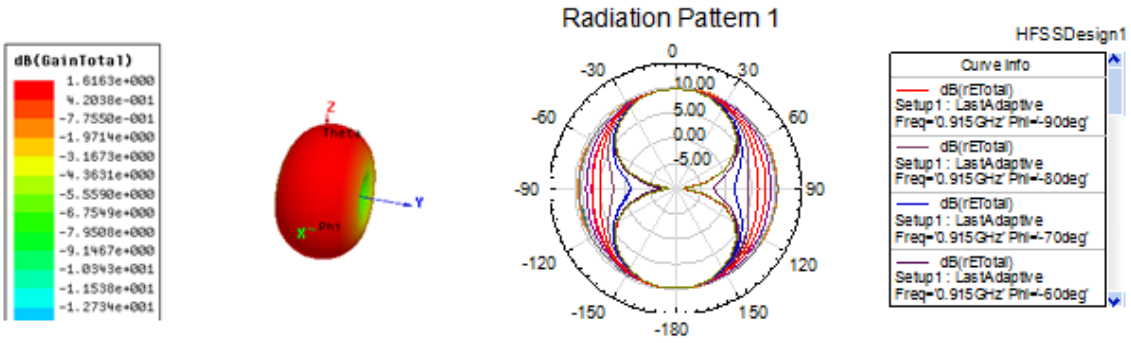

Figure 6.4b Simulated antenna 3-D gain pattern and antenna radiation pattern for antenna **B** (Directivity for phi=0 degrees (x-z plane) and phi = 90 degrees (y-z plane))

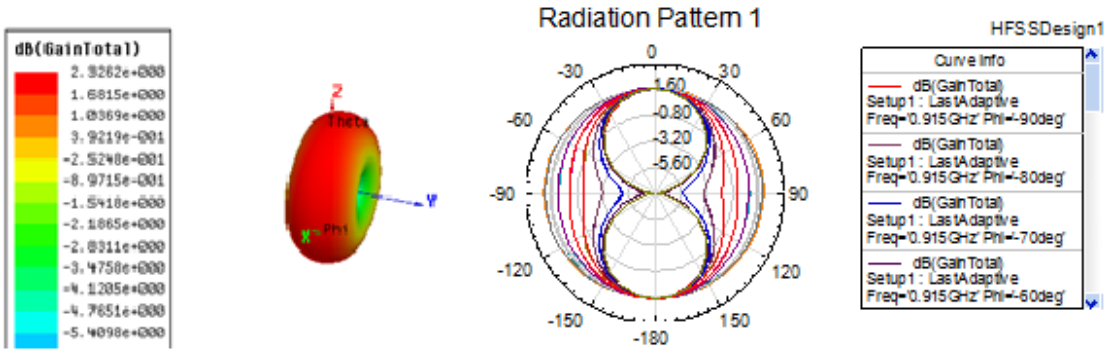

Figure 6.4c Simulated antenna 3-D gain pattern and antenna radiation pattern for antenna **C** (Directivity for phi=0 degrees (x-z plane) and phi = 90 degrees (y-z plane))

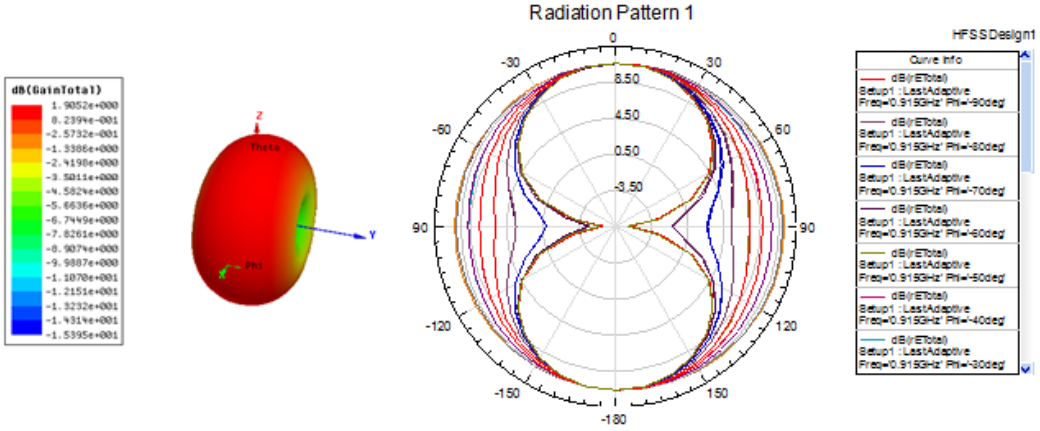

Figure 6.4d Simulated antenna 3-D gain pattern and antenna radiation pattern for antenna **D** (Directivity for phi=0 degrees (x-z plane) and phi = 90 degrees (y-z plane))

Figure 6.4 Simulation results showing the 3-D gain pattern and radiation pattern of the proposed antenna designs.

The antenna radiation efficiency is given by the formula $G = e_{rad}D$ [19]. Here, G is the gain of the antenna and D is the directivity. The read range is given by the Friis free-space formula given by [5] equations (16), (17).

The chip to be used is NXP UCODE G2XM ($P_{th} = -15\,dBm$). The reader used is Convergence Systems Ltd CS203 ($P_t = 30dbm, Gt = 6dBi$), the antenna gain as given above and λ ≅ 0.33 m. The results are shown in table 6.4. The impedance matching comparison for the antenna design is shown in table 6.5.

$$r_{max} = \frac{\lambda}{4\pi}\sqrt{\frac{P_t G_t G_r \tau}{P_{th}}} \quad (16)$$

$$\tau = \frac{4R_c R_a}{|Z_c + Z_a|^2}, \qquad and \;\; 0 \leq \tau \leq 1 \quad (17)$$

Table 6.4 Simulated Antenna Parameters

Antenna	Impedance (Ohm)	Return Loss (dB)	Gain (dB)	Directivity (dBi)	Antenna Radiation Efficiency (%)	Theoretical Read Range (m)
Antenna A	10.99 + j180.9 Ω	19.91 dB	2.193	2.929	74.8	9.86
Antenna B	18.10 + j146.5 Ω	41.16 dB	1.616	2.544	63.5	11.76
Antenna C	14.18 + j141.2 Ω	23.21 dB	2.326	2.327	99.9	8.21
Antenna D	21.05 + j148.5 Ω	35.39 dB	1.905	2.564	74.3	12.68

Table 6.5 The simulated return loss and impedance value comparison for the antenna designs.

Antenna	Return Loss	Simulated Impedance Value	Desired Impedance Value
Antenna A	19.91 dB	10.99 + j180.9 Ω	16 + j148 Ω
Antenna B	41.16 dB	18.10 + j146.5 Ω	16 + j148 Ω
Antenna C	23.21 dB	14.18 + j141.2 Ω	34 + j122 Ω
Antenna D	35.39 dB	21.05 + j148.5 Ω	16 + j148 Ω

The antennas parameters such as return loss, load impedance, read range have been calculated and presented in table 6.4. The comparison between the desired impedance value and the simulated impedance value is shown in table 6.5. The return loss for all the antenna designs is more than the 10 dB standard requirement [5]. The effect of changing the geometrical parameters (height, width) on return loss and antenna impedance is shown in the next section.

6.2.2 Simulation results with optimization

The optimization of the antenna dimensions (length, width, etc.) is studied in this section using HFSS simulations. The main goal is to observe how changing the dimensions of the proposed antenna designs impacts antenna parameters such as return loss and impedance. Furthermore, the results obtained can help antenna designers pick necessary dimensions for the proposed applications for optimal tag performance criteria such as chip impedance matching, return loss, improved read range, etc.

This section will target four specific antenna parts namely, the height, the width, the capacitive-tip and the inductive coil as shown in Figure 6.5. The four different parts of the antenna are targeted because they have a significant impact on the conjugate impedance matching, and read range as suggested by [7], [5] and discussed in detail in chapter 4. The impact on tag performance by changing the substrate value is minimal. Nevertheless, it is still studied and the results are presented at the end of this section.

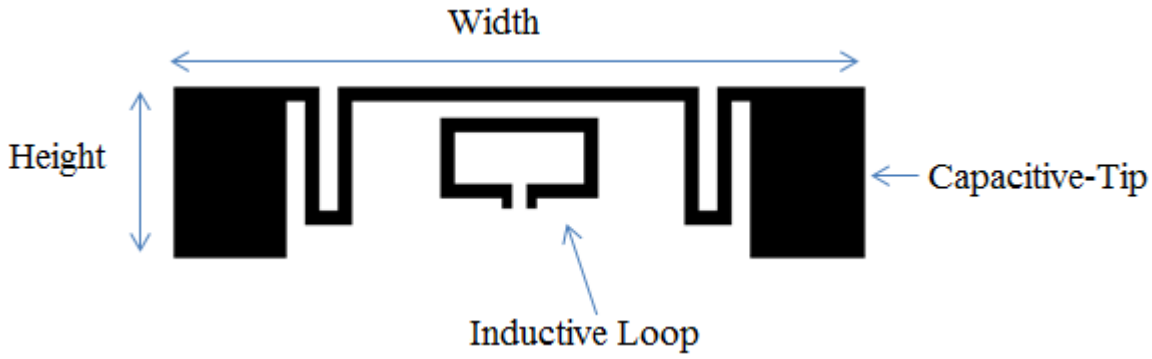

Figure 6.5 Optimization of specific antenna parts for improving tag performance

As observed from literature [5], [7], [45], [53], and [54], each of these parts affects the overall tag performance criteria. For example, the inductive loop shifts the resonant frequency of the antenna and this may impact the return loss value. In addition, if the return loss value is below the 10 dB standard then, the tag will not operate at the desired frequency (915 MHz). This scenario poses a problem because most readers are designed based on geographic frequency regulations such as 915 MHz in North America.

The optimization setup should be carried out correctly while defining dimensions using the simulation software HFSS. For example if the antenna dimensions exceed the substrate dimensions as shown in Figure 6.5 then, the results may not be valid. In addition, the designer should be aware of how the dimensions change incrementally for the optimization as illustrated in Figure 6.6.

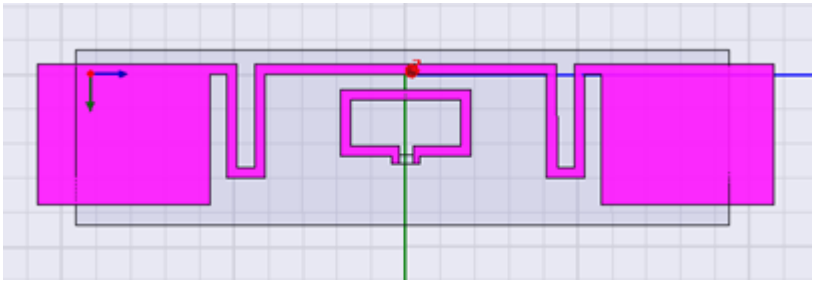

Figure 6.6 Dimensions of the antenna shown to exceed the dimensions of the substrate.

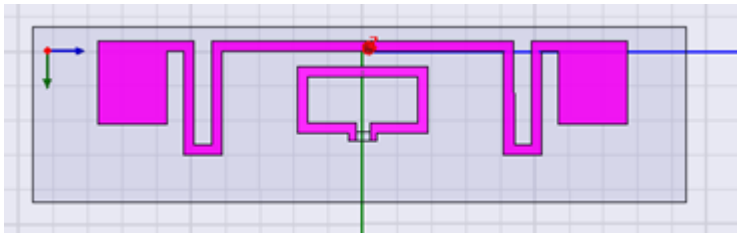

Figure 6.7 Dimensions of the antenna are within the dimensions of the substrate.

Inductive Loop Optimization: The dimensions of the inductive loop are changed and the simulation results (return loss and impedance) of Antennas **A**, **B** and **D** are presented in Figure 6.8. Antenna **C** is not included because does not have an inductive loop matching structure.

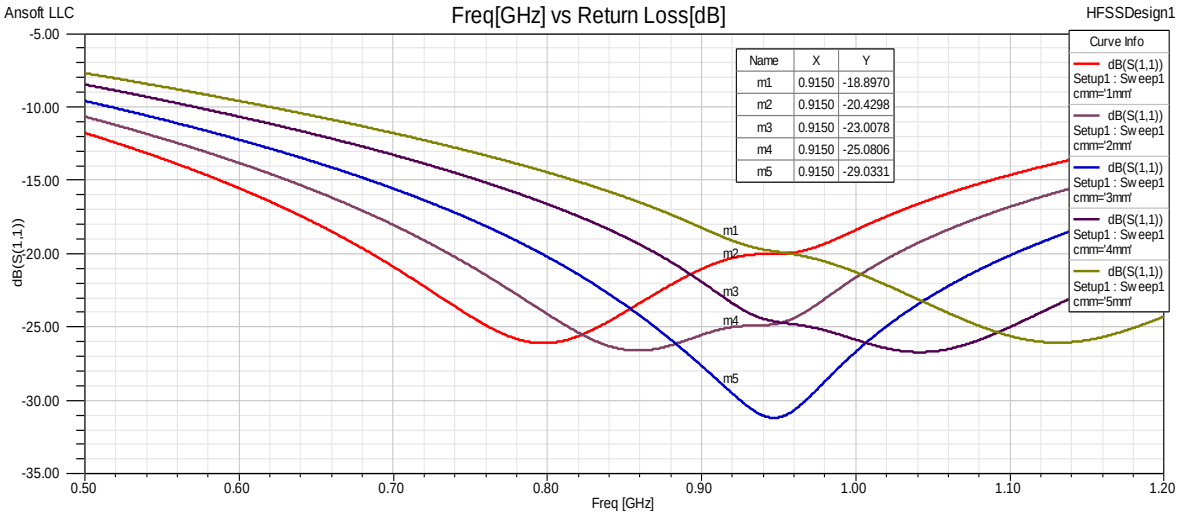

Figure 6.8a Simulation results showing the return loss of the antenna **A** after optimization of the Inductive loop.

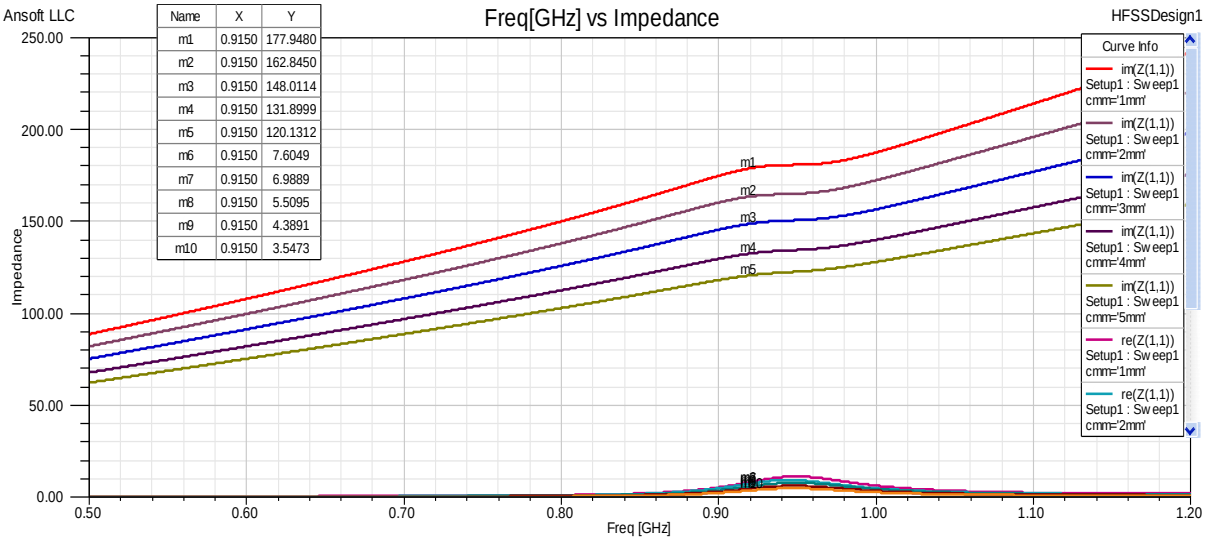

Figure 6.8b Simulation results showing the impedance of the antenna **A** after optimization of the Inductive loop.

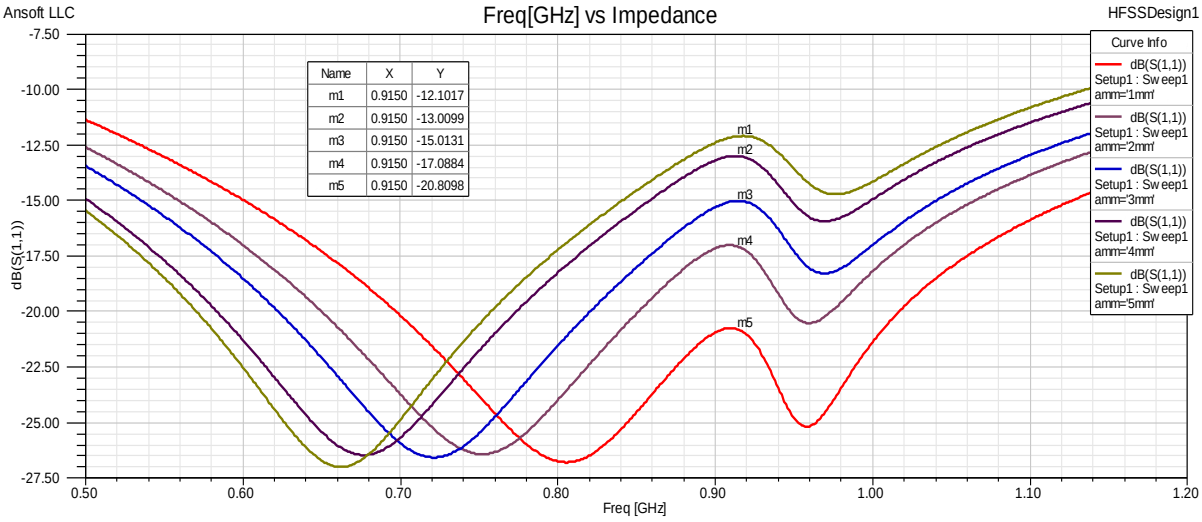

Figure 6.8c Simulation results showing the return loss of the antenna **B** after optimization of the Inductive loop.

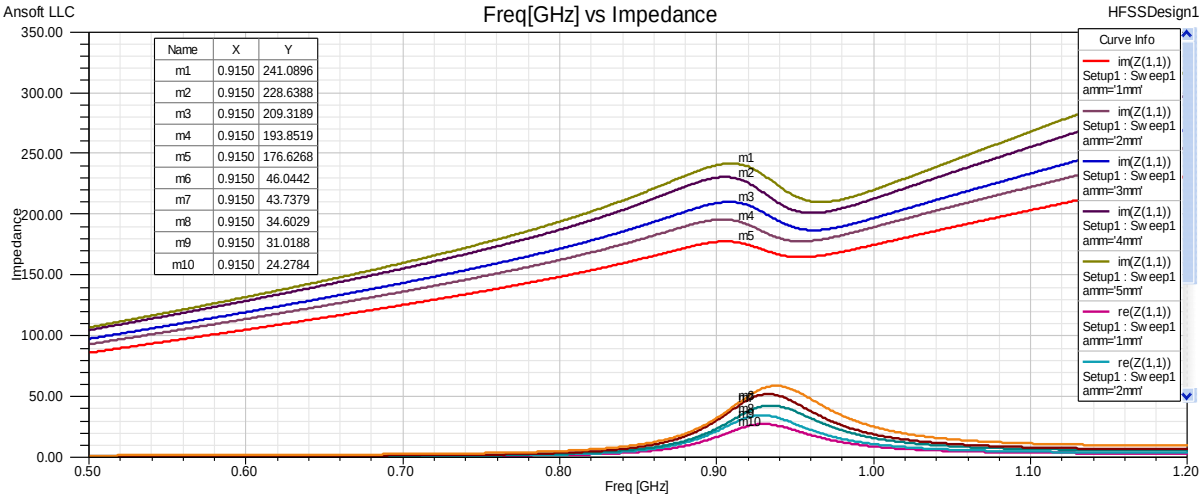

Figure 6.8d Simulation results showing the impedance of the antenna **B** after optimization of the Inductive loop.

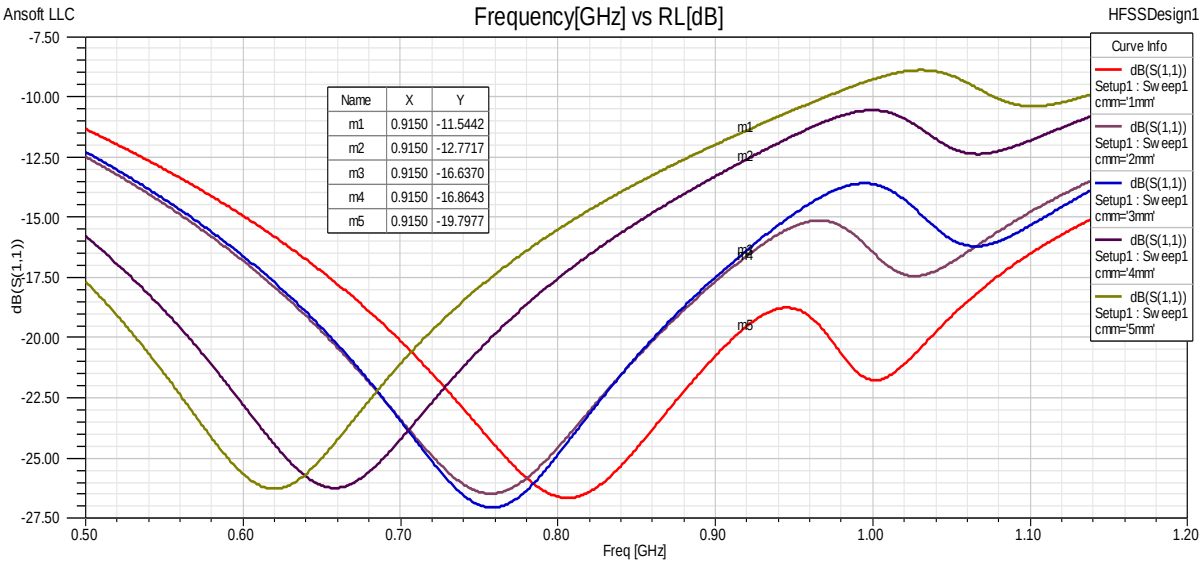

Figure 6.8e Simulation results showing the return loss of the antenna **D** after optimization of the Inductive loop.

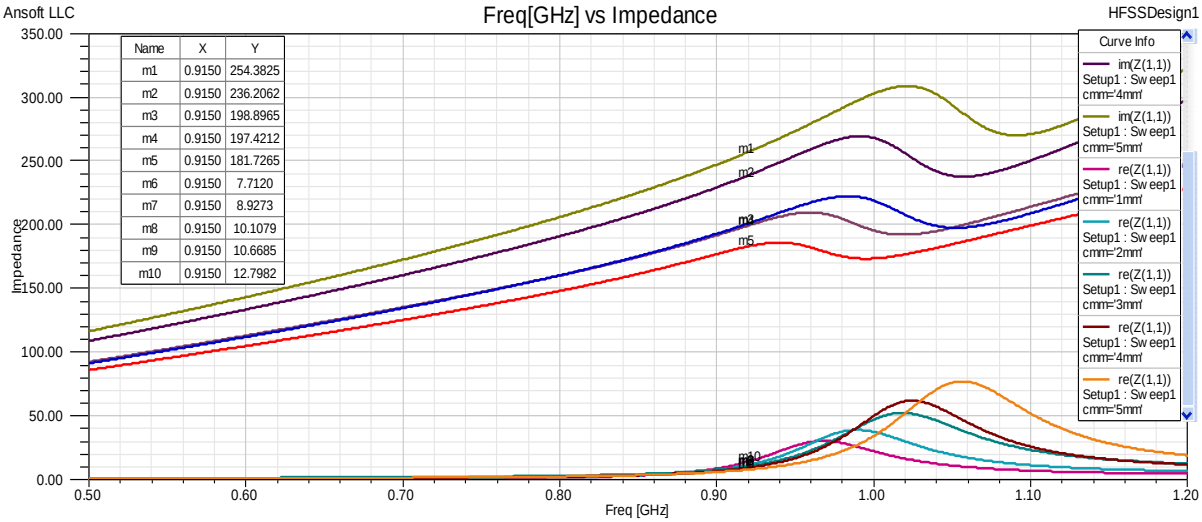

Figure 6.8f Simulation results showing the impedance of the antenna **D** after optimization of the Inductive loop.

Figure 6.8 Simulation results of inductive loop optimization of the proposed antennas

As seen from the Figure 6.8, the inductive coil has a significant impact on the resonant frequency of the antenna. In addition, the reactive part of the impedance changes more

compared to the real part. The difference in changing the dimensions will be further discussed in section 6.3.

Capacitive-Tip Optimization: The dimensions of the Capacitive-Tip are changed and the simulation results (return loss and impedance) of Antennas **A**, **C** and **D** are presented in Figure 6.9. Antenna **B** is not included because does not have a capacitive-tip structure.

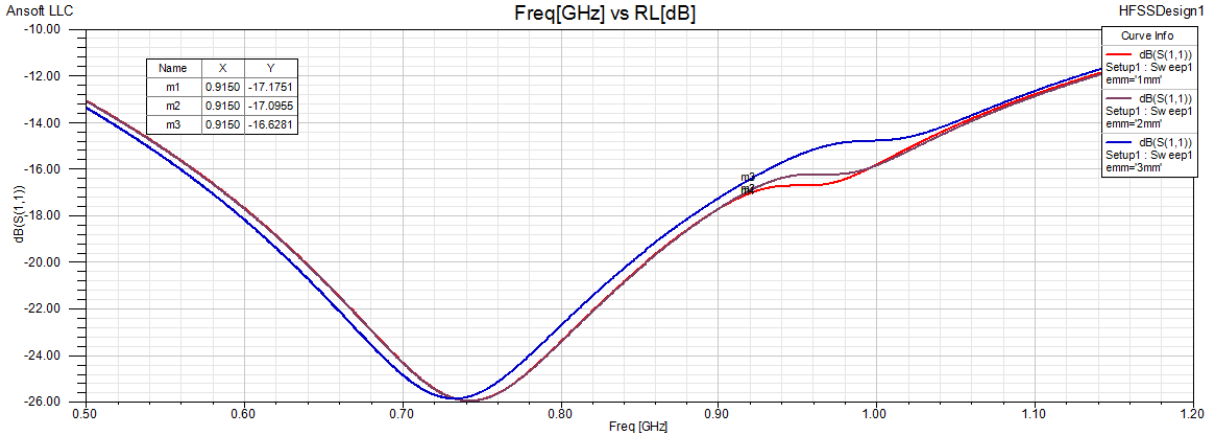

Figure 6.9a Simulation results showing the return loss of the antenna **A** after optimization of the capacitive-tip.

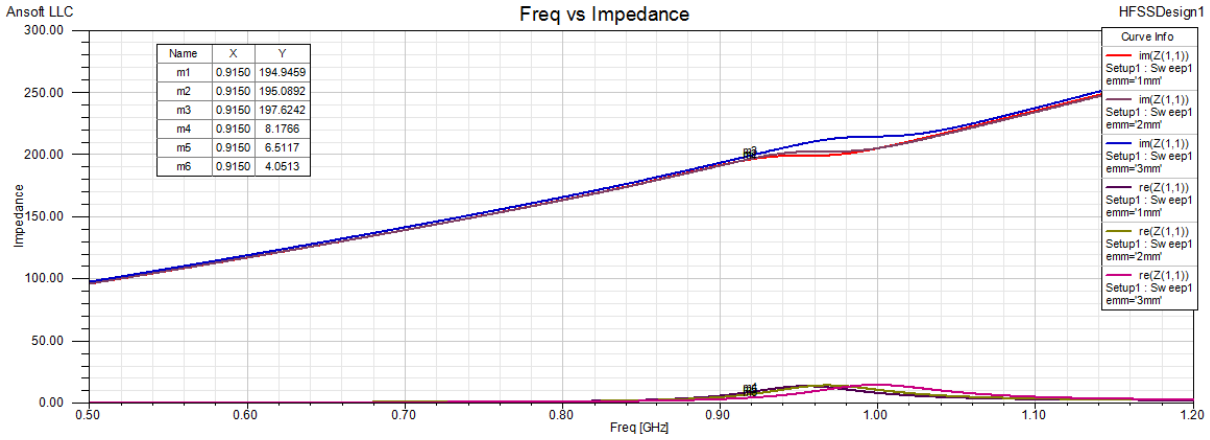

Figure 6.9b Simulation results showing the impedance of the antenna **A** after optimization of the capacitive-tip.

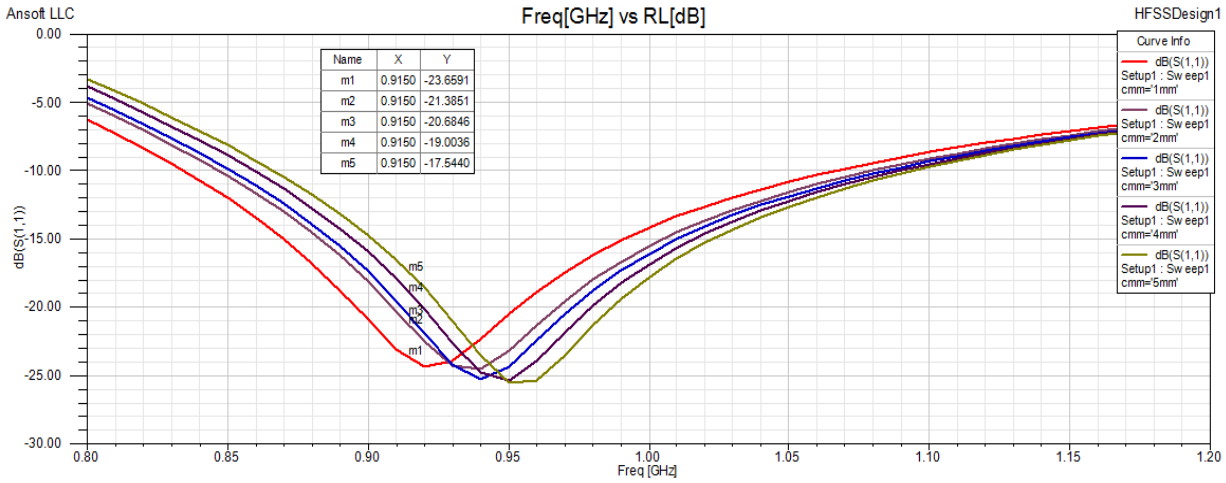

Figure 6.9c Simulation results showing the return loss of the antenna **C** after optimization of the capacitive-tip.

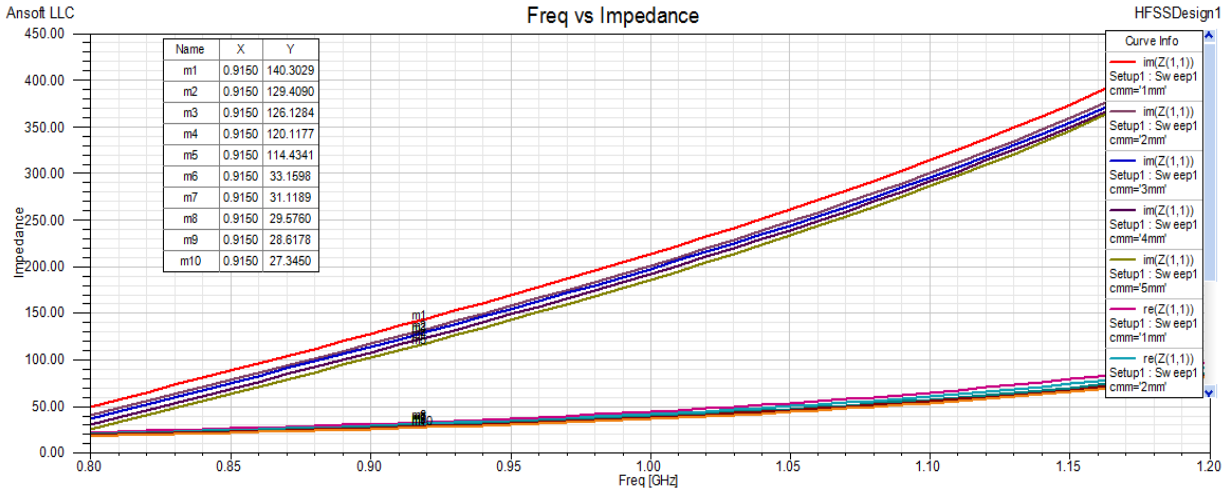

Figure 6.9d Simulation results showing the impedance of the antenna **C** after optimization of the capacitive-tip.

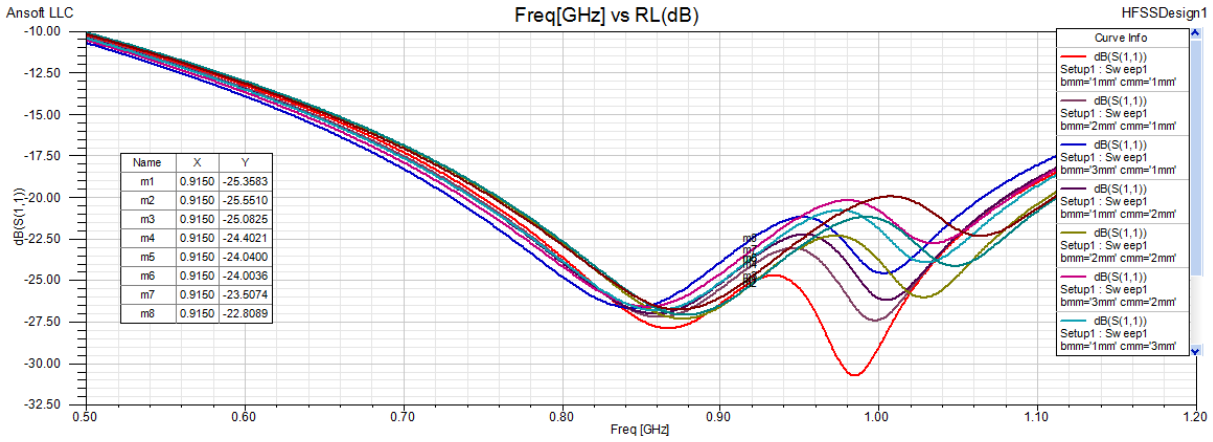

Figure 6.9e Simulation results showing the return loss of the antenna **D** after optimization of the capacitive-tip.

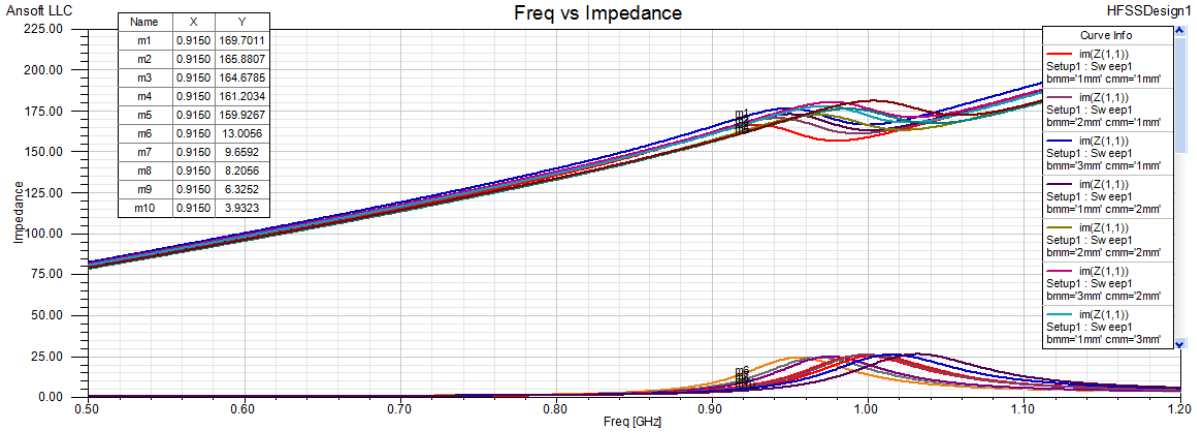

Figure 6.9f Simulation results showing the impedance of the antenna **C** after optimization of the capacitive-tip.

Figure 6.9 Simulation results of capacitive tip optimization of the proposed antennas

As seen from the Figure 6.9, the capacitive-tip has an impact on the impedance of the antenna. In addition, the resonant frequency does not change by changing the dimensions of the capacitive-tip. The difference in changing the dimensions will be further discussed in the section 6.3.

Antenna - Height Optimization: The dimensions of the antenna height are changed and the simulation results (return loss and impedance) of Antennas **A**, **B, C** and **D** are presented in Figure 6.10.

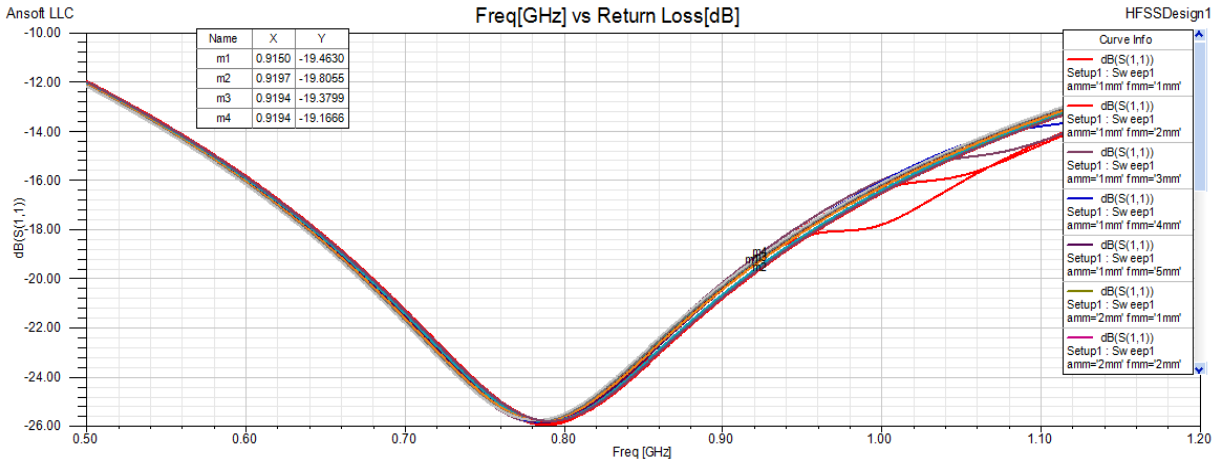

Figure 6.10a Simulation results showing the return loss of the antenna **A** after optimization of the height of the antenna.

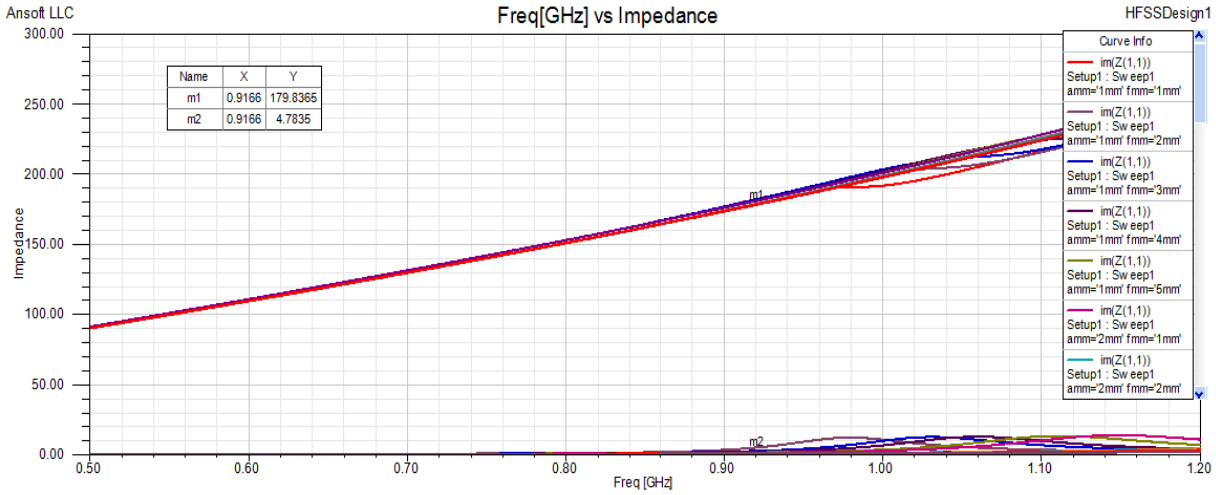

Figure 6.10b Simulation results showing the impedance of the antenna **A** after optimization of the height of the antenna.

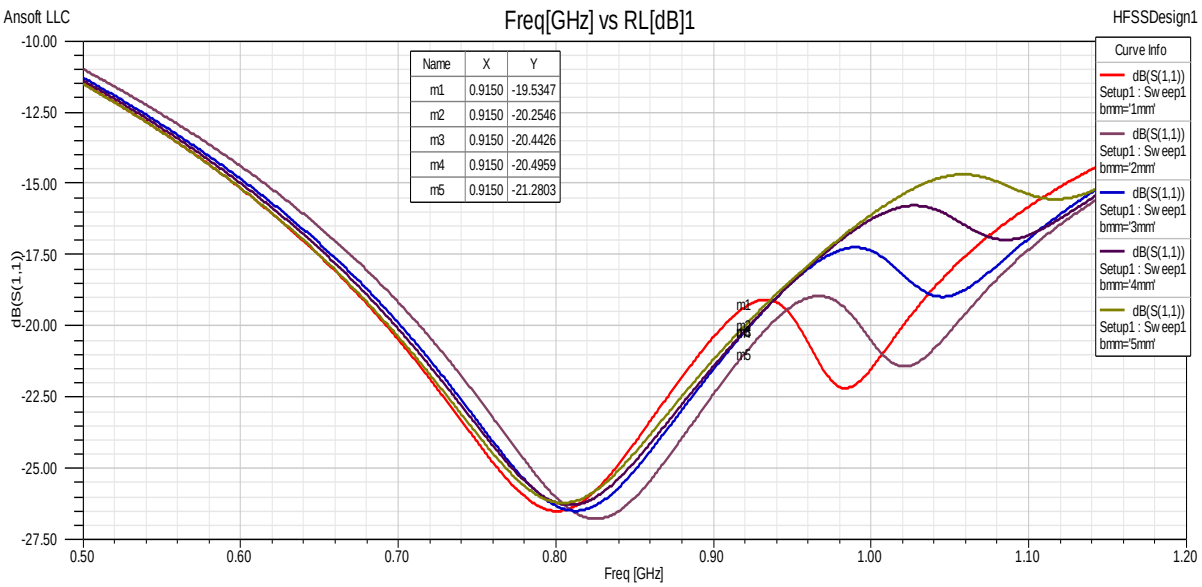

Figure 6.10c Simulation results showing the return loss of the antenna **B** after optimization of the height of the antenna.

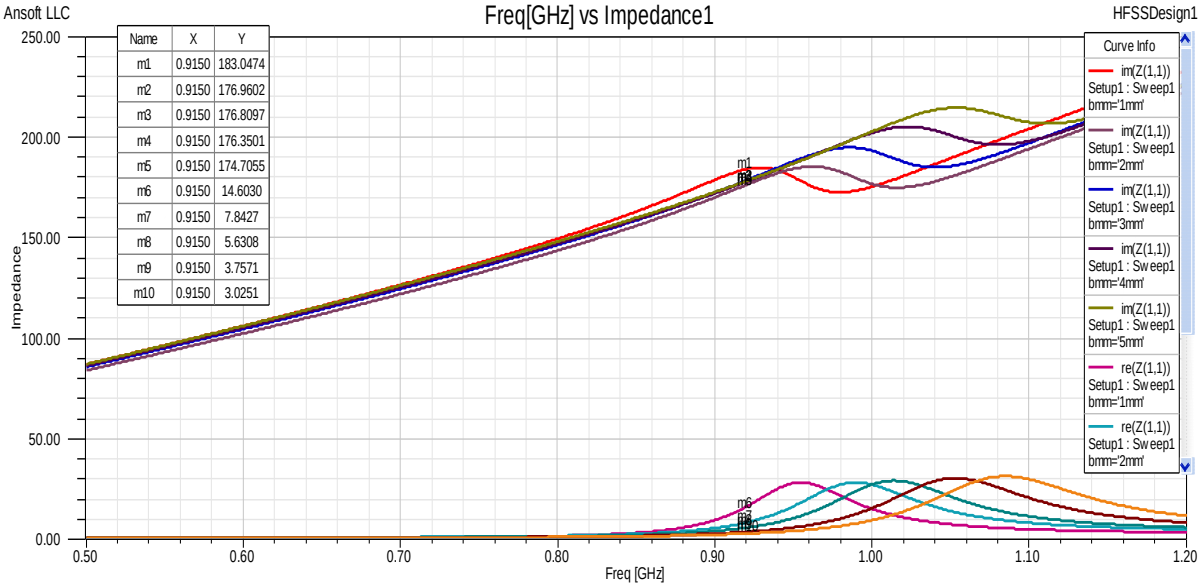

Figure 6.10d Simulation results showing the impedance of the antenna **B** after optimization of the height of the antenna.

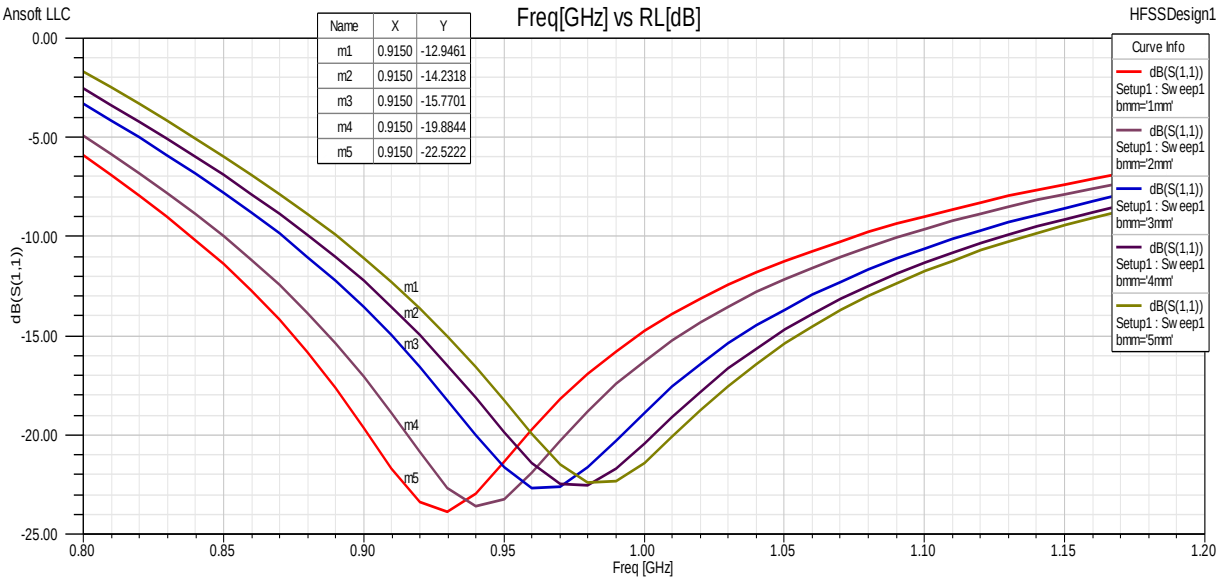

Figure 6.10e Simulation results showing the return loss of the antenna **C** after optimization of the height of the antenna.

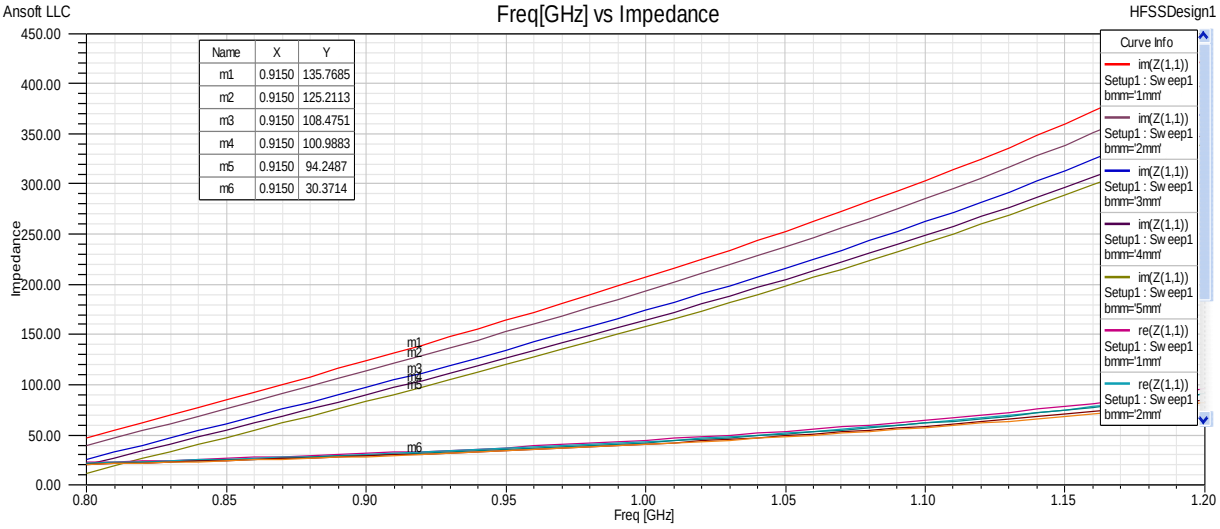

Figure 6.10f Simulation results showing the impedance of the antenna **C** after optimization of the height of the antenna.

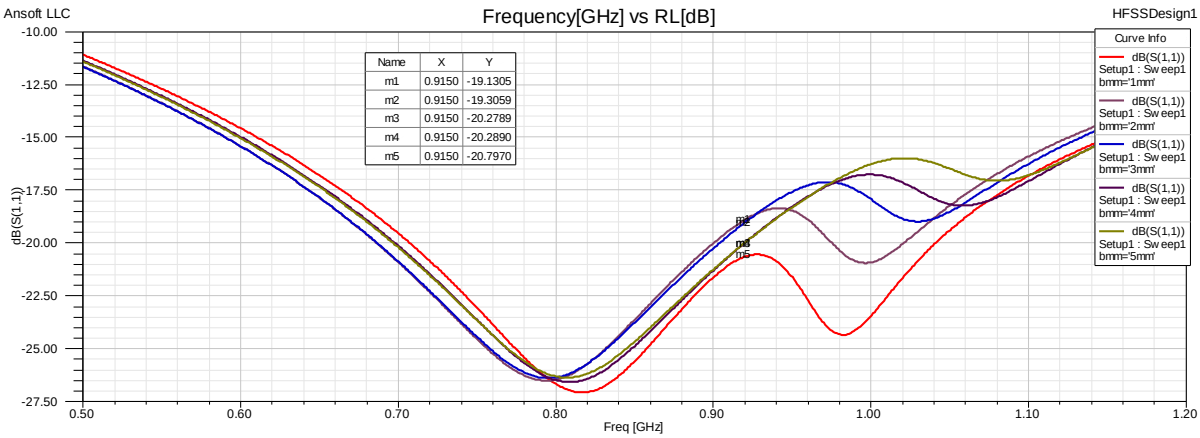

Figure 6.10g Simulation results showing the return loss of the antenna **D** after optimization of the height of the antenna.

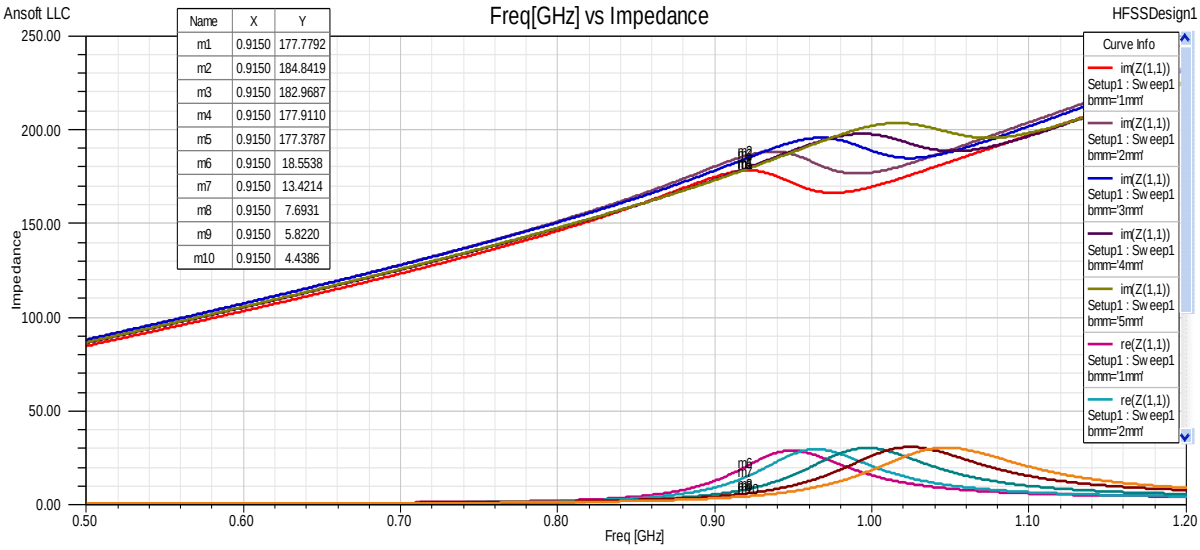

Figure 6.10h Simulation results showing the impedance of the antenna D after optimization of the height of the antenna.

Figure 6.10 Simulation results of height optimization of the proposed antennas

As seen from the Figure 6.10, the height of the antenna structures has an impact on the reactive part of the impedance at the desired frequency of 915 MHz. In addition, the resonant frequency is not affected by changing the height of the antenna designs. The difference in changing the dimensions will be further discussed in the section 6.3.

Antenna - Width Optimization: The dimensions of the antenna width are changed and the simulation results (return loss and impedance) of Antennas **A**, **B, C** and **D** are presented in Figure 6.11.

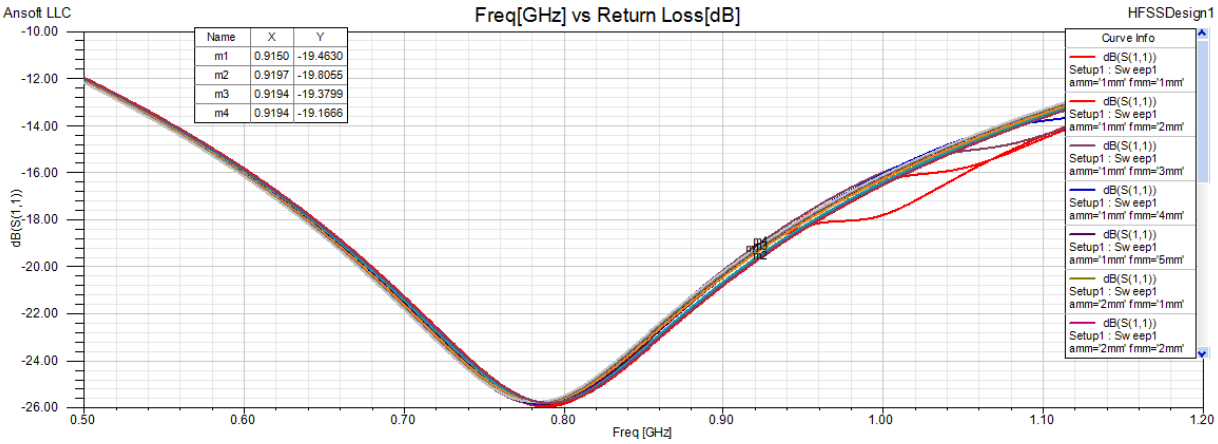

Figure 6.11a Simulation results showing the return loss of the antenna **A** after optimization of the width of the antenna.

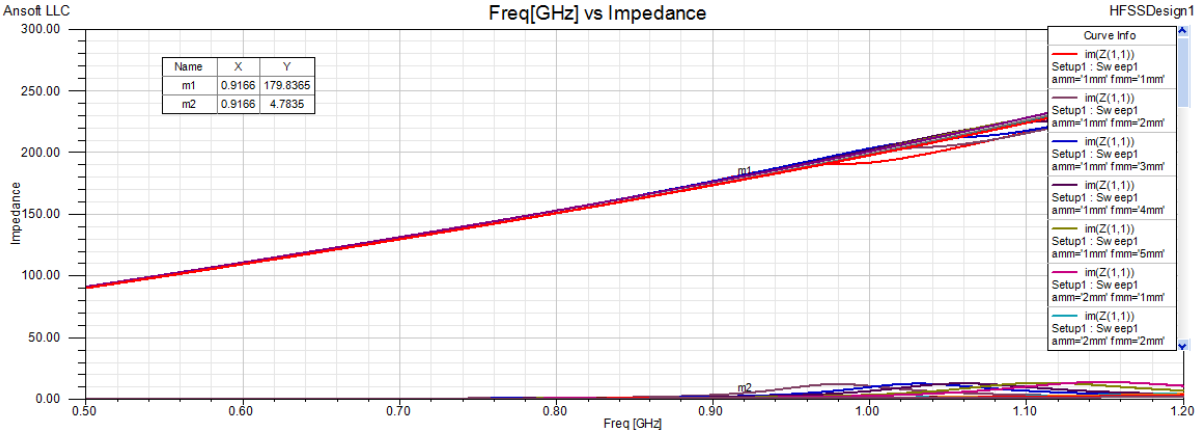

Figure 6.11b Simulation results showing the impedance of the antenna **A** after optimization of the width of the antenna.

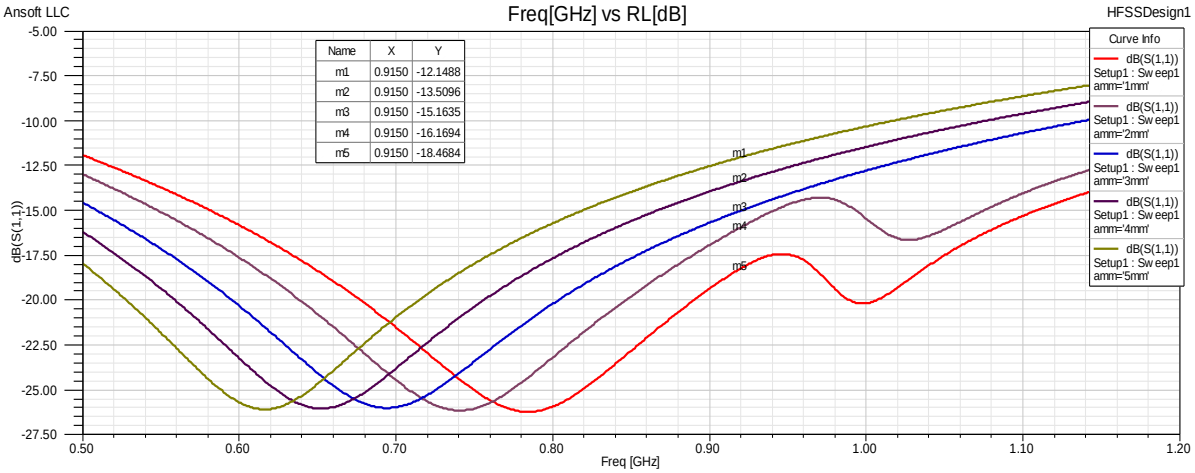

Figure 6.11c Simulation results showing the return loss of the antenna **B** after optimization of the width of the antenna.

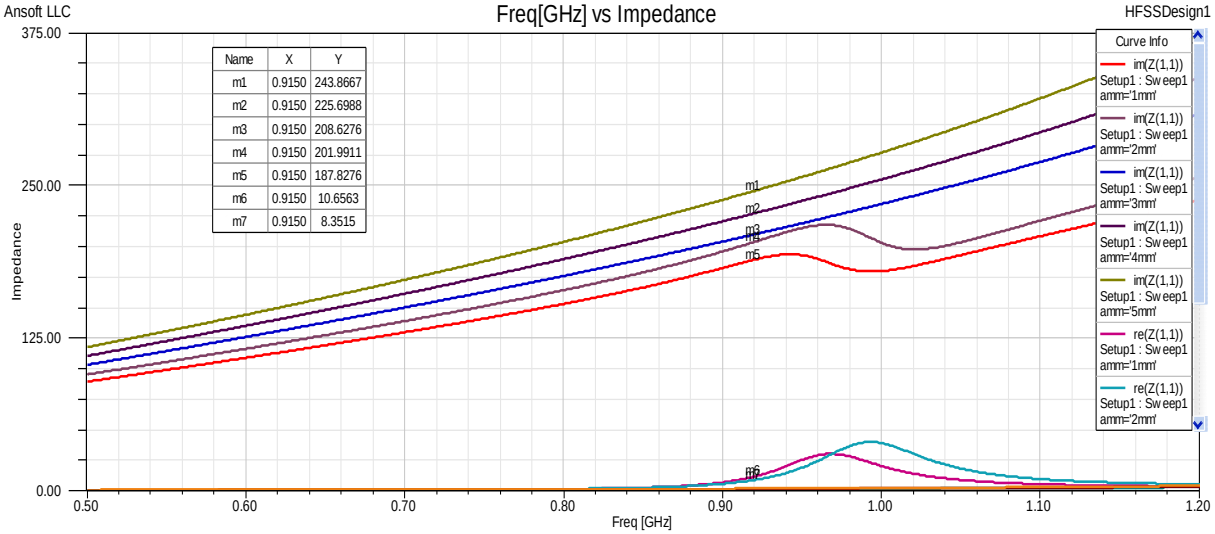

Figure 6.11d Simulation results showing the impedance of the antenna **B** after optimization of the width of the antenna.

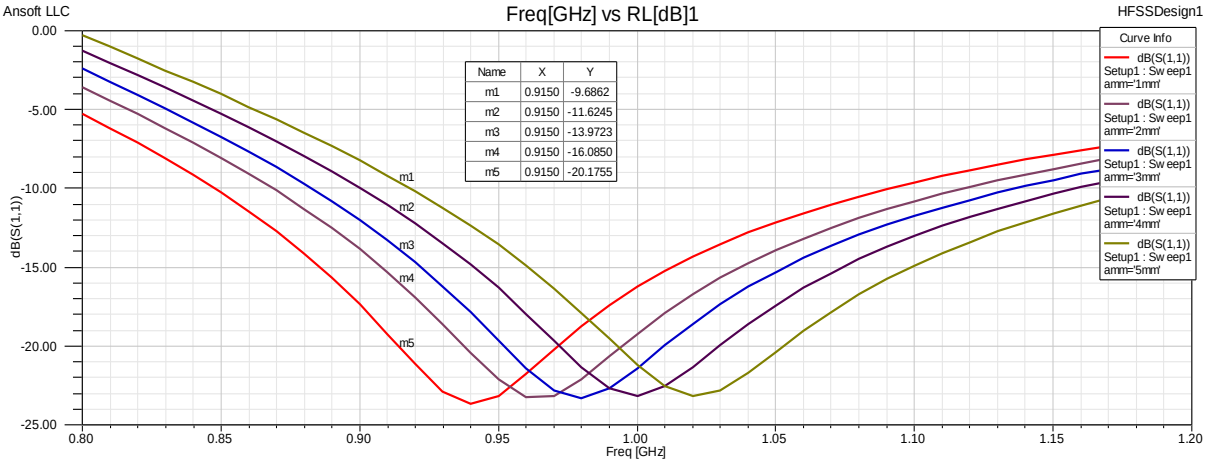

Figure 6.11e Simulation results showing the return loss of the antenna **C** after optimization of the width of the antenna.

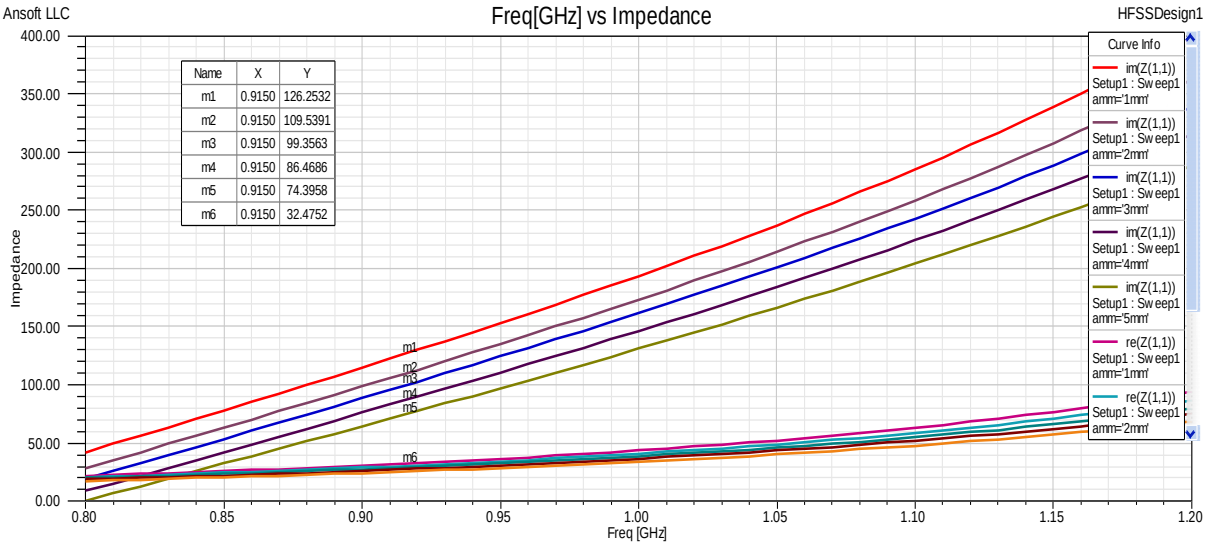

Figure 6.11f Simulation results showing the impedance of the antenna **C** after optimization of the width of the antenna.

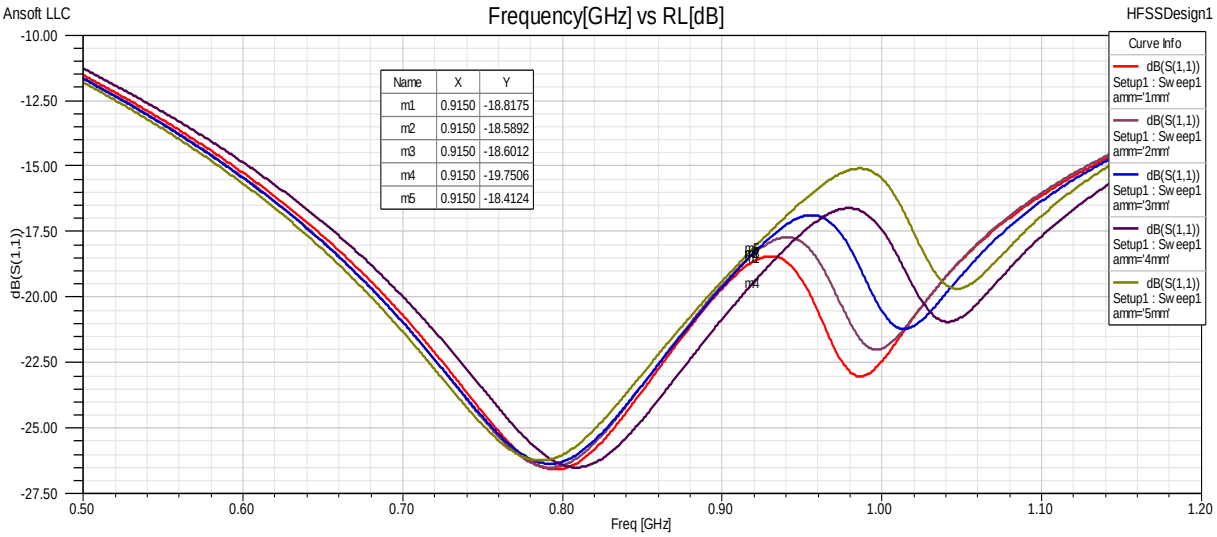

Figure 6.11g Simulation results showing the return loss of the antenna **D** after optimization of the width of the antenna.

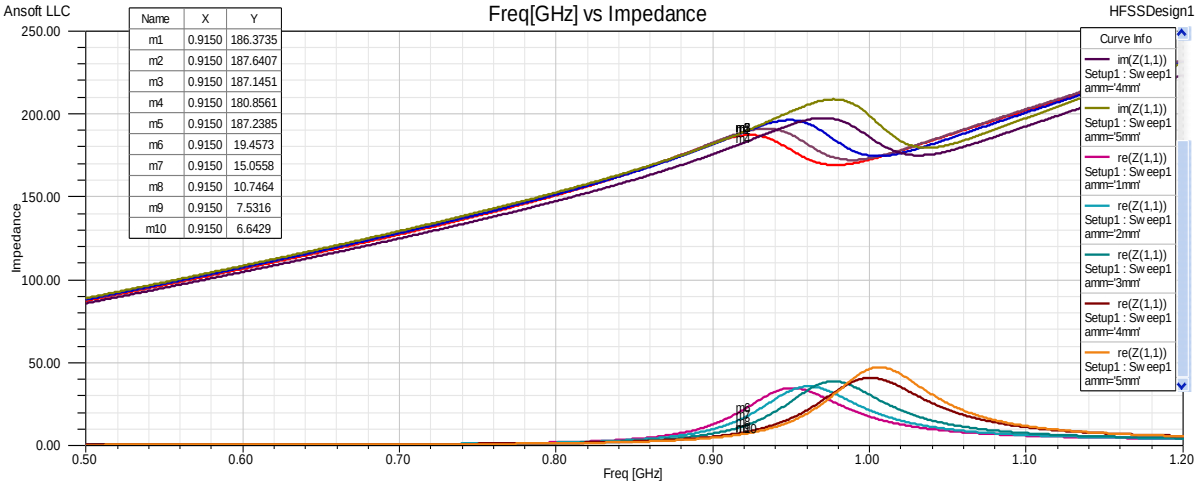

Figure 6.11h Simulation results showing the impedance of the antenna **D** after optimization of the width of the antenna.

Figure 6.11 Simulation results of width optimization of the proposed antennas.

As seen from the Figure 6.11, the width of the antenna structures has an impact on the real part of the impedance at the desired frequency of 915 MHz. In addition, the resonant frequency is not affected by changing the height of the antenna designs. The difference in changing the dimensions will be further discussed in the section 6.3.

Substrate Optimization: The dimensions of the substrate height and width are changed and the simulation results (return loss and impedance) of Antennas **A**, **B, C** and **D** are presented in Figure 6.12. The dimensions of the height and width are changed uniformly together.

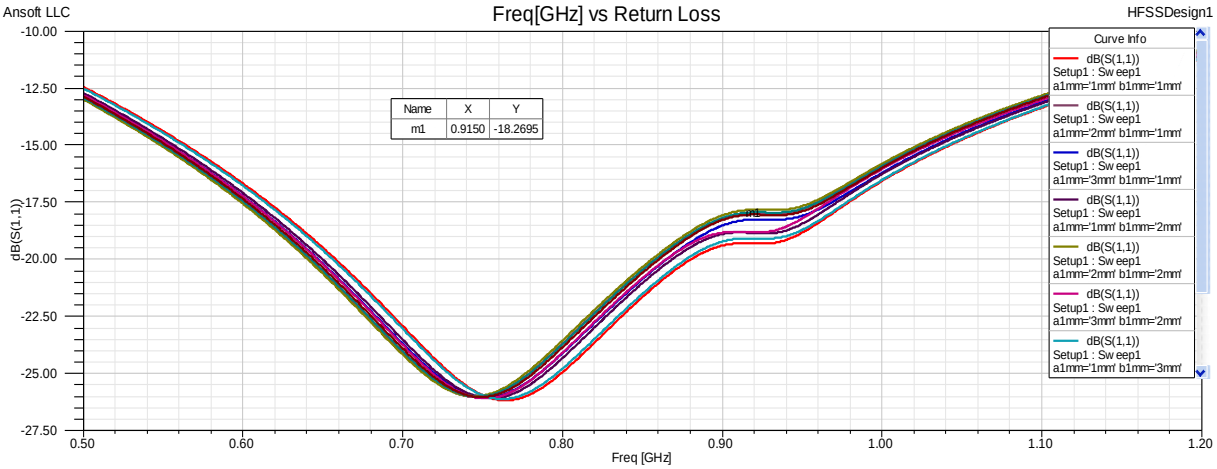

Figure 6.12a Simulation results showing the return loss of the antenna **A** after optimization of the substrate of the antenna.

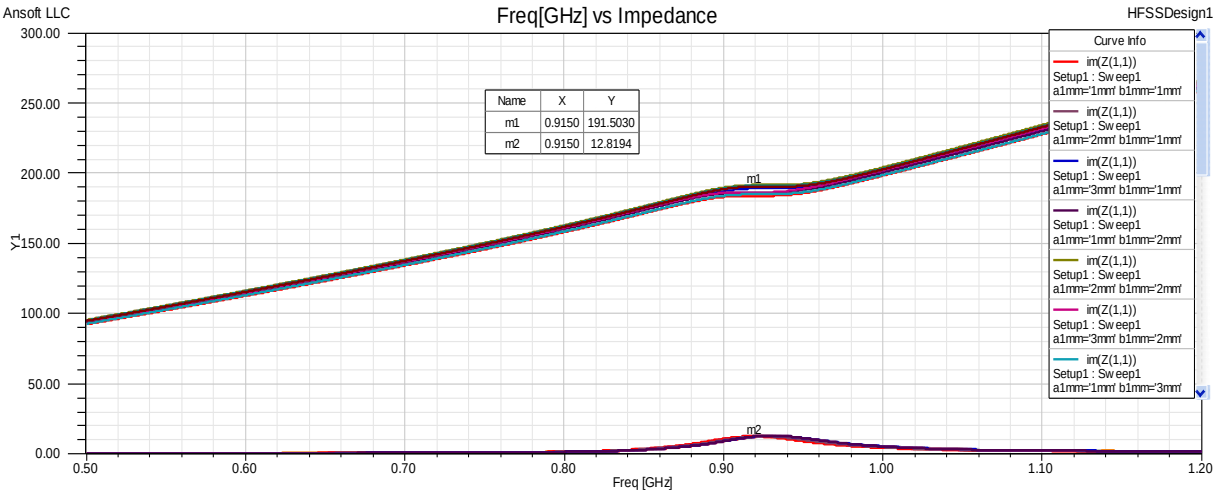

Figure 6.12a Simulation results showing the impedance of the antenna **A** after optimization of the substrate of the antenna.

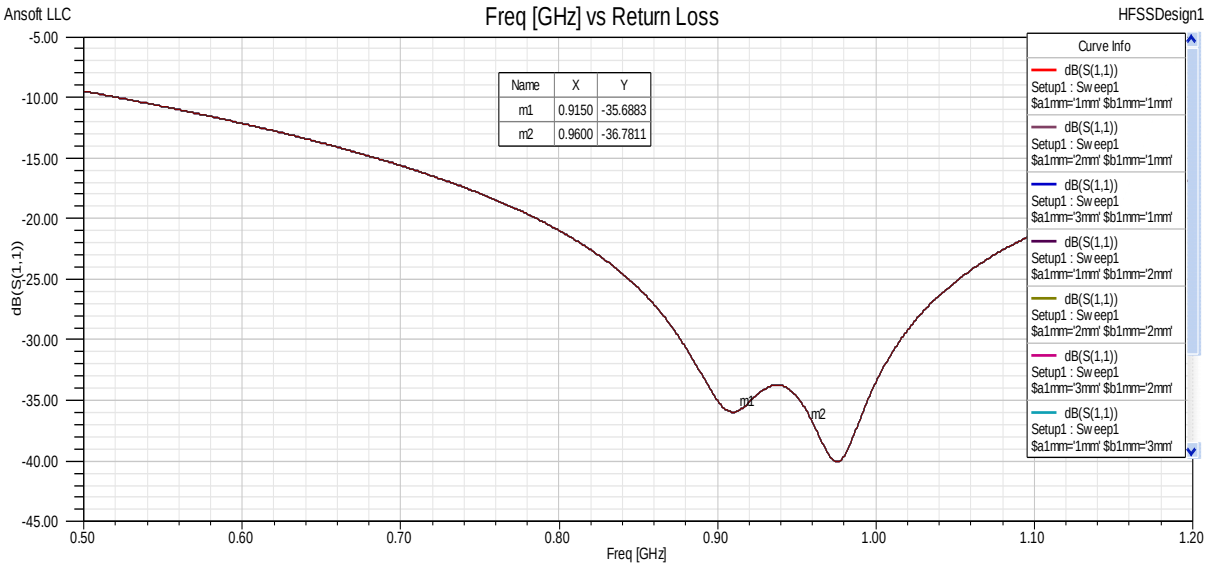

Figure 6.12c Simulation results showing the return loss of the antenna **B** after optimization of the substrate of the antenna.

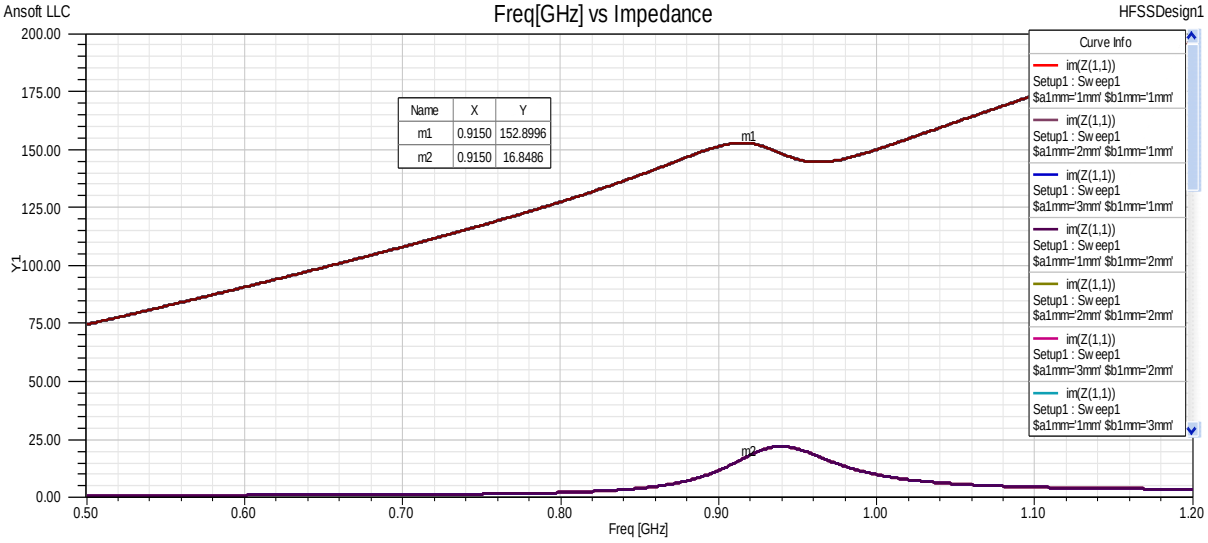

Figure 6.12d Simulation results showing the impedance of the antenna **B** after optimization of the substrate of the antenna.

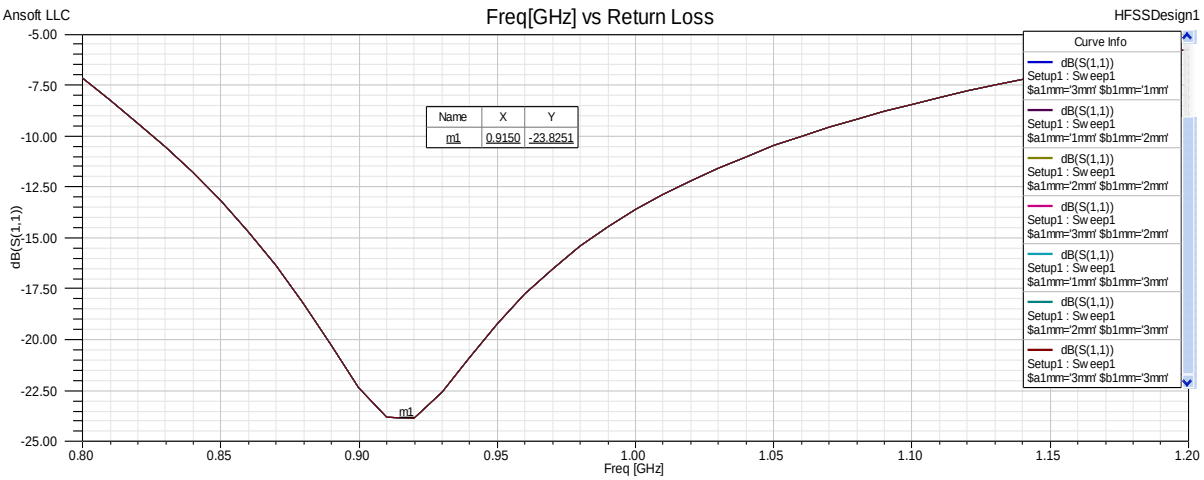

Figure 6.12e Simulation results showing the return loss of the antenna **C** after optimization of the substrate of the antenna.

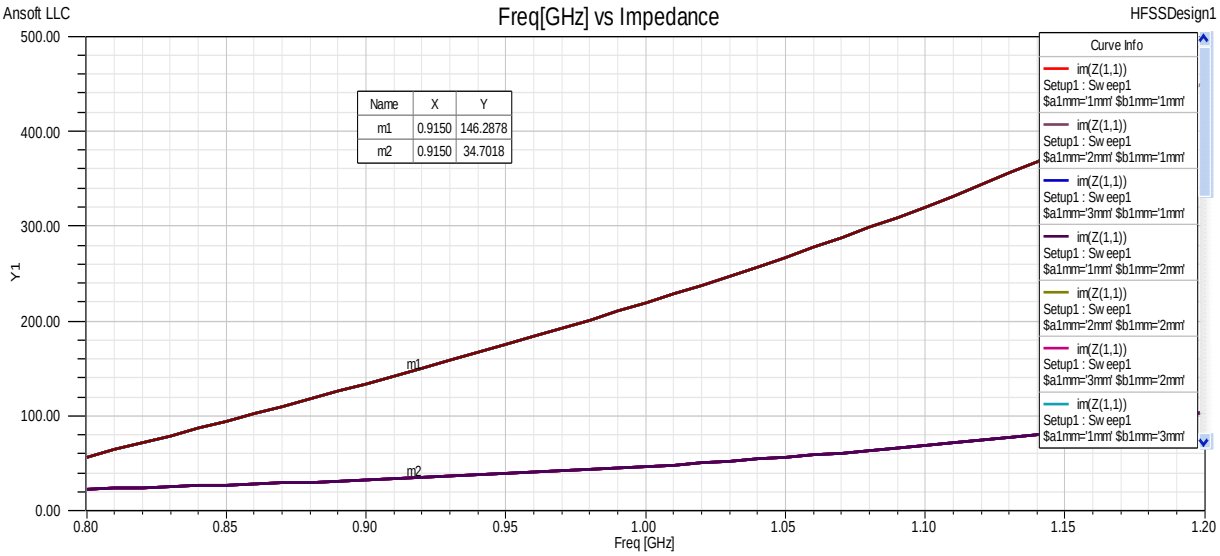

Figure 6.12f Simulation results showing the impedance of the antenna **C** after optimization of the substrate of the antenna.

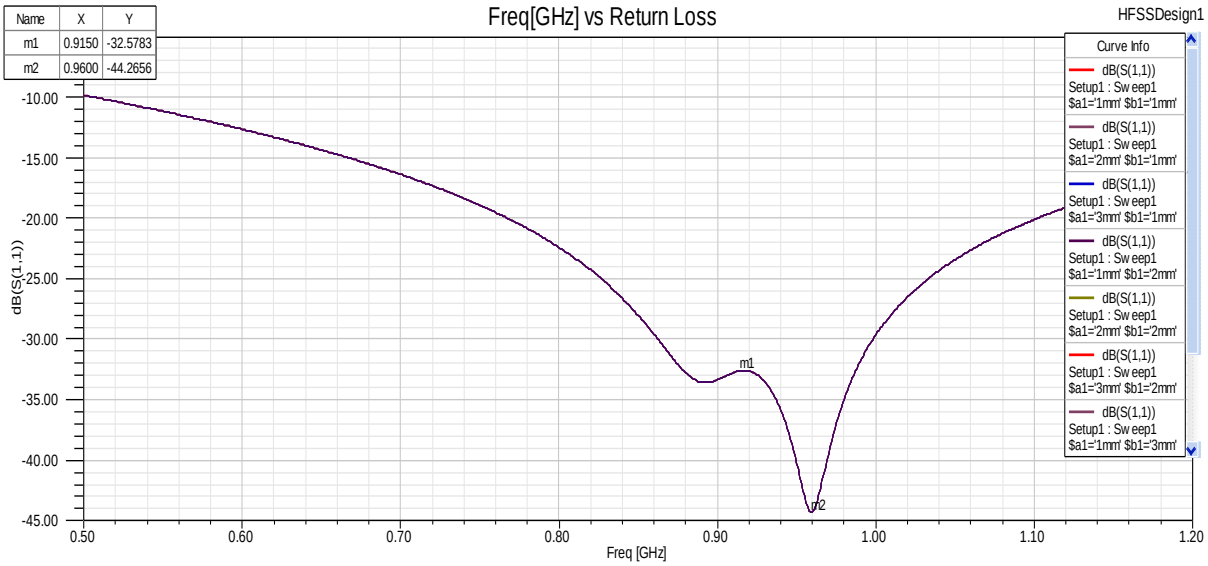

Figure 6.12g Simulation results showing the return loss of the antenna **D** after optimization of the substrate of the antenna.

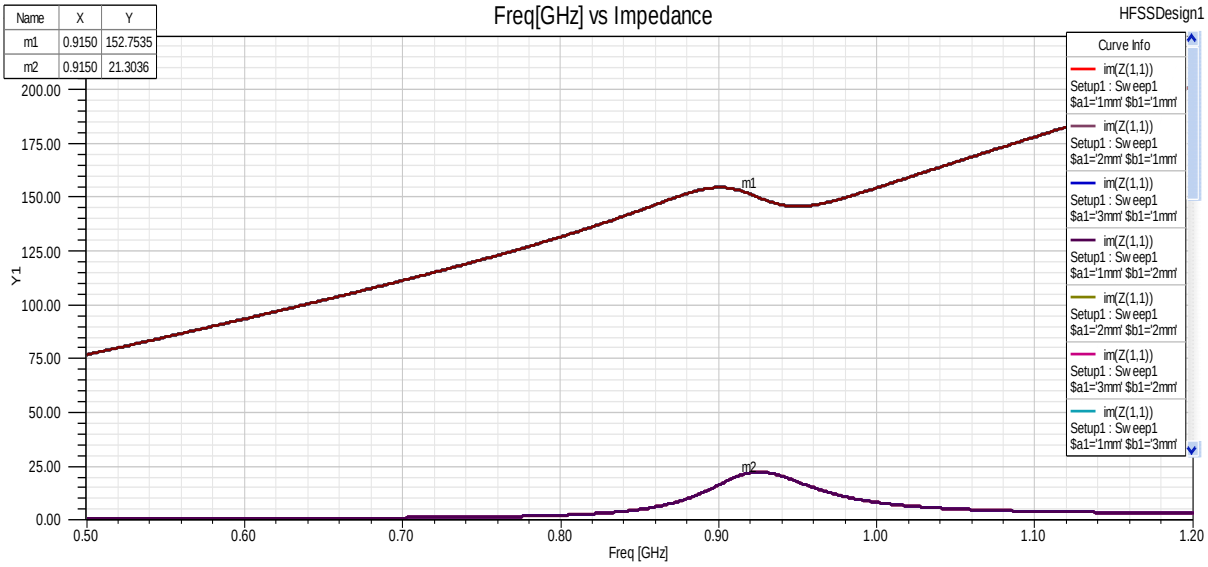

Figure 6.12h Simulation results showing the return loss of the antenna **D** after optimization of the substrate of the antenna.

Figure 6.12 Simulation results of substrate optimization of the proposed antennas

As seen from the Figure 6.12, changing the dimensions of the substrate has a minimal impact on the return loss and the impedance of the antenna designs.

6.3 Discussion of Simulation Results

All the antenna designs except antenna design **E** were simulated using HFSS. The results show that changing the dimensions of the proposed antenna impacts antenna parameters such as return loss and impedance. Furthermore, the results obtained can help antenna designers pick necessary dimensions for the proposed applications for optimal tag performance criteria such as chip impedance matching, return loss, improved read range, etc.

The optimization results show that the substrate has a minimal impact on the return loss and the impedance of the antenna designs. This effect of the four specific antenna parts namely, the height, the width, the capacitive-tip and the inductive coil are listed in table 6.6.

Table 6.6 The effect of antenna designs parts on return loss and impedance after optimization.

Antenna	Inductive loop	Capacitive-Tip	Height	Width
A	Significant Impact on return loss	Minimal impact on impedance	Minimal impact on impedance	Minimal impact on impedance
B	Significant Impact on return loss	None (no capacitve-tip)	Real part of impedance	Imaginary part of impedance
C	None (no loop)	Improves return loss and impedance	Return loss and Imaginary impedance	Return loss and Imaginary impedance
D	Significant Impact on return loss	Improves return loss only	Real part of impedance	Imaginary part of impedance

After the optimization process, the final antenna design dimensions proposed for each antenna are listed in table 6.7

Table 6.7 The final antenna design dimensions (mm) after optimization.

Antenna	A1	B1	a	b	c	D	E	f	g	H	I
A	97.5	34.7	41	15	27	2	15	15.7	-	-	-
B	94	18.5	9.8	16.5	5.5	2	6.7	9.7	-	-	-
C	120	40	50	23	32	4	19	-	-	-	-
D	94	24.5	44	20.5	19	2	7.5	5.5	15	9.7	6.7
E	100	60	80	40	-	-	-	-	-	-	-

The antenna design **E** was not discussed until now because it was not simulated using HFSS. The application of antenna design **E** is contactless proximity cards (ISO 14443) as seen in Figure 6.13. Furthermore, an industry provided antenna simulator tool [51] was used to design the antenna as shown in Figure 6.14. The antenna design **E** is designed to operate at a high frequency value of 13.56 MHz. The main design shape for this antenna is an inductive coil [51], [13] and [55].

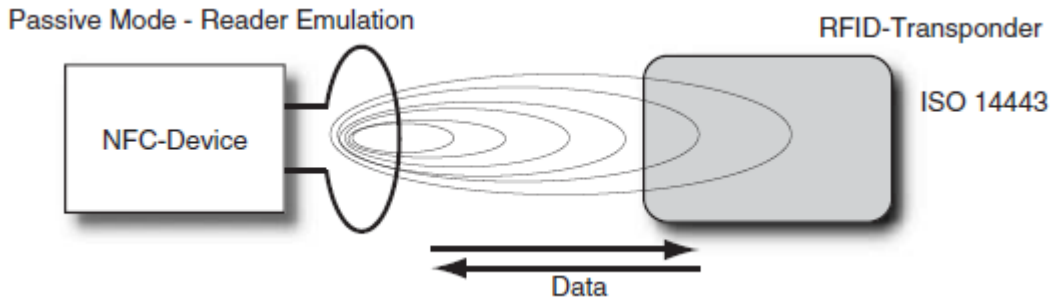

Figure 6.13 Passive RFID transponder for high frequency (13.56 MHz) application.

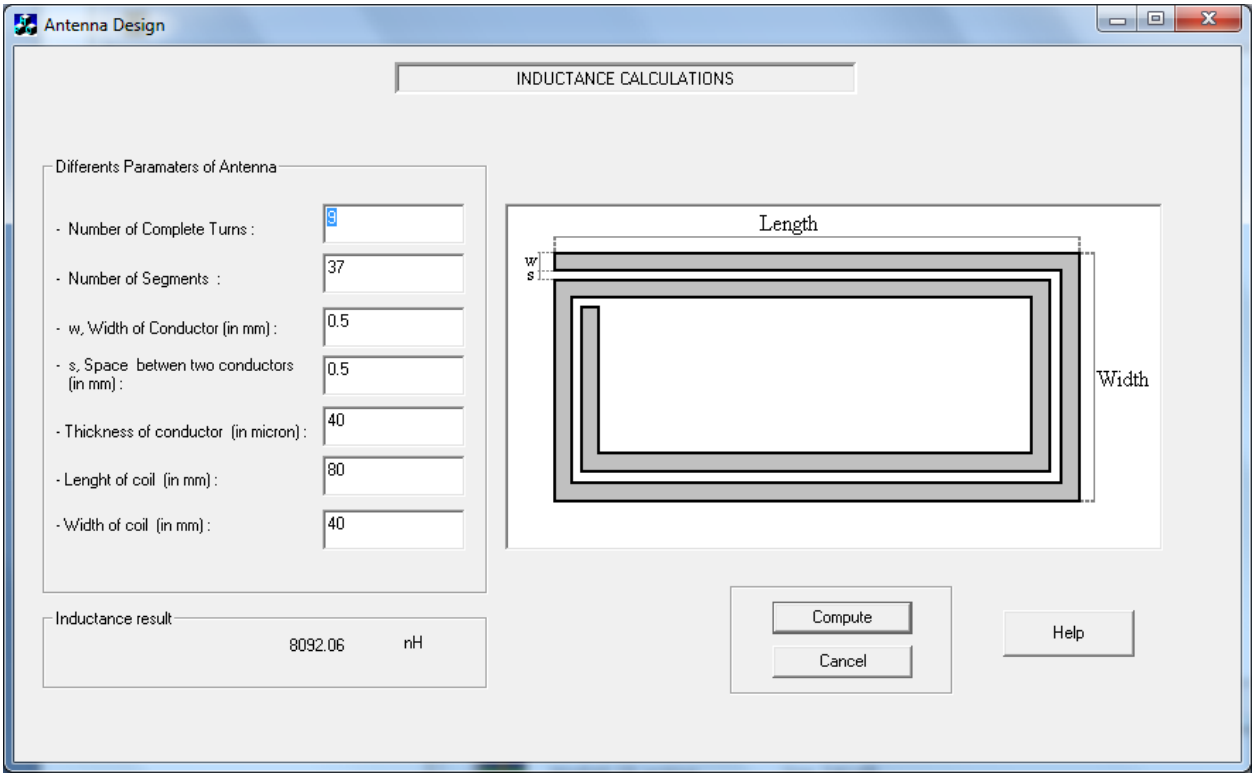

Figure 6.14 Inductive coil antenna design for high frequency (13.56 MHz) application.

As proposed by [4] equation (21), the impedance matching is achieved by calculating the right antenna coil inductance.

$$L_{ant} = \frac{1}{(2\pi f_o)^2 . C_{tun}} \quad (21)$$

In equation (21) [52], f_o is 13.56 MHz and C_{tun} is 17pF. Therefore, the required inductance value after using the antenna simulator is found to be 8.092 nH.The chip chosen for this application is the NXP Mifare and has an impedance of 17 pF. In order, to match this impedance the inductance value obtained should be 8.103 nH.

6.4 Chapter Summary

In this chapter the simulation results of the designed tags based on the application of use were presented. The simulation software HFSS was used to optimize the dimensions of the proposed antenna. The different antenna designs (A, B, C, D and E) and the advantages of using the particular geometry were discussed. The results show the impact of changing the

dimensions on antenna parameters such as return loss and impedance. Furthermore, the results obtained can help antenna designers pick necessary dimensions for the proposed applications for optimal tag performance criteria such as chip impedance matching, return loss, improved read range, etc. The parametric study and optimization of the proposed designs were achieved using the FEM design tool. The simulations results provided help select the best possible geometric dimensions for the proposed antennas before the actual fabrications process. Therefore, the RF designers can be confident in the tag antenna design before the fabrication process, thereby assuring a low cost solution to RFID system. Finally, antenna design **E** was discussed briefly as it involves high frequency (13.56 MHz) applications such as contactless cards.

CHAPTER 7 – Experimental Measurements and Results

Passive RFID tags are usually fabricated after the antenna design dimensions are fixed after the optimization process. The fabrication is the last step in the RFID tag design process. After fabrication, the design is tested using a Vector Network Analyzer (VNA) for the antenna impedance and the read range distance (m) is measured inside an anechoic chamber both of which have been discussed in detail in chapter 3, section 3.3.

In this chapter the proposed antenna design A,B,C,D are tested using tag testing procedures for long range RFID tags. The antenna design **E** is tested using a near-field reader because it represents a contactless near-field application. The experimental results are shown in sections 7.1 (read range) and 7.2 (impedance measurement). The comparison of measurement results versus simulation results are presented in section 7.3. The fabricated antenna designs are shown in Figure 7.1. The goal is to match experimental results to the simulated results from Chapter 6 in order to verify that the optimization results have improved the RFID tag antenna design process.

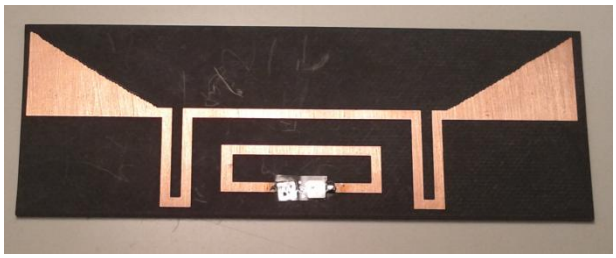

Figure 7.1a Antenna deign **A** (Broadband)

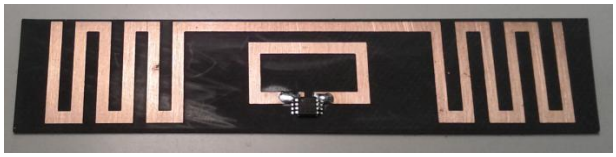

Figure 7.1b Antenna deign **B** (Meander dipole)

Figure 7.1c Antenna deign **C** (Two-Wire folded dipole)

Figure 7.1d Antenna deign **D** (Baggage tag dipole)

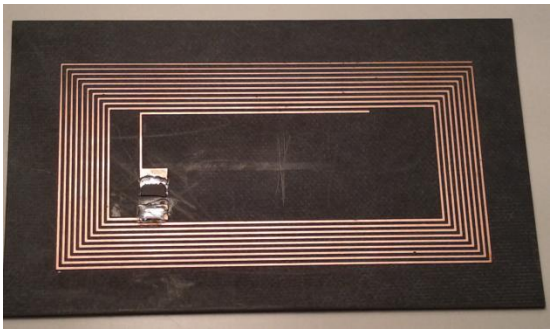

Figure 7.1e Antenna deign **E** (Contactless card)

Figure 7.1 Pictures of the fabricated antenna designs

7.1 Read Range

The read range distance measurement for RFID tags was carried out in an anechoic chamber. The tags are placed at a fixed distance of 5 meters from the reader as seen in Figure 7.2a, 7.2b. The frequency of interest is 915 MHz and the RFID reader used is Convergence Systems Limited CSL CS203. The power of the reader was set to 30 dbm and the read-count was observed on the computer attached to the reader.

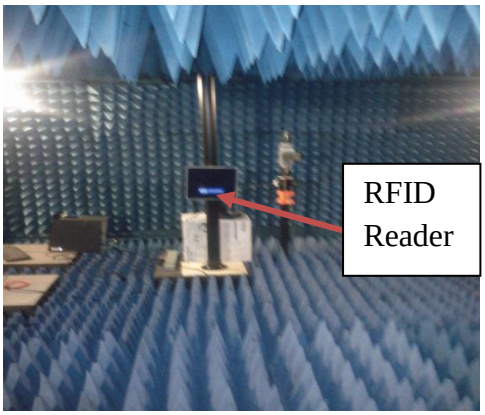

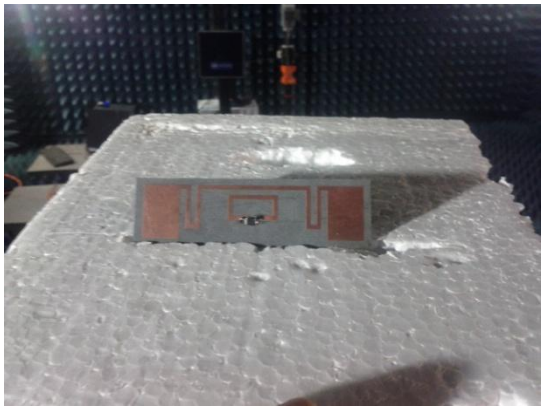

Figure 7.2a measurement setup [3]. **Figure 7.2b** RFID tag placed on a foam stand [3].

The range can be calculated using equation (4) from chapter 3, section 3.3.

$$r_0 = d\sqrt{\frac{EIRP}{P_{min}LG_t}} \quad (9)$$

At each frequency, the minimum power P_{min}, needed to communicate with the tag is recorded. Since the loss L of the connecting coaxial cable, the gain of the transmitting antenna G_t, the distance d to the tag are known, the tag range for any transmitter EIRP (effective isolated radiated power) can be determined from (9).

The anechoic chamber facility has a length of approximately 5 meters and all four antenna designs were read at the distance of 5 meters inside the chamber. The distance outside the anechoic chamber was recorded as well and the results are presented in Table 7.1. However, the results taken outside the anechoic chamber do not account for reflections and multipath signal interference.

Table 7.1 Read distance of the antenna designs in a corridor

Antenna	**Distance (meters)**
A	6.09 m
B	7.16 m
C	13.9 m
D	9.44 m

7.2 Impedance Measurement

Most RFID tags are balanced dipoles [21] and this makes it harder to measure the electrically small antennas directly using a vector network analyzer (VNA). To overcome this problem an experimental setup was used as proposed by [21] and discussed in detail in chapter 3, section 3.3. The tag antennas were cut in half and mounted on brass sheet (16cm x 16cm) and placed on the metal plate (0.46m x 0.8m) as shown in Figure 7.3.

Figure 7.3a Half tag placed on plate.

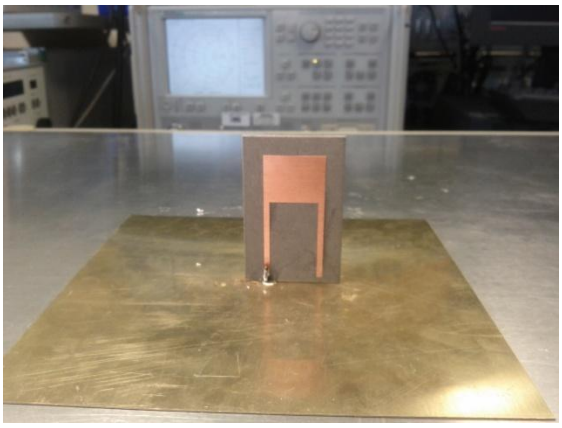

Figure 7.3b Half-tag mounted on brass sheet.

The measurement taken by the VNA shows only half the impedance as well as half the return loss. For example, if the VNA reading shows 4 + j 55Ω then, the full tag impedance will be double this value, 8 + j 55Ω. The impedance to be matched for antenna designs A, B, D is 16 + j148 Ω. For this experiment, the VNA has to be calibrated properly before use. The RF cable is connected from the VNA to a SMA connector placed underneath the metal plate as shown in Figure 7.4.

Figure 7.4 RF cable connecting VNA to the SMA connector.

The calibration of the VNA is a very important step. It is typically done with a 50 Ohm balanced load. The results of the VNA calibration are shown in Figure 7.5.

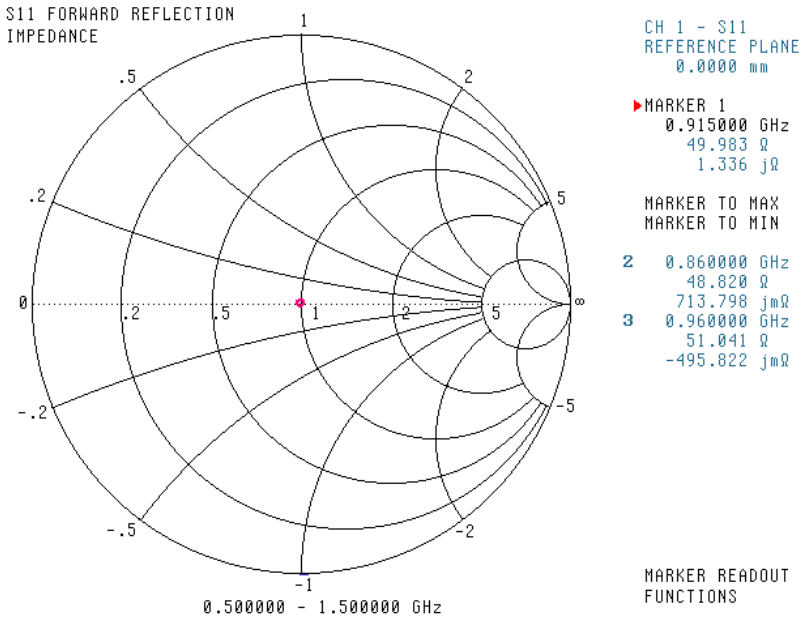

Figure 7.5a Impedance of the VNA with a matched 50 Ohm load.

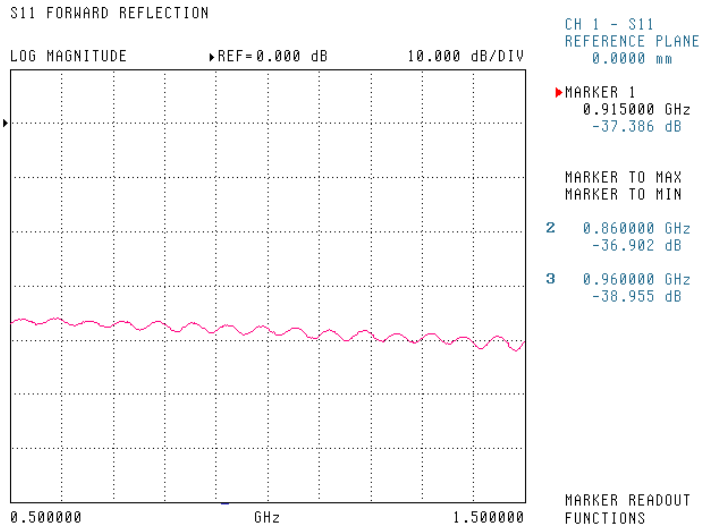

Figure 7.5b Return Loss of the VNA with a matched 50 Ohm load.

It was observed that the brass plate has minimal impact on the impedance value when connected to the VNA. The results below show the return loss as well as the impedance for the four antenna designs.

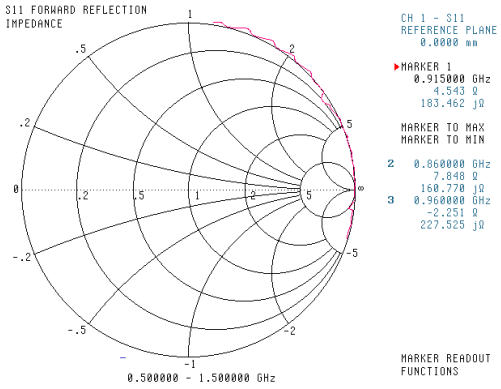

Figure 7.6a Impedance of Antenna **A**.

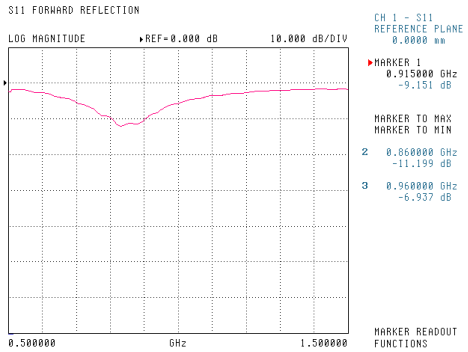

Figure 7.6b Return Loss (dB) of Antenna **A**

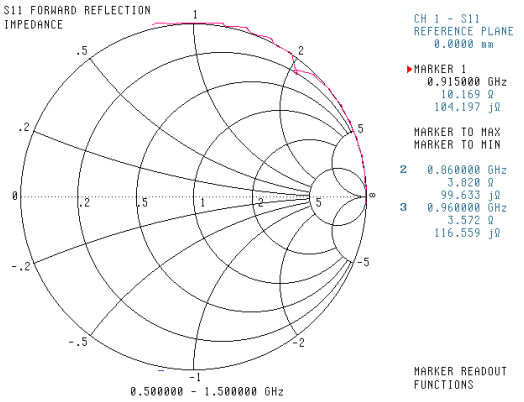

Figure 7.6c Impedance of Antenna **B**.

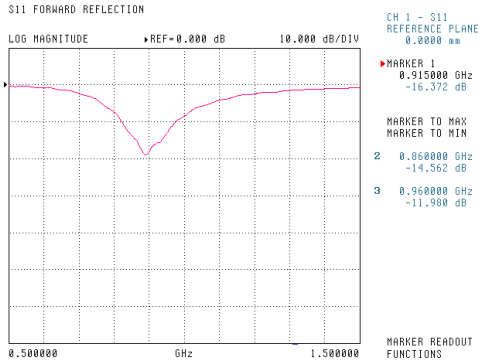

Figure 7.6d Return Loss (dB) of Antenna **B**

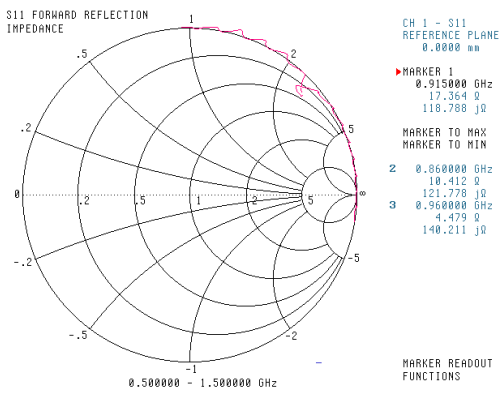

Figure 7.6f Impedance of Antenna **C**

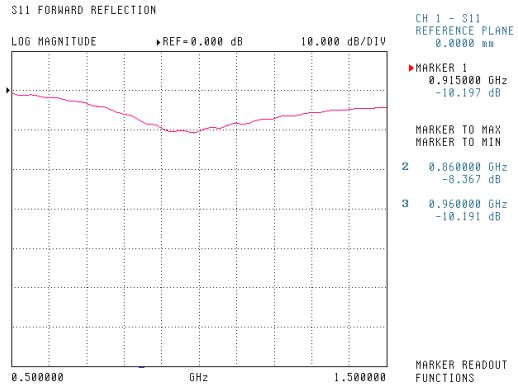

Figure 7.6g Return Loss (dB) of Antenna **C**

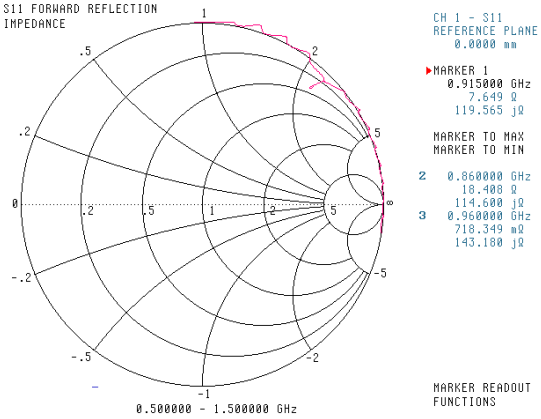

Figure 7.6h Impedance of Antenna **D**

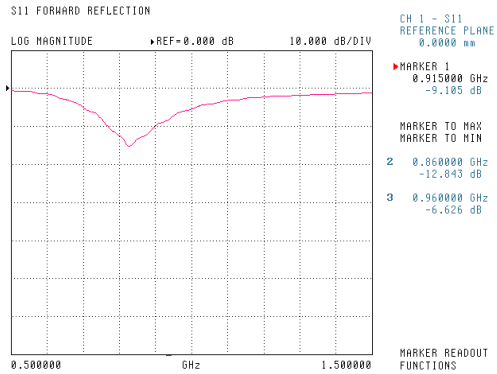

Figure 7.6i Return Loss (dB) of Antenna **D**

Figure 7.6 Measured impedance and return loss of the proposed antennas.

7.3 Comparison of simulated and measured results

This section provides the comparison of the measured versus the simulated results. The impedance at 915 MHz of the antenna designs A, B, C and D and other antenna parameters such as read range, gain and return loss are displayed in table 7.2.

Table 7.2 Simulated and measured results.

Antenna	Simulated Impedance (Ohm)	Measured Impedance (Ohm)	Simulated Return Loss (dB)	Measured Return Loss (dB)	Theoretical Read Range (m)	Measured Read Range (m)
A	10.9 + j 180.9 Ω	9 + j 320 Ω	19.91	18.2	9.86	6.09
B	18.1 + j 146.5 Ω	20 + j 205 Ω	41.20	32.8	11.76	7.16
C	14.2 + j 141.2 Ω	34.6 + j 240 Ω	23.20	20.4	8.21	13.9
D	21.1 + j 148.5 Ω	15 + j 240 Ω	35.34	18.20	12.68	9.44

The results from the simulation and measurement show close agreement when comparing the return loss (dB) values. Furthermore, it was observed that the RF cable when connected to the 50 Ohm matched load showed perfect matching. However, the SMA connector connected to the experimental table was found to show some discrepancy. Therefore, the measured impedance values do not exactly match the simulated impedance values. In addition, the simulation setup is not entirely the same as the experimental setup i.e. no table or connector or large radiation boundary was modeled in the simulation. Nevertheless, the measured results show very good read range values which indicates good tag performance characteristics and satisfies the requirements of the application such as pharmaceutical, clothing, inventory, etc.

The return loss graph for the simulated and measured values is shown in 7.7.

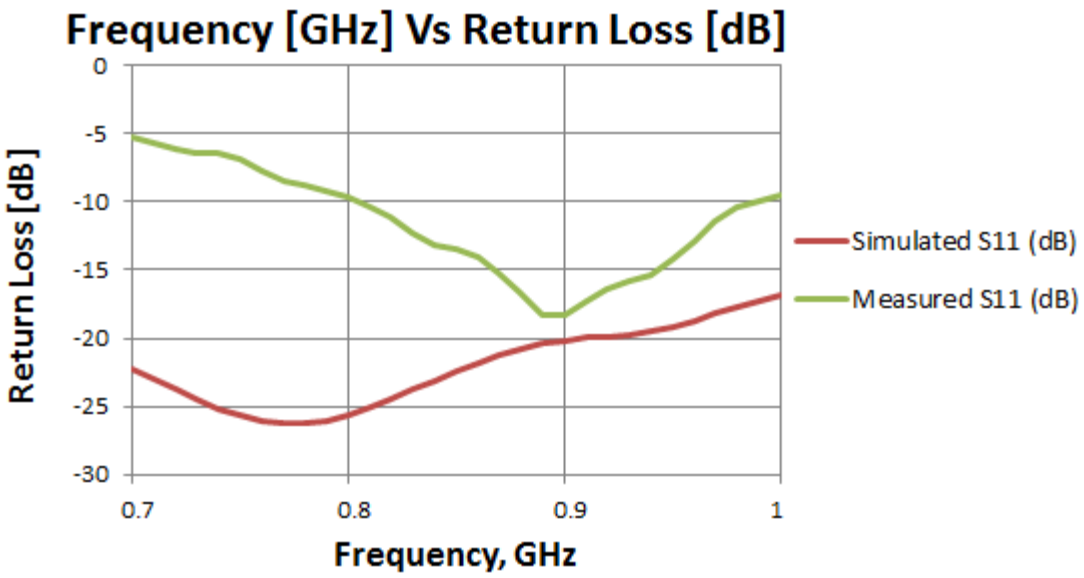

Figure 7.7a Return Loss (dB) of Antenna **A**

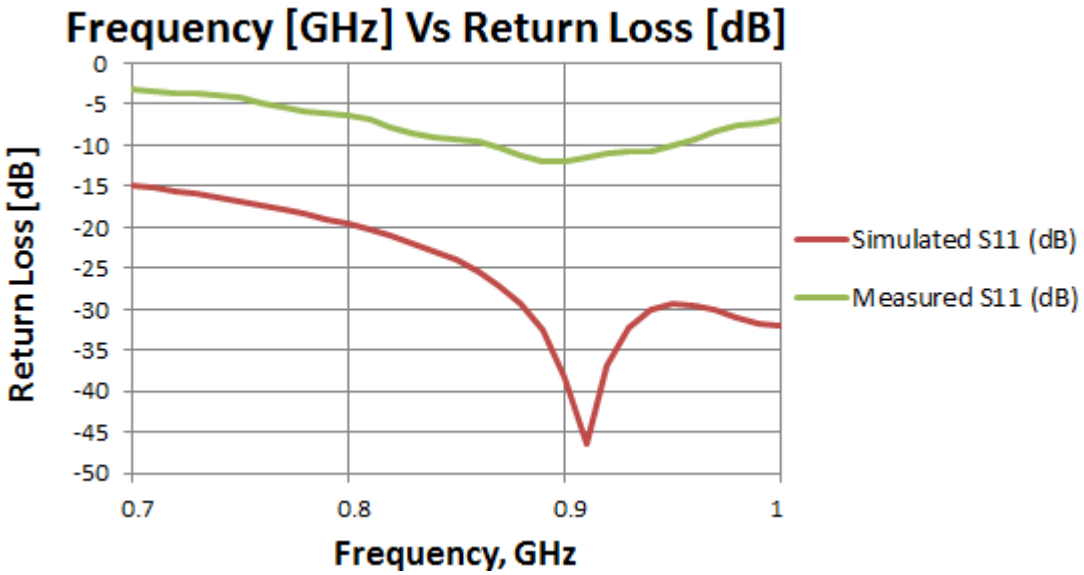

Figure 7.7b Return Loss (dB) of Antenna **B**

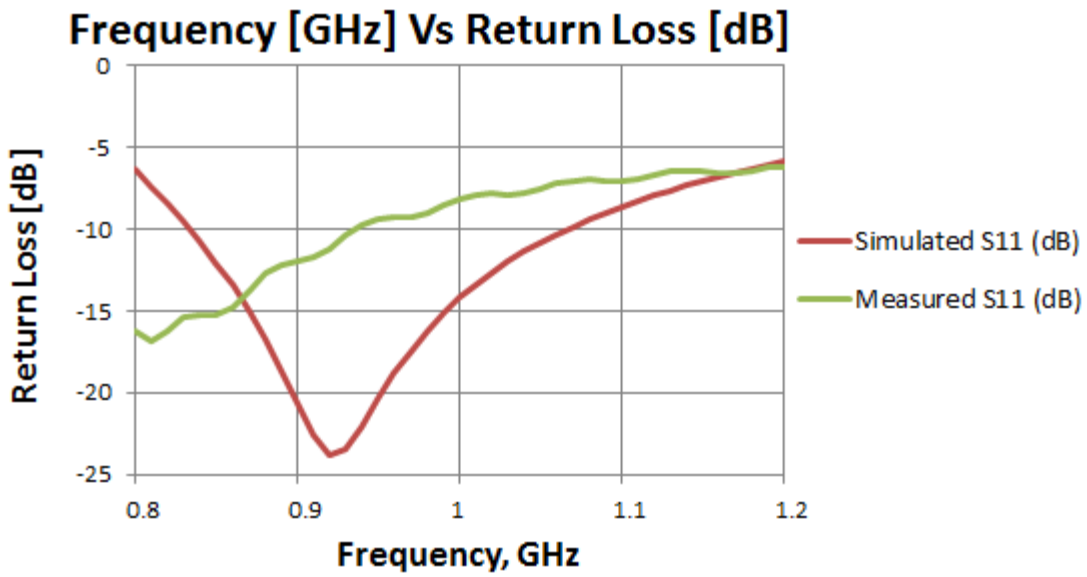

Figure 7.7c Return Loss (dB) of Antenna **C**

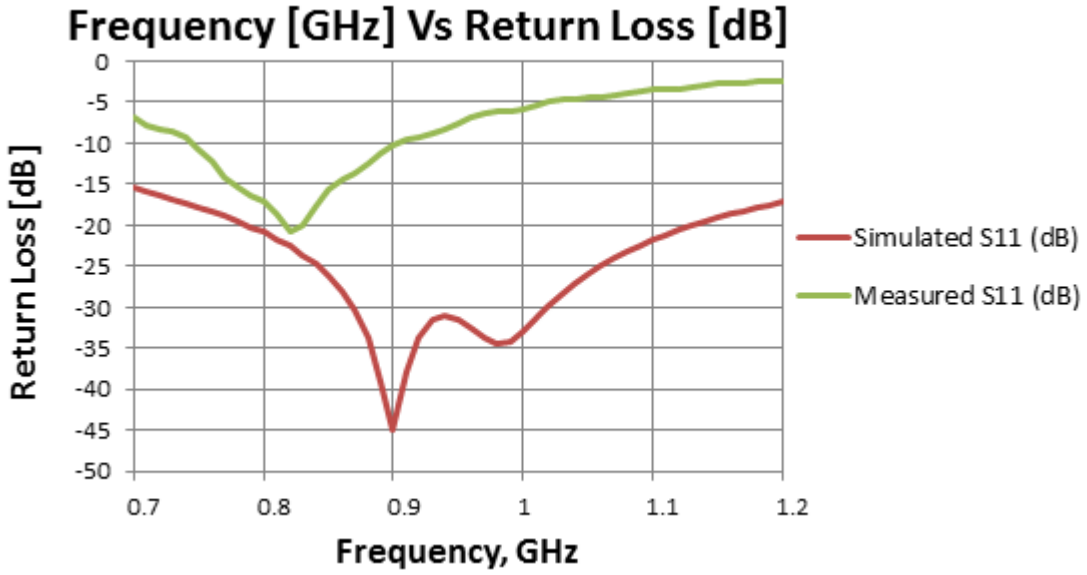

Figure 7.7d Return Loss (dB) of Antenna **D**

Figure 7.7 Measured results versus the simulation results for the proposed antennas.

The figure 7.7 shows the measured return loss values versus the simulation return loss values for each of the antenna designs, A, B, C and D. As shown by [22] the return loss values are simply doubled to indicate an approximate return loss value for the full antenna

i.e. not just half the antenna. The antenna design **E** was fabricated according to the theory outlined for HF tags used for contactless cards as explained in chapter 6, section 6.3. The Figure 7.8 shows the typical antenna design for the HF tag used for contactless cards.

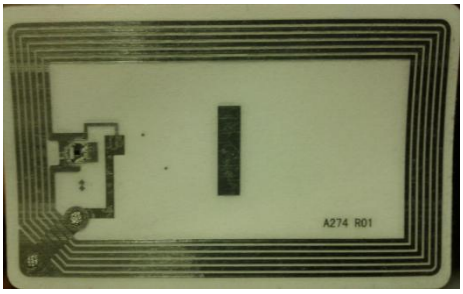

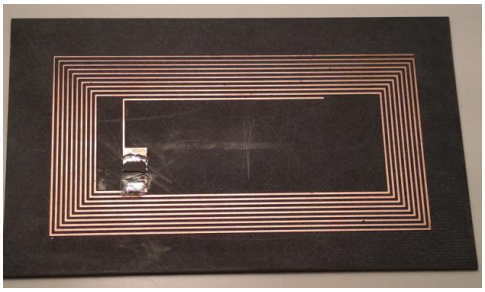

Figure 7.8a Industry HF tag antenna design [55]. **Figure 7.8b** Fabricated Antenna **E**.

The typical application of the designs shown in figure 7.8 is proximity contactless cards. The antenna design **E** used a Nxp Mifare chip with an impedance value of 17pf. The results of using this card with a smartphone reader and the 'nxp info' mobile application is shown in figure 7.9.

** TagInfo scan (version 1.30) 2012-04-17 04:44:44 **

IC manufacturer:
NXP Semiconductors
IC type:
MIFARE Ultralight C (MF0ICU2)
NFC Forum NDEF-compliant tag:
Type 2 Tag

NFC data set information:
Current message size: 18 bytes
Maximum message size: 137 bytes
NFC data set access: Read & Write
Can be made Read-Only
Text record:
type: "T"
encoding: UTF-8
lang: en
text: "Hi Mohamed."

Figure 7.9a Mobile application 'Tag Info' used to read the contactless card with the smartphone.

Memory size:
192 bytes
* 48 pages, with 4 bytes per page

Technologies supported:
ISO/IEC 14443-3 (Type A) compatible
ISO/IEC 14443-2 (Type A) compatible

Figure 7.9b Mobile application 'Tag Info' used to read the contactless card with the smartphone.

The antenna design **E** was designed to be read by similar devices and HF readers. However, the design **E** did not function as intended because of the possible factors listed below.

1) The thickness of the substrate was found to be greater than a typical plastic card such as a credit card.
2) The coil structure on the antenna might be disconnected at specific locations. Therefore, it needs to be thoroughly viewed using a microscope.

The separation of the inductive loop lines is 0.5mm and this makes it hard to fabricate using techniques such as 'etching'.

7.4 Chapter Summary

In this chapter the simulation results and the measured results of the proposed antennas were compared. The results from simulation and measurement show close agreement when comparing the return loss (dB) values as shown in table 7.2. In addition, the measurement results for the impedance values were shown to match closely in terms of the real component of the impedance. For antenna design E the application of use is contactless card. Furthermore, the demonstration of the application of antenna design E is demonstrated in figure 7.9. The fabricated antenna did not function as intended because of the thickness of the substrate and the difficulties encountered in the fabrication process. However, the design can be implemented with the help of industry RFID tag printers that are customized to print tags of applications such as contactless cards.

Chapter 8 – Conclusion

This thesis demonstrated the RFID tag antenna design process for passive UHF RFID tags (915 MHz) as well as passive HF RFID tags (13.56 MHz). Although RFID technologies have become very popular in recent years, there is still a significant gap when it comes to accurate design of tags based on specific application or use such as inventory, clothing, pharmaceuticals, etc.

The main problem that antenna designers face is chip-impedance matching. This matching is necessary for optimal tag performance characteristics such as read range, antenna radiation, antenna efficiency, etc. Some impedance matching techniques have been presented namely, T-match, inductively coupled loop and nested slot techniques. Furthermore, optimization of the antenna dimensions with the help of commercial electromagnetic (EM) simulation tools was successfully achieved. The proposed antenna designs for specific applications were thus fabricated and tested.

The RFID antenna design process required necessary evaluation of the application of use. For example, the tag designed for pharmaceutical products requires the tag to be in close vicinity of liquids and can significantly impact tag performance characteristics such as read range, antenna efficiency, etc. Furthermore, as discussed in this work, RF designers can select the best geometrical dimensions of the antenna based on impedance-matching charts for optimal tag performance. Furthermore, as highlighted in this document, multiple applications (baggage tag, clothing, inventory, etc.) can use the same ASIC-chip with different antenna geometry.

8.1 Contribution

The main contribution of this thesis is the systemization of the RFID antenna design process for RF designers by providing techniques to develop application-specific passive RFID tags. Currently, industry RFID design procedures give more attention to the application requirements of the RFID tags by means of fabrication and measurement procedures as shown in [10] rather than precise chip impedance matching process. This

thesis proposes to fill this gap by providing a systemized passive RFID tag antenna design procedure. As an example of this process, tag antenna designs (A, B, C, D and E) were achieved through simulations and tag performance measurements. Furthermore, the results obtained help RF designers select optimal impedance-matching antenna dimensions before the fabrication process. As a result, this process will significantly reduce the RFID tag development costs.

8.2 Future work

After analyzing the simulated/experimental results and considering previous research work in this area, there are many possible future extensions to the RFID antenna design. One extension of this work is to find applications where the RFID tags are affected by the surrounding environment such as metals, water, glass wine bottle, etc. Some RFID antenna designs such as planar inverted-F (PIFA) configurations and microstrip antennas form a partial solution to this problem. However, the PIFA and microstrip design increase the overall cost of the tag.

Another possible extension of is the design of a dual UHF/HF RFID tag to incorporate item level tagging as well as distance-read tracking. Furthermore, the dual band tags research will give way to dual band readers and reduce the overall cost of the RFID system.

REFERENCES

[1] D. C. Wyld, *RFID: The right frequency for the government*. A research monograph from the IBM Center for the Business of Government, 2005.

[2] D. Dobkin and T. Wandinger, "A Radio-Oriented Introduction to Radio Frequency Identification," *High Frequency Electronics*, pp. 46-51, 2005.

[3] D. Dobkin, pp. 69: *The RF in RFID: Passive UHF RFID in Practice*. Oxford: Elsevier, 2007.

[4] G. De Vita, G. Iannaccone, "Design criteria for the RF section of UHF and microwave passive RFID transponders", *IEEE Trans. on Microw. Theory and Tech.*, vol. 53(9), pp. 2978-2990, Sept. 2005

[5] K.V.S. Rao, P.V. Nikitin, and S. Lam, "Antenna design for UHF RFID tags: a review and a practical application," *IEEE Trans. on Antennas and Propag.*, vol. 53, pp. 3870-3876, Dec. 2005.

[6] P.V. Nikitin, *et al*. Power reflection coefficient analysis for complex impedances in RFID tag design, *IEEE Trans. on Microw. Theory and Tech., 53*(9): 2712–2725, Dec. 2005

[7] G. Marrocco, "The Art of UHF RFID antenna design: impedance-matching and size-reduction techniques", *IEEE Antennas and Propag. Mag.*, vol. 50, Issue. 1, pp. 66-79, Feb 2008.

[8] J.W. Lee et al. Design Consideration of UHF RFID Tag for Increased Reading Range. *IEEE MTT-S Int. Microw. Symp. Digest, 2006.* pp. 1588 – 1591. 20 November 2006

[9] Avery Dennison, UHF RFID Inlays, Internet: *http//rfid.averydennison.com /product_ cat/uhf-rfid-inlays*, Accessed, Nov. 5, 2011.

[10] M. Bolic, D. Simplot-Ryl, and I. Stojmenovic, *RF Systems: Research Trends and Challenges*. Wiley Online Library: John Wiley & Sons, 2010.

[11] N.C. Karmakar, *Handbook of smart antennas for RFID systems.* John Wiley & Sons. Hoboken, New Jersey, 2010.

[12] K. Finkenzeller, *RFID Handbook*, 3rd edition, John Wiley & Sons, Hoboken, NJ, 2010.

[13] M. Myer, M. Brown, S. Patadia, and S. Dua, *Passport for Comptia RFID+ Certification*, McGraw-Hill, New York, 2007.

[14] R. Mark, *The History of RFID Technology* [Online], Available: http://www.rfidjournal.com/article/view/1338/1, accessed 20 February 2012.

[15] H. Stockman, "Communication by Means of Reflected Power", *Proc. of the IRE*, vol. 36, pp.1196-1204, October 1948.

[16] EPC Global Home Page [Online], Available: http://www.gs1.org/epcglobal, accessed 20 February 2012.

[17] Class 1 Generation 2 UHF Air Interface Protocol Standard. http://www.epcglobalinc.org /standards/. Accessed Nov 10, 2011.

[18] A. Petosa, *Antennas and Arrays*, Carleton University Course Notes, Sep. 2011.

[19] C. Balanis, *Antenna Theory*, 3rd edn. Chichester: John Wiley & Sons, Ltd, 2005.

[20] L.J. Chu, "Physical limitations of omni-directional antennas," *J. Applied Physics*, vol. 19, pp. 1163–1175. 1948.

[21] Y. Tikhov, Y. Kim, Y.-H. Min, "Compact low cost antenna for passive RFID transponder," *IEEE Int. Symp. Antennas Prop.*, pp. 10 15-1018, 2006.

[22] G. Marrocco, "RFID antennas for the UHF remote monitoring of human subjects," *IEEE Trans. Antennas Prop.*, vol. 55, pp. 1862-1870, 2007.

[23] Avery Dennison, UHF RFID Inlays, *http//rfid.averydennison.com/product_cat/uhf-rfid-inlays*, Accessed in Oct. 13, 2011.

[24] T. Hu, C. Liu, Z. Wang, "Design and analysis of UHF tag antenna structure," *China-Japan Joint Microw. Conf.*, pp. 1-4, 2011.

[25] J.W. Lee *et al*., "Design consideration of UHF RFID tag for increased reading range," *IEEE MTT Int. Microw. Symp.*, pp. 1588-1591, 2006.

[26] High-Frequency Structure Simulator, HFSS v12, Pittsburgh, PA, USA.

[27] A.C. Polycarpou, *Introduction to Finite Element Methods in Electromagnetics*, Arizona: Morgan & Claypool, 2006.

[28] H. Hirvonenen, P. Pursula, K. Jaakkola and K. Laukkanen, "Planar Inverted-F Antenna for Radio Frequency Identification," *Electronics Letters*, 40, 14, July 2004, pp. 848-850.

[29] L. Ukkonen, M. Schaffrath, J. A. Kataja, L. Sydanheimo and M. Kivikoski, "Evolutionary RFID tag antenna design for pape industry applications," *Int. J. RFID and App.*, vol. 1, 2006, pp. 107-122.

[30] G. Marrocco, "Body-matched antennas for wireless biometry," *European Conf. on Antennas and Propag.*Nice, France, p. 795, 2006.

[31] G. Marrocco and C. Calabrese, "Automatic design of miniaturized slot-line RFID antennas," *European Conf. Antennas and Propag.*, Edinburgh, Scotland, 2007.

[32] L. Korowajczuk, *LTE, WiMAX and WLAN Network Design, Optimization, and Performance Analysis*, Wiley & Sons, West Sussex, UK, 2011.

[33] B.C. Wadell, *Transmission Line Design Handbook*, Artech House, Wilmington, DE, 1991

[34] W. Choi, H.W. Son, C. Shin, J.-H. Bae, G. Choi, "RFID tag antenna with a meandered dipole and inductively coupled feed," *IEEE Int. AP-S Symp. Antennas Propag.*, Albuquerque, NM, pp. 619-622, 2006.

[35] N. Michishita, Y. Yamada, "A novel impedance matching structure for a dielectric loaded 0.05 wavelength small meander line antenna," *IEEE Int. AP-S Symp. Antennas Propag.*, Albuquerque, NM, pp. 1347-1350, 2006.

[36] A. Toccafondi, P. Braconi, "Compact load-bars meander line antenna for UTHF RFID transponder," *European Conf. on Antennas and Propag.*, Nice, France, 2006.

[37] C. Cho, H. Choo and I. Park, "Design of novel RFID tag antennas for metallic objects," *IEEE Int. AP-S Symp. Antennas Propag.*, Albuquerque, NM, pp. 3245-3248, 2006.

[38] M. Keskilammi, M. Kivikoski, "Using text as a meander line for RFID transponder antennas," *IEEE Antennas and Propag.*, vol. 3, pp. 372-374, 2004.

[39] H. Hirvonenen, P. Pursula, K. Jaakkola and K. Laukkanen, "Planar Inverted-F Antenna for Radio Frequency Identification," *Electronics Letters*, 40, 14, July 2004, pp. 848-850.

[40] B. Yu, S.-J. Kim, B. Jung, F. J. Harackiewicz, M.-J. Park, B. Lee, "Balanced RFID tag antenna mountable on metallic plates," *IEEE Int. AP-S Symp. Antennas Propag.*, Albuquerque, NM, pp. 3237-3240, 2006.

[41] C.H. Cheng, R.D. Murch, "Asymmetric RFID tag antenna," *IEEE Int. AP-S Symp. Antennas Propag.*, Albuquerque, NM, pp. 1363 1366, 2006.

[42] Avery Dennison, UHF RFID Inlays, *http//rfid.averydennison.com/product_cat/uhf-rfid-inlays*, accessed Oct. 13, 2011.

[43] A.E. Abdulhadi, R. Abhari, "Dual printed meander monopole antennas for passive UHF RFID tags," *IEEE AP-S Int. Symp. Antennas Prop.*, Spokane, WA, pp. 988-991, 2011.

[44] J.W. Lee *et al*., "Design consideration of UHF RFID tag for increased reading range," *IEEE MTT-S Int. Microwave Symp.*, pp. 1588-1591, 2006.

[45] T. Hu, L. Caifeng, Z. Wang, "Design and analysis of UHF tag antenna structure," *China-Japan Joint Microw. Conf.*, pp. 1-4, 2011.

[46] G. Jihui, *et al*., "A design of RFID tag antenna for clothing," *Cross Strait Quad-Regional Radio Science and Wireless Technology Conf.*, pp. 1075-1077, 2011.

[47] Y. Nishioka, *et al*., "Novel antenna configuration for HF- and UHF band hybrid card-type RFID Tags," *European Conf. on Antennas and Propag.*, pp. 1-5, 2010.

[48] K. Riad, A. Ataollah, "UHF RFID transponders antenna design for metal and wood surfaces," *IEEE Int. Conf. on RFID*, pp. 270 - 277, 2009.

[49] R. Bhattacharyya, *et al*., "RFID tag antenna based sensing: does your beverage glass need a refill?," *IEEE Int. Conf. on RFID*, pp. 126–133, 2010.

[50] Internet resource, Rogers Corp., http://www.rogerscorp.com/documents/606/acm/RT-duroid-5870-5880-Data-Sheet.aspx, accessed March 15, 2012.

[51] Internet Resource STMicroelectronics, http://www.st.com/internet/com/TECHNICAL_RESOURCES/TECHNICAL_LITERATURE/APPLICATION_NOTE/CD00221490.pdf, accessed February 20, 2012.

[52] B. Yang, Q.Feng, (2008) A folded dipole antenna for RFID tag, *Int. Conf. on Microw. and Millim. Wave Tech., 2008. ICMMT*, *IEEE Conf. publications, pp. 1047-1049,* 2008.

[53] C.R.Medeiros, J.R. Costa, "Passive UHF RFID Tag for Airport Suitcase Tracking and Identification", *IEEE Antennas and Wireless Propag. Letters*, Vol. 10, 2011.

[54] Internet resource, STMIcroelectronics, http://www.st.com/internet/mcu/product /219471.jsp, accessed February 20, 2012.

[55] Internet resource, Identive NFC, http://www.identivenfc.com/nfc-tags.htm, accessed February 20, 2012.